Transportation Consortium of South-Central States

Solving Emerging Transportation Resiliency, Sustainability, and Economic Challenges through the Use of Innovative Materials and Construction Methods: From Research to Implementation

Engineered Geopolymer Composites (EGCs) for Sustainable Transportation Infrastructure

Project No. 19CLSU04

Lead University: Louisiana State University

Collaborative Universities: Texas A & M University and ESPOL

Final Report

November 2020

TECHNICAL DOCUMENTATION PAGE

1. Project No. 19CLSU04	2. Government Accession No.	3. Recipient's Catalog No.	
4. Title and Subtitle Engineered Geopolymer Composites (EGCs) for Sustainable Transportation Infrastructure		**5. Report Date** Nov. 2020	
		6. Performing Organization Code	
7. Author(s) PI: Gabriel Arce https://orcid.org/0000-0002-3610-8238 PI: Marwa Hassan https://orcid.org/0000-0001-8087-8232 Co-PI: Miladin Radovic https://orcid.org/0000-0003-4571-2848 Co-PI: Svetlana Sukhishvili https://orcid.org/0000-002-2328-4494 GRA: Ruwa AbuFarsakh https://orcid.org/0000-0002-3596-864x GRA: Oscar Huang https://orcid.org/0000-0001-7004-3506 GRA: Sang Zhen https://orcid.org/0000-0002-9703-6311 SP: Mauricio Cornejo https://orcid.org/0000-0003-4483-5125 SP: Haci Baykara https://orcid.org/0000-0002-8319-0836		**8. Performing Organization Report No.**	
9. Performing Organization Name and Address Transportation Consortium of South-Central States (Tran-SET) University Transportation Center for Region 6 3319 Patrick F. Taylor Hall, Louisiana State University, Baton Rouge, LA 70803		**10. Work Unit No. (TRAIS)**	
		11. Contract or Grant No. 69A3551747106	
12. Sponsoring Agency Name and Address United States of America Department of Transportation Research and Innovative Technology Administration		**13. Type of Report and Period Covered** Final Research Report Aug. 2019 – Nov. 2020	
		14. Sponsoring Agency Code	

15. Supplementary Notes

Report uploaded and accessible at Tran-SET's website (http://transet.lsu.edu/).

16. Abstract

The objective of this study was to develop novel Engineered Geopolymer Composite (EGC) materials implementing locally available ingredients to produce practical and cost-effective EGCs for repair and new construction of transportation infrastructure in the region. To this end, geopolymers (GPs) were synthesized by alkali activation of metakaolin (MK) or a combination of metakaolin and fly ash (MKFA) as GP precursors. MK-GPs were activated using sodium silicate and potassium silicate solutions prepared by dissolving silica fume (SiO_2) and KOH or NaOH in deionized water. MKFA-GPs replaced silica fume using fly ash and were activated using only KOH solution. GP binders, GP mortars and fiber-reinforced GP composites were manufactured and thoroughly evaluated. Based on the experimental findings, it was concluded that MK based GP matrices are promising for the development of EGCs as these GPs produce high mechanical strength at ambient curing conditions and allow for pseudo strain hardening (PSH) behavior to occur when reinforced with low contents of PVA fiber (i.e., 1.6% volume fraction). However, attaining proper fiber dispersion in MK-GP matrices was challenging. MKFA GP matrices developed in this study exhibited low mechanical strength and did not produce PSH behavior when reinforced with PVA fibers. Low strengths were associated to the low reactivity of fly ash in contrast to silica fume. A feasibility study was conducted in Ecuador to evaluate use of natural zeolite, volcanic ash, and metakaolin for the development of GP matrices, the maximum compressive strength attained was ~20 MPa.

17. Key Words Geopolymer, Metakaolin, PVA Fibers, Na, K		18. Distribution Statement No restrictions. This document is available through the National Technical Information Service, Springfield, VA 22161.	
19. Security Classif. (of this report) Unclassified	**20. Security Classif. (of this page)** Unclassified	**21. No. of Pages** 64	**22. Price**

Form DOT F 1700.7 (8-72)   **Reproduction of completed page authorized.**

SI* (MODERN METRIC) CONVERSION FACTORS

APPROXIMATE CONVERSIONS TO SI UNITS

Symbol	When You Know	Multiply By	To Find	Symbol
LENGTH				
in	inches	25.4	millimeters	mm
ft	feet	0.305	meters	m
yd	yards	0.914	meters	m
mi	miles	1.61	kilometers	km
AREA				
in^2	square inches	645.2	square millimeters	mm^2
ft^2	square feet	0.093	square meters	m^2
yd^2	square yard	0.836	square meters	m^2
ac	acres	0.405	hectares	ha
mi^2	square miles	2.59	square kilometers	km^2
VOLUME				
fl oz	fluid ounces	29.57	milliliters	mL
gal	gallons	3.785	liters	L
ft^3	cubic feet	0.028	cubic meters	m^3
yd^3	cubic yards	0.765	cubic meters	m^3
NOTE: volumes greater than 1000 L shall be shown in m^3				
MASS				
oz	ounces	28.35	grams	g
lb	pounds	0.454	kilograms	kg
T	short tons (2000 lb)	0.907	megagrams (or "metric ton")	Mg (or "t")
TEMPERATURE (exact degrees)				
^oF	Fahrenheit	5 (F-32)/9 or (F-32)/1.8	Celsius	^oC
ILLUMINATION				
fc	foot-candles	10.76	lux	lx
fl	foot-Lamberts	3.426	candela/m^2	cd/m^2
FORCE and PRESSURE or STRESS				
lbf	poundforce	4.45	newtons	N
lbf/in^2	poundforce per square inch	6.89	kilopascals	kPa

APPROXIMATE CONVERSIONS FROM SI UNITS

Symbol	When You Know	Multiply By	To Find	Symbol
LENGTH				
mm	millimeters	0.039	inches	in
m	meters	3.28	feet	ft
m	meters	1.09	yards	yd
km	kilometers	0.621	miles	mi
AREA				
mm^2	square millimeters	0.0016	square inches	in^2
m	square meters	10.764	square feet	ft^2
m	square meters	1.195	square yards	yd^2
ha	hectares	2.47	acres	ac
km	square kilometers	0.386	square miles	mi^2
VOLUME				
mL	milliliters	0.034	fluid ounces	fl oz
L	liters	0.264	gallons	gal
m	cubic meters	35.314	cubic feet	ft^3
m	cubic meters	1.307	cubic yards	yd^3
MASS				
g	grams	0.035	ounces	oz
kg	kilograms	2.202	pounds	lb
Mg (or "t")	megagrams (or "metric ton")	1.103	short tons (2000 lb)	T
TEMPERATURE (exact degrees)				
C	Celsius	1.8C+32	Fahrenheit	^oF
ILLUMINATION				
lx	lux	0.0929	foot-candles	fc
cd/m^2	candela/m^2	0.2919	foot-Lamberts	fl
FORCE and PRESSURE or STRESS				
N	newtons	0.225	poundforce	lbf
kPa	kilopascals	0.145	poundforce per square inch	lbf/in^2

TABLE OF CONTENTS

LIST OF FIGURES

LIST OF TABLES

ACRONYMS, ABBREVIATIONS, AND SYMBOLS

ASTM	American Society for Testing and Materials
CV	Coefficient of Variation
DI	Deionized
GP	Geopolymer
GGBS	Ground-Granulated Blast-Furnace Slag
ECC	Engineered Cementitious Composite
EDS	Energy Dispersive Spectroscopy
EGC	Engineered Geopolymer Composite
E_m	Modulus of Elasticity of the Matrix
FA	Fly Ash
FRC	Fiber Reinforced Concrete
J_b'	Complementary Energy of the Fiber-Bridging Relation
J_{tip}	Crack-Tip Matrix Toughness
JSCE	Japan Society of Civil Engineers
K_m	Fracture Toughness of the Matrix
LOI	Loss on Ignition
LVDT	Linear Variable Displacement Transducer
MK	Metakaolin
MS	Microsilica Sand
PCC	Portland Cement Concrete
PSH	Pseudo Strain Hardening
PVA	Polyvinyl Alcohol
RS	River Sand
SE	Secondary Electron
SEM	Scanning Electron Microscopy
STD	Standard Deviation
UHMWPE	Ultra-High Molecular Weight Polyethylene
XRF	X-ray Fluorescence Spectroscopy
σ_{fc}	First Cracking Strength
σ_0	Fiber-Bridging Capacity
δ_0	Crack Opening Corresponding to σ_0
$\sigma(\delta)$	Fiber-Bridging Relationship

EXECUTIVE SUMMARY

The objective of this study was to develop novel Engineered Geopolymer Composite (EGC) materials implementing locally available ingredients to produce practical and cost-effective EGCs for repair and new construction of transportation infrastructure in the region. To this end, geopolymers (GPs) were synthesized by alkali activation of metakaolin (MK) or a combination of metakaolin and fly ash (MKFA) as GP precursors. MK-GPs were activated using sodium silicate and potassium silicate solutions prepared by dissolving silica fume (SiO_2) and potassium hydroxide (KOH) or sodium hydroxide (NaOH) in deionized water. On the other hand, MKFA-GPs were activated using only potassium hydroxide (KOH) solution. GP binders, GP mortars and fiber-reinforced GP composites were manufactured and thoroughly evaluated. Properties of GP materials evaluated included water loss, shrinkage, density, setting time, compressive strength, tensile strength and strain capacity, flexural strength and deflection capacity, and slant shear bond strength to Portland cement concrete (PCC).

Based on the experimental findings, it was determined that regardless of the starting water composition, the water content of all K- and Na-based MK-GP binders stabilized at ~5-10wt% and ~10-15wt%, respectively, after four weeks of curing. A similar situation was observed for K- and Na-based MK-GP mortars were the water content converged to ~2-3% and ~3-4%, respectively. It was observed that in contrast to K-based compositions, Na-based compositions exhibited a greater tendency to retain water. This observation was attributed to Na ion's smaller ionic radius in contrast to K ion, which is able to attract more water molecules. Another important tendency observed was that the density of the dried MK-GP decreased as the initial water content increased. This phenomenon was attributed to excess water being released during the geopolymerization process, which create voids within the GP structure. Generally, the strength of Na-based MK-GP binders increased as the SiO_2/Al_2O_3 ratio increased and/or the water/solids ratio decreased. On the other hand, for K-based MK-GP binders, the strength increased significantly when the SiO_2/Al_2O_3 ratio was equal or greater than 2.5. Furthermore, the strength of the MK-GPs significantly increased with the addition of sand, which was attributed to the likely formation of a strong ITZ between the GP binder and aggregate particles. SEM analysis of MK-GPs revealed that larger quantities of unreacted metakaolin within the GP microstructure correlated with low strengths. From the MK-GP mortars evaluated, K321, K331, and Na431 compositions were selected for further evaluation as fiber reinforced composites for the development of EGCs. These compositions were selected due to their satisfactory strength and workability characteristics.

The inclusion of PVA fibers in MK-GP mortars produced noticeable compressive strength improvements. In addition, the increment in fiber content produced further enhancements in the compressive strength. Furthermore, MK-GP mortars using microsilica sand (MS) generally presented greater compressive strengths compared to those using river sand (RS). From the MK-GP compositions evaluated for EGC development, K321 produced the composites with the greatest compressive strengths. This was counter intuitive since K331 and Na431 pure MK-GP binders presented higher strength compared to K321 pure MK-GP. This observation was explained by the excessive workability of K331 and Na431 MK-GP binders, which caused some aggregate and fiber segregation problems (specially for Na431 MK-GP materials). The greatest compressive strength (i.e., 57.52 MPa) was obtained for the composite K321 MK-GP using MS and 1.6% PVA fiber content by volume (i.e., K321 MK-GP-MS-1.6%PVA). In contrast to conventional PCC, the density of this composite was approximately 22.9% lower, yet it fell in the classification of high-strength concrete. Consequently, the K321 MK-GP-MS-1.6%PVA composite and its RS

counterpart (i.e., K321 MK-GP-RS-1.6%PVA) were selected for further evaluation in uniaxial tension and bending. Experimental findings revealed a mild PSH behavior the composites in uniaxial tension, with K321 MK-GP-MS-1.6%PVA outperforming in terms of tensile strength and strain capacity. The absence of robust PSH performance of the materials was principally attributed to deficient fiber distribution. A such, a modified mixing procedure was attempted to improve fiber dispersion. This produced significant enhancements in the tensile properties of the materials allowing K321 GP-MS-1.6%PVA to exhibit significant PSH characteristics (i.e., tensile strain capacity up to 2.02%). Flexural performance test results agreed with uniaxial tensile test findings were the K321 GP-MS-1.6%PVA composite presented the highest flexural strength and deflection capacity. Being the best performing composite, K321 GP-MS-1.6%PVA was selected to evaluate the bond strength of MK EGCs with conventional concrete through slant shear test. Test findings implied excellent bond characteristics of the MK-based EGC as failure of the slant shear specimens consistently occurred in the concrete substrate. Generally, it was concluded that MK based GP matrices are promising for the development of EGCs yet attaining proper fiber dispersion is challenging. Therefore, future research should be directed towards optimizing the rheological characteristics of the MK-GP matrices and mixing procedures to consistently produce appropriate fiber dispersion. To produce more cost-effective composites, the development of K321 MKFA-GP compositions was evaluated by replacing silica fume with fly ash. In contrast to K321 MK-GP compositions, the K321 MKFA-GP materials presented low mechanical strength and exceedingly high setting times. This was attributed to the low reactivity of fly ash compared to silica fume. Furthermore, MKFA-GP composites did not produce PSH behavior. This was attributed to the low matrix strength, which likely yield a produced a poor fiber/matrix interface. The pH of the different GP binders evaluated for EGC application (i.e., K321, K331, Na431, and MKFA K321) was assessed. The pH of all these binders was more alkaline than that of conventional PCC. As such, safety precautions should be taken when working with these materials including the use personal protective equipment and appropriate training of the workforce.

A feasibility study was conducted in Ecuador to evaluate the combination of different solid precursor, i.e., natural zeolite, volcanic ash and metakaolin for the development of geopolymer matrices. Experimental results showed that the combination of these precursors was only possible when zeolite and MK were used under the experimental conditions evaluated. Experimental findings suggested that an optimal Si/Al ratio may be achieved by mixing 70% of zeolite and 30 of MK. Furthermore, the highest of compressive strength obtained was approximately 20 MPa.

1. INTRODUCTION

Concrete is a durable, low-cost, and widely available material that exhibits high compressive strength, leading to its widespread use in civil infrastructure (e.g., bridges, buildings, pavements, etc.), However, it has low tensile strength and ductility resulting in brittle failure and cracking. Cracks tend to develop and propagate when concrete is subjected to loading or changes in environmental conditions, thus granting easy access for water and other detrimental agents into the structure allowing for enhanced deterioration (*1*). To counteract this problem, discrete fibers admixed in concrete materials have been used to hinder the crack growth and propagation, therefore mitigating the brittle behavior of concrete. However, traditional fiber-reinforced concrete (FRC) present marginal improvement in ductility and tensile strength as well as exhibit strain-softening after cracking (single localized crack growth associated with a decrease in load carrying capacity) when subjected to tensile stresses. Consequently, high-performance fiber-reinforced cementitious composites (HPFRCC) were developed as an alternative to mitigate concrete brittleness and its weak behavior under tensile stresses. In contrast with FRC, HPFRCC exhibit strain-hardening performance after cracking under tensile stresses. One novel type of HPFRCC known as Engineered Cementitious Composites (ECCs) has been studied over the past three decades to mitigate the brittle nature of concrete. The uniqueness of ECCs arises from its high tensile strain capacity ranging between 1 to 8% (i.e., 100 to 800 times that of regular concrete or FRC), which is achieved at relatively low fiber contents (i.e., typically 1.5 to 2% volume fraction) by means of a micromechanics and fracture mechanics based design approach (*2–6*). The implementation of the micromechanics and fracture mechanics concepts allow to efficiently mitigate the brittleness of concrete by transforming the Griffith crack propagation mode of regular concrete and FRC to a steady-state flat crack propagation mode. Consequently, this enables a tensile pseudo strain-hardening (PSH) behavior in ECCs through the formation of multiple steady-state microcracks, which gives rise to the extraordinary tensile ductility of these composites (*7*).

ECCs are typically composed of cement (mostly Portland Cement), supplementary cementitious materials (SCMs), fine aggregate, water, and polymer microfibers (*7–12*). Polyvinyl alcohol (PVA) fibers have been principally used to manufacture ECCs (*3, 6, 12–19*). However, ultra-high-molecular weight polyethylene (UHMWPE) fibers have also been used; yet, these have been mainly limited to the development of high performance ECCs due to its high cost (*4, 12, 20–23*). Since ECCs do not use coarse aggregate, the amount of cement required to manufacture these composites increases relative to conventional concrete. In turn, this increments ECCs environmental impact, as the cement industry consumes vast amounts of energy and produces immense amounts of carbon dioxide (CO_2) emissions, which accounts for nearly 8% of CO_2 global anthropogenic emissions (*24*). As such, there is a significant motivation to find alternative binders that can replace cement in the manufacture of ECC materials without negatively affecting the mechanical properties of these novel composites. Recently, geopolymer (GP) binders have been proposed as a promising and sustainable alternative to cement based binders in the manufacture of ECCs (*3, 25, 26*). These composites implementing GP binders are recognized in the literature as strain-hardening geopolymer composites (SHGC) or Engineered Geopolymer Composites (EGCs). Previous studies suggest that GP matrices exhibit comparable compressive strengths to cementitious matrices while exhibiting lower fracture toughness (*3, 25–27*).In turn, EGCs can achieve high tensile ductility at remarkably low fiber contents (i.e., less than 2%) (*2, 16, 25, 26, 28*).

EGC Design

EGCs follow the same fiber/matrix micromechanics and fracture mechanics concept of ECCs, which allow for these composites to exhibit robust pseudo strain-hardening (PSH) behavior. To attain PSH behavior, two conditions must be met: the strength criterion and the energy criterion presented in Equations 1 and 2, respectively (*2, 8, 29*). The strength criterion assures that the composite will not fail (by fiber rupture or pullout) upon crack initiation from any defect site in the matrix (*2, 15, 17, 29*). Conversely, the energy criterion guarantees steady-state flat crack propagation that occurs when the crack-tip matrix toughness (J_{tip}) is lower than the complementary energy of the fiber bridging relation (J_b') as first demonstrated by Marshall and Cox using J-integral analysis (*30*). When both criteria are satisfied, then PSH behavior of the composite is possible. Otherwise, the post-cracking strain-softening behavior commonly observed in regular FRC will prevail as illustrated in Figure 1b.

$$\sigma_{fc} \leq \sigma_0 \tag{1}$$

where:
σ_0 = Fiber-bridging capacity; and
σ_{fc} = First-cracking strength.

From Equation 1, σ_{fc} is defined by the matrix fracture toughness (K_m) and the initial flaw size, while σ_0 depends on the fiber and fiber/matrix interface properties (*2, 26*).

$$J_b' = \sigma_0 \delta_0 - \int_0^{\delta_0} \sigma(\delta)d\delta \geq J_{tip} \approx \frac{K_m^2}{E_m} \tag{2}$$

where:
J_b' = Complementary energy of the fiber-bridging relation;
J_{tip} = Crack-tip matrix toughness;
δ_0 = Crack opening corresponding to σ_0;
$\sigma(\delta)$ = Fiber-bridging relationship;
K_m = Fracture toughness of matrix; and
E_m = Modulus of elasticity of matrix.

From Equation 2, J_{tip} is sensitive to K_m and E_m, which depend on the matrix composition. On the other hand J_b', represents the net energy available for crack propagation (illustrated in Figure 1a) and is defined by the fiber-bridging relation, which depends on the properties of the fiber and fiber/matrix interface. Relevant fiber properties include the fiber length (L_f), diameter (d_f), modulus of elasticity (E_f), and tensile strength (σ_{fu}) (*31*). On the other hand, key fiber/matrix micro-scale interfacial properties, which are often referred in the literature as micromechanical parameters, include the frictional bond (τ_0), chemical bond (G_d), and slip-hardening coefficient (β) (*31*). Jointly, these fiber and fiber/matrix properties define the fiber-bridging relation. In fact, micromechanics-based models have been developed by Li and co-workers to obtain the fiber-bridging relation of the composite from the aforementioned properties (*12, 29, 31, 32*).
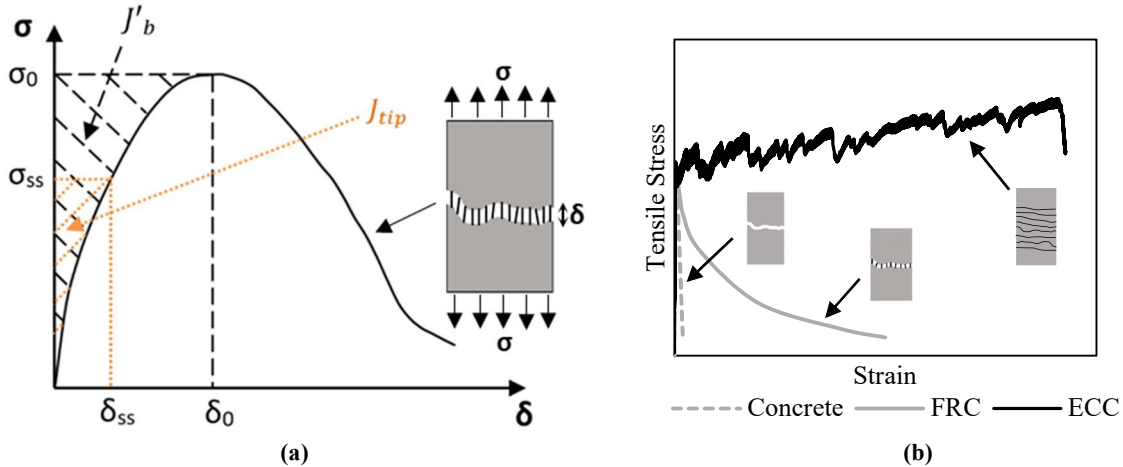
Figure 1. (a) Fiber bridging relation (σ-δ curve) and (b) stress vs. strain behavior of cementitious materials in tension (adapted from (*10*)).

For simplicity, Equations 1 and 2 are typically expressed in the form of $\sigma_0/\sigma_{fc} \geq 1$ and $J_b'/J_{tip} \geq 1$ where the σ_0/σ_{fc} and J_b'/J_{tip} ratios are reffered to as the PSH strength and the PSH energy performance indexes, respectively. As such, succesful design of ECCs or EGCs is achieved when both the PSH strength and PSH energy indexes are greater than one. However, it is important to note that Equations 1 and 2 assume a perfectly homogeneous material; and therefore, for robust PSH behaviour of the composites, PSH perfomance indexes greater than one are necessary. Based on experimental evidence, it has been determined that PSH strength and PSH energy indexes greater than 1.3 and 2.7, respectively, correlate with robust PSH performance (*33*). Figure 1b illustrates an ECC with robust PSH behavior.

In contrast to the cementitious matrices of ECC materials, GP matrices exhibit lower fracture toughness (K_m) and lower tensile strength (σ_{fc}) while attaining comparable compressive strengths (*2*). Therefore, it is favorable for meeting both the strength and energy criteria used in the design of ductile cementitious composites (*25*). Consequently, EGC materials can produce robust high tensile ductility at remarkably low fiber contents (as low as 1.5% volume fraction utilizing PVA fibers); thus, significantly enhancing the cost-effectiveness and greenness of these novel composites (*2*).

2. OBJECTIVES

The objective of this study was to develop novel Engineered Geopolymer Composite (EGC) materials implementing locally available ingredients to produce practical and cost-effective EGCs for repair and new construction of transportation infrastructure in the region.

3. LITERATURE REVIEW

In 2017, the report card on US infrastructure performed by the American Society of Civil Engineers (ASCE) rated the US infrastructure with an overall D+ grade. Regarding transportation infrastructure, roads and bridges obtained grades of D and C+, respectively. This in turn, highlights the urgent need to rebuild or rehabilitate transportation infrastructure in the US, which will require vast amounts of construction materials with Portland cement concrete (PCC) being at the forefront. Given that the cement industry worldwide is responsible for large amounts of CO_2 emissions, in light of global warming, there is a need to develop novel material alternatives to PCC that are less emission intensive and more energy efficient, durable, and resilient. As such, geopolymer (GP) based concrete materials have caught the attention of the scientific community worldwide.

3.1 Geopolymers

The word polymer comes from the Greek words poly (i.e., many) and meros (i.e., part). Polymers are substances that consist of large molecules (macromolecules) that are made of many repeating subunits called monomers. The reaction of these monomers is called polymerization (*34*). Polymers can be classified in two broad groups: organic and inorganic. Organic polymers exhibit chain backbones which are mainly composed of carbon atoms whereas inorganic polymers do not (*35*). Polymers can also be classified as natural or synthetic polymers, where natural polymers are naturally occurring, and synthetic polymers are man-made.

Geopolymers (GPs) are inorganic aluminosilicate polymers, which can be processed at room temperature from natural sources (e.g., calcined clays, volcanic rocks, mine tailings, etc.) or industrial byproducts (e.g., fly ash, slag, rice husk ash, etc.) that provide for a rich source of soluble silicon (Si) and aluminum (Al) species (*36–38*). The formation of GP rigid gels emerges from the geopolymerization of Al and Si species, which occurs through the activation of the GP precursor with an alkaline solution.

The term geopolymer was first introduced by Joseph Davidovitis in the 1970s. While GPs are relatively new materials, several useful applications have been found including coatings, adhesives, waste encapsulation, and binders for concrete and fiber-reinforced composites (*36*). Specifically in concrete materials applications, GPs prevent extensive corrosion of rebar in steel-reinforced concrete , are more resistant to acid attack (*39*, *40*) and fire (*41*), and can reach maximum strength faster than ordinary Portland cement (OPC) . Furthermore, the production of GPs is more energy efficient and can reduce the CO_2 emission by 44-64% when compared to OPC (*42–44*). Last but not least, they can be produced sustainably from natural sources or waste materials.

3.2 Geopolymerization

Geopolymerization is a complex process involving several chemical reactions that occur at different rates. The geopolymerization process is divided in the following stages: (1) dissolution of the Al and Si species of the GP precursor in the alkaline solution; (2) polymerization, which occurs when the hydrolyzed $[AlO_4]^{5-}$ (aluminate) and $[SiO_4]^{4-}$ (silicate) species react forming geopolymer gel; (3) reorganization and precipitation of formed geopolymer gel; (4) final hardening of the polymer chains through the polycondensation process releasing water as it cures; and (5) polymerization and growth of the amorphous to semi-crystalline structure (*36–38*). The

geopolymerization process is summarized in Figure 2. Three types of 3-dimensional amorphous polymer structures consisting of Si, O, and Al form during a geopolymerization chemical reaction: poly-sialate (Si-O-Al-O-), poly-sialate-siloxo (Si-O-Al-O-Si-O), and poly-sialate-disiloxo (Si-O-Al-O-Si-O-Si-O) (36–38). Sialate refers to the Si-O-Al link, while siloxo refers to the Si-O-Si link. The resulting chemical formula (Equation 3) of a GP composition is the following:

$$M_n[-(SiO_2)_z -AlO_2]_n \cdot wH_2O \qquad\qquad [3]$$

where;
M= alkali metal cation (usually Na+ or K+);
n= M/Al ratio;
z= Si/Al ratio; and
w= molar water quantity

Geopolymers are usually prepared with a Si/Al ratio of 1.8-2.2, a $H_2O/(Al_2O_3+SiO_2)$ ratio of 2.0-5.0, and a M/Al ratio of 0.9-1.2 (36–38). Several studies suggested that an increase in SiO_2/Al_2O_3 results in an increase in compressive strength, hardness, and fracture toughness, due to the GPs increased density and Si-O-Si bonds (45, 46). It has been established that an Si-O-Si bond is stronger than Si-O-Al bond (36, 45). Furthermore, similar to cement binders, an increase in water content (i.e., $H_2O/(Al_2O_3+SiO_2)$) negatively affects the geopolymer mechanical properties as excess water evaporates from the material leaving a lower density solid with an increased open porosity (26, 47). An increase in the alkali/Al ratio is theorized to act as a chain terminator during the polycondensation and prevent the geopolymer chains from fully developing (37, 48). Therefore, an appropriate amount of alkali metal is needed to balance the negatively charged IV-fold coordination of Al^{3+} in an Si^{4+} network and contribute to the catalysis of the condensation process(45).
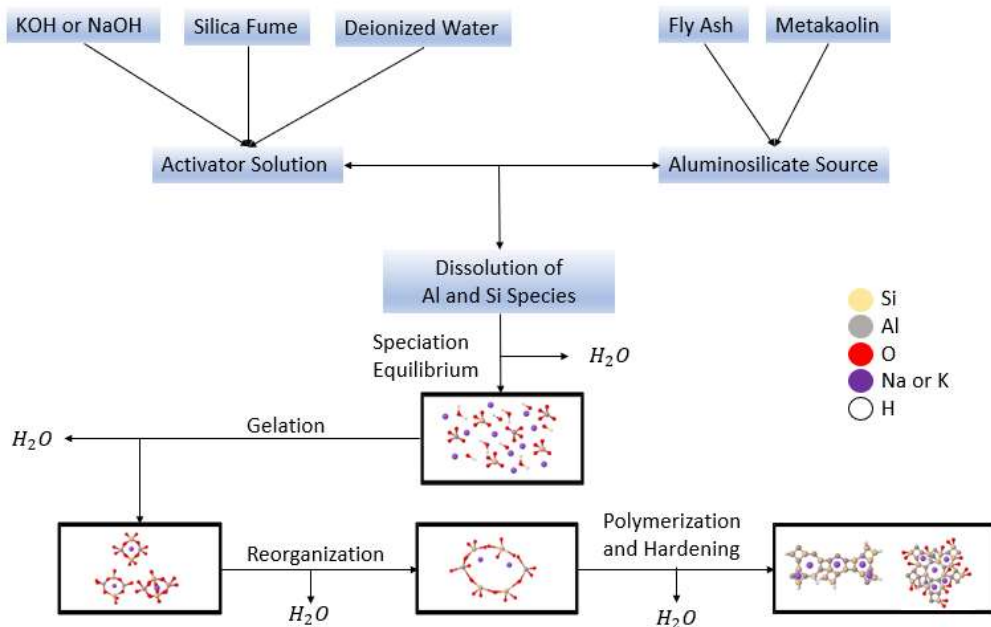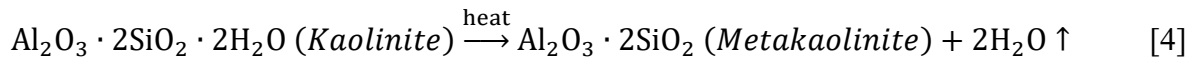

Figure 2. Geopolymerization process.

3.3 Metakaolin

The most abundant product of the chemical breakdown of potassium feldspar is the clay mineral kaolinite (*49*). Kaolinite is very stable under surface conditions and is used as a coating for high-gloss paper, such as that used in textbooks (*50*). When kaolinite is thermally treated (i.e., calcinated within a definite temperature range, 600-800°C), metakaolin is formed as shown in equation 4 through a process called dehydroxylation (*51*). Metakaolin is a highly reactive pozzolan that is classified as a SCM (*51*). It is a high purity white mineral that is used to replace part of the clinker in cement or replace cement in concrete mixtures (*52*). Furthermore, metakaolin is manufactured specifically for cementing applications to maintain high whiteness, high reactivity, ultrafine particle size distribution and consistency. It meets ASTM C-618 Class N pozzolans as well as strength activity index per ASTM C-1240 (*52*).

$$Al_2O_3 \cdot 2SiO_2 \cdot 2H_2O \, (Kaolinite) \xrightarrow{heat} Al_2O_3 \cdot 2SiO_2 \, (Metakaolinite) + 2H_2O \uparrow \qquad [4]$$

3.4 Fly Ash

Fly ash also known as coal ash is a byproduct of the combustion reaction of coal. ASTM C618 identifies two different types of fly ash (Class C and Class F) based on the presence of calcium oxide (CaO), silicon dioxide (SiO_2), iron (III) oxide (Fe_2O_3), and aluminum oxide (Al_2O_3). The main difference between the two types of fly ash is the CaO composition. Class F fly ash contains of less than 10% CaO, while Class C fly ash contains of greater than 10% CaO (*36*). It is important to mention that when Class C fly ash is used, the CaO interferes with the geopolymerization reaction forming calcium silicate hydrate as well as linear polymer chains and flash set properties (*36*).

3.5 Silica Fume

Silica Fume is a byproduct from the industrial manufacturing of elemental silicon or alloys (i.e., ferrosilicon steel) in electric arc furnaces (*36, 53*). At high temperatures of over 2000 °C high purity quartz reduces forming SiO gas, which mixes with oxygen forming SiO_2 and condenses at low temperature resulting in silica fume as shown in Equation 5 (*36, 53*). Silica fume is composed ultrafine amorphous SiO_2 sphere ranging from 50 to 100 nanometers in diameter with a specific surface area of 15000 to 30000 m^2/kg (*36*). High purity silica fume can also be produced from the vapor phase hydrolysis of silicon tetrachloride ($SiCl_4$) in a flame of hydrogen and oxygen as shown in Equation 6 (*36*). Silica fume is usually added to MK or FA to modify Si/Al ratio in GPs. The chemical reactions for both processes are as follows:

$$2SiO + O_2 \rightarrow 2SiO_2 \qquad\qquad\qquad\qquad\qquad\qquad\qquad [5]$$

$$2H_2 + O_2 + SiCl_4 \rightarrow SiO_2 + 4HCl \qquad\qquad\qquad\qquad\qquad [6]$$

3.6 Engineered Geopolymer Composites (EGCs)

The first efforts to develop ECCs utilizing geopolymer (GP) binders were reported in 2014 by Ohno and Li (*25*). In the literature, GP-based ECCs are referred to as Engineered Geopolymer Composites (EGCs). Since then, scientists around the world began extensively studying these emerging composites including their processing, curing, mechanical properties, microstructure,

etc. To date, EGCs using mainly fly ash as precursor for GP binders have been studied (*2*, *4*, *16*, *18*, *19*, *54*). However, combinations of fly ash and ground granulated blast-furnace slag (GGBS) (*4*, *14*), as well as a combination of fly ash and metakaolin (*18*, *19*) have also been evaluated. Recently, a few studies have also investigated the use of pure metakaolin binders for the manufacture of EGCs (*55*, *56*). To date, the alkaline activators studied by researchers include water glass solutions of potassium or sodium hydroxide pellets and silica fume dissolved in DI water (*55*, *56*), solutions of commercially-available aqueous sodium silicate (Na_2SiO_3) and sodium hydroxide (NaOH) pellets (*2*, *18*, *19*), aqueous 8 M NaOH and Na_2SiO_3 (*16*, *54*, *57*), aqueous 8 M KOH and potassium silicate (K_2SiO_3) (*16*), and anhydrous sodium metasilicate powder (*4*). These studies show that the most important factors affecting the strength of the EGCs are aluminosilicate source, SiO_2/Al_2O_3 ratio in GP binder composition, water to solids ratio used during synthesis, type and amount of alkali activator, mixing and curing conditions, etc. (*18*, *19*, *54*, *58*). The sand used to make EGC is microsilica sand at 0, 14.5, 20, 30, 40, 50, and 80 wt% (*2*, *4*, *18*, *19*, *54–56*).

The fibers studied to produce EGCs with ductile PSH capabilities include 1.2 wt% oil coated and uncoated PVA (*2*, *3*, *18*, *19*, *54–57*), UHMWPE (*4*, *55*), and copper coated steel fibers (*4*). PVA fibers ranging from 1- 2 vol.% were used to increase the compressive, tensile, and flexural strengths (*2–4*, *18*, *19*, *54–57*). After conducting compression and uniaxial tensile tests, Ohno and Li concluded that 1.5 vol.% was the optimum PVA fiber content balancing material sustainability indices (MSI) and compressive and tensile properties (*2*). Kan et al. further studied fly ash based PVA-EGCs using metakaolin as partial fly ash replacement (at 0, 0.8, 1.6 wt.%) and PVA fiber at 1.50, 1.65, and 1.8 vol.%. It was concluded that 1.5 vol.% PVA with 1.6 wt.% metakaolin cured at 80°C was the optimum composition due to its high compressive and tensile properties (*18*, *19*).

It is important to mention that two types of curing methods were observed: heat curing (*2–4*, *18*, *19*, *54*, *57*) and room temperature curing (*4*, *55*, *56*). To perform heat curing, several researchers kept the specimens in the mold for 24 hours, the demolded specimens were placed in an oven for 24 hours at 60 °C, and then placed in room temperature 20±1°C and 70±5% relative humidity until the day of testing (*2–4*, *54*, *57*). Kan et al., 2020 observed a different heat curing method where the specimens were placed in an oven for 2h at 60, 70, and 80°C before being placed in room temperature. It was concluded that heat curing the specimens at 80°C produced the most ductile composite with a tensile strain capacity of 5.2% and tensile strength of 3.8 MPa. To perform room temperature curing, Alrefaei & Dai cured the EGC specimens by placing a wet burlap and plastic sheets for 24 h to prevent plastic shrinkage cracks and submerging the specimens in a water tank until testing day (*4*). On the other hand, Trindade et al. kept the samples exposed to the atmosphere at room temperature for 48 hours and then placed them in plastic bags until testing day (*55*, *56*).

4. METHODOLOGY

4.1 Materials

4.1.1 Activator Solution

In this study all activator solutions were prepared using a mixture of sodium hydroxide pellets with 99% purity (Noah Technologies, TX) or potassium hydroxide flakes with 99.9% purity (Noah Technologies, Tx), amorphous fumed silicon (IV) oxide (Alfa Aesar, MA), and deionized water were used.

To produce the activator solutions, a beaker and a magnetic stirrer were used. First, deionized (DI) water is added. Next, the amount of hydroxide needed to make the solution is added in fifths to prevent overheating from the exothermic reaction during the dissolution of the hydroxide. Between each addition, the beaker must be clear and warm or cold to the touch. For solutions implementing silica fume, once all the hydroxide is dissolved, the silica fume is added in the beaker. Subsequently, the solution is stirred to dissolve the silica fume. Finally, the solution (Figure 3) remains on the magnetic stirrer for 24 hours before being filtered into a glass storage container. It is important to note that the beaker is continuously sealed during the solution manufacturing process by means of a plastic sheet to prevent water evaporation and reaction with ambient CO_2.

Figure 3. Activator solution.

4.1.2 Geopolymer Precursors

The precursors used to manufacture MK-based and MFA-based geopolymer binder, mortars, and EGCs were metakaolin (MetaMax, BASF) and Class F fly ash. The oxide composition of these precursors was determined using a PANalytical Epsilon 3XLE X-ray Fluorescence Spectroscopy (XRF). The powdered samples (0.6 g) were fused with a mix of Li-tetraborate, Li-metaborate and Li-iodide (total mass of 6 g) in a Clarisse LENeo fluxer to glass beads. The beads were analyzed using the Omnian programme of the Epsilon 3 software. Per ASTM D7348-13, the loss on ignition (LOI) values were calculated using the weight difference of the dry samples (before fusion) and the glass beads (*59*). The oxide composition and loss of ignition (LOI) of each material is listed in Table 1. Per XRF, the metakaolin used in this study was mainly composed of SiO_2 and Al_2O_3, with contents of 51.04 and 46.70% (atomic %), respectively. Similarly, fly ash was composed of 51.88% SiO_2 and 17.78% Al_2O_3 along with 5.45% CaO. Furthermore, the loss on ignition (LOI) of metakaolin and fly ash were 0.64% and 0.77%, respectively.

To determine the particle size distribution of the fly ash GP precursor, a Beckman LS200 Laser Diffraction Particle Size Analyzer was used. The analysis was performed in a micro-volume module where the sample was suspended in water and agitated for 60 seconds. Figure 4 presents the particle size distribution, mean particle size, and maximum nominal particle size of the fly ash. It can be observed that the fly ash particles are small, and exhibit mean particle size of 17.71 μm. Finally, the morphological details of the metakaolin and fly ash particles are presented in Figure 5a and b, respectively, per SEM micrographs at a voltage of 20 kV, a current of 4 nA, and a 1000x magnification.

Table 1. XRF oxide composition.

Chemical	Concentration wt%									
	Na_2O	MgO	Al_2O_3	SiO_2	P_2O_5	SO_3	K_2O	CaO	TiO_2	Fe_2O_3
Metakaolin	0.05	0.00	46.70	51.04	0.02	0.03	0.08	0.02	1.53	0.38
Fly Ash	0.92	1.28	17.78	51.88	0.32	1.02	2.46	5.45	0.79	10.83

4.1.3 Fine Aggregates

For the evaluation of pure GP binder and GP mortar, standard Ottawa testing sand (Humboldt Mfg Co., Elgin, IL) that follows ASTM C778 is used. For the evaluation of EGC, two types of sand were utilized: locally available river sand (RS) and microsilica sand (MS) (U.S. Silica Company, Ottawa, IL). The specific gravity of the RS and MS were evaluated per ASTM C128-15 (*60*) to be 2.62 and 2.65, respectively. The particle size distribution of both sands presented in Figure 4 was also determined using the Beckman LS200 Laser Diffraction Particle Size Analyzer. Furthermore, the mean particle size and maximum particle size of both sands are also shown in Table 2. As shown in Figure 4 and Table 2, RS consists of coarser particles than MS. Moreover, SEM images presenting the morphological details of RS and MS are shown in Figure 5c and d, respectively. It can be seen that MS has a highly angular particle shape in contrast to the more rounded shape of RS particles.

Table 2. Mean and maximum nominal particle size.

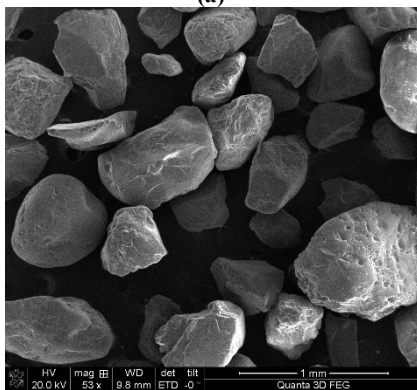| Material Properties	River Sand	Microsilica Sand	Fly Ash
Mean Particle Size (μm)	474.63	15.20	17.71
Maximum Particle Size (μm)	1377.20	146.82	309.64
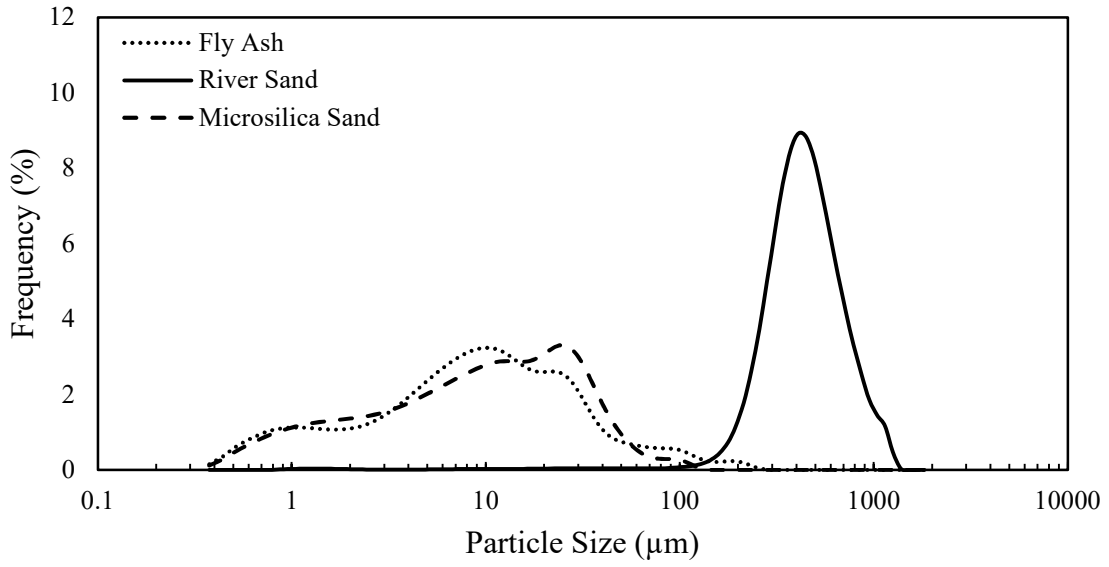
Figure 4. Particle Size distribution of fly ash, river sand, and microsilica sand.

(a)

(b)

(c)

(d)

11
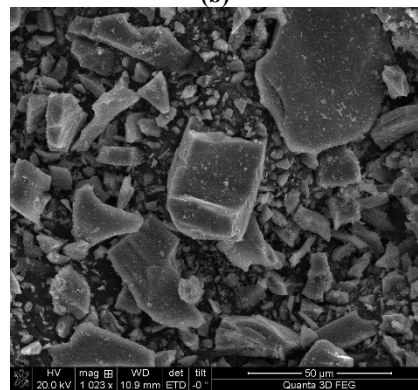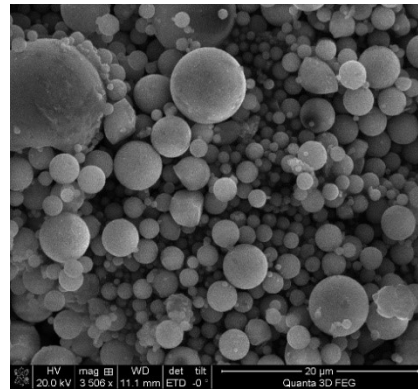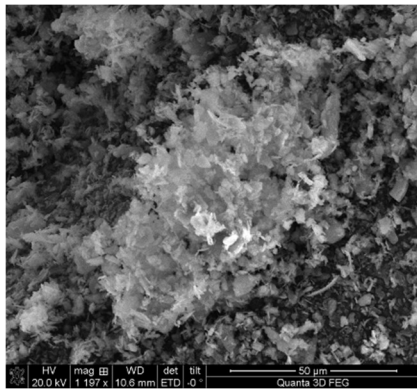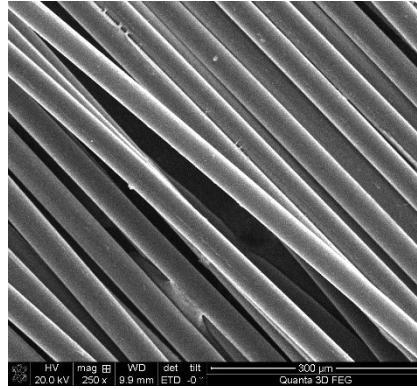
(e)

Figure 5. Secondary electron SEM images of: (a) metakaolin, (b) fly ash (c) silica sand, (d) microsilica sand, (e) PVA fiber.

4.1.4 Fibers

The fiber used in this study was non-oil-coated RECS15 Polyvinyl Alcohol (PVA) fibers (Nycon, US). The PVA fiber properties provided by the manufacturer are shown in Table 3. Furthermore, an SEM image presenting the morphology of the PVA fiber is shown in Figure 5e.

Table 3. Fiber properties.

Fiber Type	Diameter (μm)	Length (mm)	Elongation (%)	Specific Gravity	Modulus of Elasticity (GPa)	Strength (MPa)
PVA	38	8	6	1.3	41	1600

4.1.5 Ingredients for GP Feasibility Study in Ecuador

Parallel to the main work conducted in this study, an investigation of the feasibility of the usage of zeolite-rich tuff, metakaolin, and volcanic ashes as solid precursors in the elaboration of GP matrices for the development of EGC was conducted in Ecuador by ESPOL University. The ingredients used for this part of the study were selected due to its readily availability all over Ecuador.

The zeolite tuff was received from ZEONATEC that previously milled up to passing N 325 mesh. Volcanic ash was collected from Riobamba close to Chimborazo volcano, and kaolinite, from La Joya at the rain forest of Ecuador. The tuff and volcanic ashes were firstly dried at 100°C using an oven for 24 h. Afterwards, the dried volcanic ash was grounded using a roll crusher and a disk miller up to pass a sieve N 325 mesh.

The geopolymer mortars were prepared using a mixture of zeolite tuff, volcanic ashes and metakaolin, and river sand collected from the banks of the Chimbo River. This sand was carefully obtained to avoid impurities and washed its use in geopolymer mortar preparation. Besides, the sand was dried at 80°C for 24h, then sieved by ASTM mesh between No. 30 and 40. XRD was used to elaborate the mineralogical composition of the sand, and the results are as follows: anorthite (~0.2%), albite (~74 %), quartz (~11%), amorphous content (~4%).

Chemical reagents used for GP synthesis were NaOH (Merck) and $Na_4Si_5O_{12}$ (Sigma Aldrich). The molar concentration of NaOH solution (SH) was of 8 M. Sodium silicate solution (SS) with SiO_2/Na_2O ratio of 2.4 was used to prepare solutions with $Na_4Si_5O_{12}/NaOH$ ratio of 3, at least 24h

prior to use. To synthesize the geopolymers, a liquid to solid ratio of 0.5 and curing temperature of 60°C for 24 h were applied.

4.2 Mixture Proportions and Mixing

4.2.1 Task I: GP Binder and Mortar Development for EGC Application

As mentioned above, GP can be defined as the combination of 4 chemical parameters, therefore, the number of possible combinations is endless. Every composition was also evaluated separately as pure binder and mortar at the standard sand to binder ratio of 2.75:1 according to ASTM C109. The samples were demolded after 7 days, then left in a sealed environment for another 7 days, and then left to dry under ambient laboratory condition for another 14 days for a total of 28 days before testing.

The GP compositions developed were labeled as KXYZ or NaXYZ, where the first letter denotes potassium (K) or sodium (Na), while X, Y, and Z are numbers that denote the molar ratios of SiO_2/Al_2O_3, water to solids (W/S), and K_2O/Al_2O_3 or Na_2O/Al_2O_3, respectively (*47*). The comprehensive list of compositions can be found in

Table 4. It can be noted that all the compositions have an alkali/Al ratio of 1 since that is the minimum stoichiometric molar ratio to charge balance the GP.

Table 4. Preliminary MK GP and mortar mixture proportions (units in kg/m^3)

Binder Type	Mix ID	Mix Type	SiO_2/Al_2O_3 (molar ratio)	$H_2O/(SiO_2+Al_2O_3)$ (molar ratio)	Cation/Al_2O_3 (molar ratio)	Sand/Binder (mass ratio)
Na241	1p	GP	2	4	1	2.75
Na241	1m	GP-RS	2	4	1	2.75
Na251	2p	GP	2	5	1	2.75
Na251	2m	GP-RS	2	5	1	2.75
Na(2.5)31	3p	GP	2.5	3	1	2.75
Na(2.5)31	3m	GP-RS	2.5	3	1	2.75
Na(2.5)41	4p	GP	2.5	4	1	2.75
Na(2.5)41	4m	GP-RS	2.5	4	1	2.75
Na3(2.5)1	5p	GP	3	2.5	1	2.75
Na3(2.5)1	5m	GP-RS	3	2.5	1	2.75
Na331	6p	GP	3	3	1	2.75
Na331	6m	GP-RS	3	3	1	2.75
Na421	7p	GP	4	2	1	2.75
Na421	7m	GP-RS	4	2	1	2.75
Na431	8p	GP	4	3	1	2.75
Na431	8m	GP-RS	4	3	1	2.75
K231	9p	GP	2	3	1	2.75
K231	9m	GP-RS	2	3	1	2.75
K241	10p	GP	2	4	1	2.75
K241	10m	GP-RS	2	4	1	2.75
K(2.5)21	11p	GP	2.5	2	1	2.75

	11m	GP-RS		
K(2.5)31	12p	GP		3
	12m	GP-RS		
K321	13p	GP	3	2
	13m	GP-RS		
K331	14p	GP		3
	14m	GP-RS		
K4(1.5)1	15p	GP		1.5
	15m	GP-RS	4	
K421	16p	GP		2
	16m	GP-RS		

The manufacture of MK-based specimens for water loss measurement, shrinkage measurement, density measurement, and compressive strength test was conducted using a VPM2 Vacuum Shear Mixer (Whip Mix, KY), shown in Figure 6a. The manufacturing procedure started by mixing the metakaolin with the activator solution for 180 seconds at 200 rpm to produce GP binder. After the initial mixing, the GP binder was further mixed at speeds of 300 and 400 rpm for 180 seconds each (for a total of 360 seconds) (48). In the case of GP mortar manufacturing, after the completion of the GP binder mixing process, sand was added and mixed at 200 rpm for 180 seconds. The mixing procedure is summarized in Figure 6. For the development of pure GP binder and GP mortar, 1 in. diameter by 1 in. height molds are used to make 12 duplicates for each composition, where 10 are for compressive strength, 1 for density measurement, and 1 for SEM for a total of 384 samples.
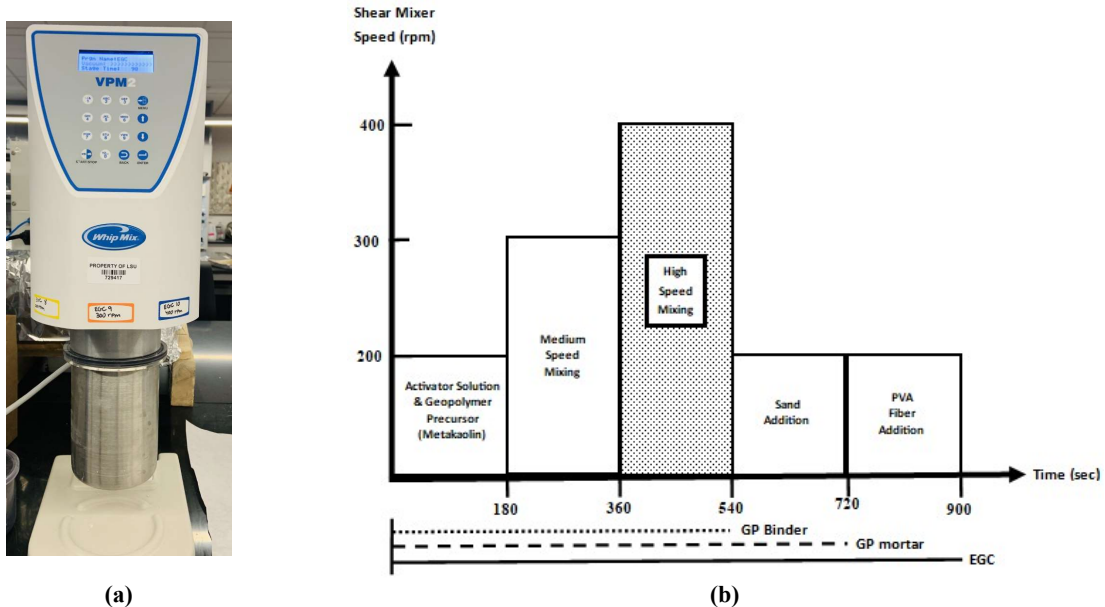

Figure 6. Geopolymer manufacturing: (a) vacuum shear mixer and (b) mixing procedure.

4.2.2 Task II: EGC Performance Evaluation and Composite Optimization

For the formulation of EGCs, three types of MK-based GP binder (i.e., K321, K331, and Na431) and one type of MKFA-based GP binder (i.e., K321), two sand types (i.e., RS and MS), and three

14

different levels of PVA fiber content were evaluated (i.e., 0.8-1.7% volume fraction). It is important to mention that the three GP binders used were selected based on the GP binder and mortar work described in section 4.2.1, where these compositions exhibited satisfactory workability and strength characteristics. However, the MKFA-based GP binder composition was selected based on the optimum MK-based composition. In total, 36 different GP materials were manufactured, including pure GP binders, GP mortars, and fiber-reinforced GP mortars (i.e., EGCs). Table 5 and

Binder Type	Mix #	Type of Mix	SiO_2/Al_2O_3	$H_2O/(SiO_2+Al_2O_3)$	Cation/Al_2O_3	Sand/Binder (wt.%)	Fiber (vol.%)
K321	1	GP	3	2	1	0.36	0
	2	GP-RS					0
	3	GP-MS					0
	4	GP-RS-0.8%PVA					0.8
	5	GP-RS-1.2%PVA					1.2
	6	GP-RS-1.6%PVA					1.6
	7	GP-MS-0.8%PVA					0.8
	8	GP-MS-1.2%PVA					1.2
	9	GP-MS-1.6%PVA					1.6
K331	10	GP		3			0
	11	GP-RS					0
	12	GP-MS					0
	13	GP-RS-0.9%PVA					0.9
	14	GP-RS-1.3%PVA					1.3
	15	GP-RS-1.7%PVA					1.7
	16	GP-MS-0.9%PVA					0.9
	17	GP-MS-1.3%PVA					1.3
	18	GP-MS-1.7%PVA					1.7
Na431	19	GP	4				0
	20	GP-RS					0
	21	GP-MS					0
	22	GP-RS-0.8%PVA					0.8
	23	GP-RS-1.2%PVA					1.2
	24	GP-RS-1.5%PVA					1.5
	25	GP-MS-0.8%PVA					0.8
	26	GP-MS-1.2%PVA					1.2
	27	GP-MS-1.5%PVA					1.5

Table 6 present the experimental matrix mixture proportions in molar ratio for all the GP materials produced in this study, excepting sand to binder ratio in wt% and fiber dosage in volume fraction. While the compressive strength of GP binders and mortars was evaluated in the work described in section 4.2.1, these tests were repeated for comparative purposes given that EGC materials were evaluated on larger sized specimens (i.e., 2-inch cube specimens). As shown in Table 5, the MK-based GP binder consists of a mixture of the GP precursor (i.e., metakaolin) and the activator solution (i.e., a combination of SiO_2, MOH, and H_2O). On the other hand, as shown in

Binder Type	Mix #	Type of Mix	SiO₂/Al₂O₃	H₂O/(SiO₂+Al₂O₃)	Cation/Al₂O₃	Sand/Binder (wt.%)	Fiber (vol.%)
K321	1	GP	3	2			0
	2	GP-RS					0
	3	GP-MS					0
	4	GP-RS-0.8%PVA					0.8
	5	GP-RS-1.2%PVA					1.2
	6	GP-RS-1.6%PVA					1.6
	7	GP-MS-0.8%PVA					0.8
	8	GP-MS-1.2%PVA					1.2
	9	GP-MS-1.6%PVA					1.6
K331	10	GP		3	1	0.36	0
	11	GP-RS					0
	12	GP-MS					0
	13	GP-RS-0.9%PVA					0.9
	14	GP-RS-1.3%PVA					1.3
	15	GP-RS-1.7%PVA					1.7
	16	GP-MS-0.9%PVA					0.9
	17	GP-MS-1.3%PVA					1.3
	18	GP-MS-1.7%PVA					1.7
Na431	19	GP	4				0
	20	GP-RS					0
	21	GP-MS					0
	22	GP-RS-0.8%PVA					0.8
	23	GP-RS-1.2%PVA					1.2
	24	GP-RS-1.5%PVA					1.5
	25	GP-MS-0.8%PVA					0.8
	26	GP-MS-1.2%PVA					1.2
	27	GP-MS-1.5%PVA					1.5

Table 6, MKFA-based GP binders consisted of a mixture of two GP precursors (i.e., metakaolin and fly ash) and a pure hydroxide solution as the activator solution. For all mixtures GP mortars and fiber-reinforced GP mortars (i.e., EGCs), the sand to GP solids ratio was maintained constant at 0.36.

Table 5. MK GP mixture proportions (molar ratio).

Binder Type	Mix #	Type of Mix	SiO₂/Al₂O₃	H₂O/(SiO₂+Al₂O₃)	Cation/Al₂O₃	Sand/Binder (wt.%)	Fiber (vol.%)
K321	1	GP	3	2	1	0.36	0
	2	GP-RS					0
	3	GP-MS					0
	4	GP-RS-0.8%PVA					0.8
	5	GP-RS-1.2%PVA					1.2
	6	GP-RS-1.6%PVA					1.6
	7	GP-MS-0.8%PVA					0.8
	8	GP-MS-1.2%PVA					1.2

Binder Type	Mix #	Type of Mix	SiO₂/Al₂O₃	H₂O/(SiO₂+Al₂O₃)	Cation/Al₂O₃	Sand/Binder (wt.%)	Fiber (vol.%)
	9	GP-MS-1.6%PVA					1.6
	10	GP					0
	11	GP-RS					0
	12	GP-MS					0
	13	GP-RS-0.9%PVA					0.9
K331	14	GP-RS-1.3%PVA					1.3
	15	GP-RS-1.7%PVA					1.7
	16	GP-MS-0.9%PVA	3				0.9
	17	GP-MS-1.3%PVA					1.3
	18	GP-MS-1.7%PVA					1.7
	19	GP					0
	20	GP-RS					0
	21	GP-MS					0
	22	GP-RS-0.8%PVA					0.8
Na431	23	GP-RS-1.2%PVA	4				1.2
	24	GP-RS-1.5%PVA					1.5
	25	GP-MS-0.8%PVA					0.8
	26	GP-MS-1.2%PVA					1.2
	27	GP-MS-1.5%PVA					1.5

Table 6. MKFA GP mixture proportions (molar ratio).

Binder Type	Mix #	Type of Mix	SiO₂/Al₂O₃	H₂O/(SiO₂+Al₂O₃)	Cation/Al₂O₃	Sand/Binder (wt.%)	Fiber (vol.%)
	28	MFA					0
	29	MFA-RS					0
	30	MFA-MS					0
	31	MFA-RS-0.8%PVA					0.8
MKFA K321	32	MFA-RS-1.2%PVA	3	2	1	0.36	1.2
	33	MFA-RS-1.6%PVA					1.6
	34	MFA-MS-0.8%PVA					0.8
	35	MFA-MS-1.2%PVA					1.2
	36	MFA-MS-1.6%PVA					1.6

4.2.2.1 Manufacturing of MK Based GP Materials

The manufacturing procedure for MK-based GP binders and mortars evaluated in this stage of the study was the same described in section 4.2.1. and summarized in Figure 6b. In the case of GP mortars containing fibers (i.e., EGCs), fibers were added to the material upon completion of the mortar mixing procedure and preliminary dispersed using a steel spatula. Subsequently, the fibers and the GP mortars were mixed for an additional 180 seconds at 200 rpm as illustrated in Figure 6b. Upon completion of the preparation of the different GP materials, the mixtures were casted into cube molds to prepare specimens for compressive strength test. Furthermore, dog-bone shaped specimens were also cast for uniaxial tensile test evaluation; yet, only for EGC materials were prepared for this test. Immediately after casting, all specimens were placed inside sealed plastic bags to prevent moisture loss as shown in Figure 7a. Cube specimens were demolded within 24

hours; yet, dog-bone specimens were demolded after 48 hours. This was the case since dog-bone specimens are thin and prone to cracking at early stages of curing; therefore, additional time was given to these specimens to allow for strength gain prior to demolding. Right after demolding, specimens were placed back in sealed plastic bags and were allowed to cure under ambient laboratory conditions (i.e., 22±1°C) until their respective testing date (as shown in Figure 7b).

To produce EGC specimens for third-point bending test (i.e., flexural test), a tabletop planetary mixer was used for mixing. This was the case since large volumes of material were required; and therefore, the capacity of the VPM2 Vacuum Shear Mixer was not sufficient. It was observed that the tabletop planetary mixture enhanced the homogeneity of the mixture resulting in better fiber distribution. As such, the uniaxial tensile specimens previously cast using the VPM2 Vacuum Shear Mixer were repeated using the tabletop mixer to evaluate the effect of mixing procedure on composite performance. To manufacture the EGC specimens using the tabletop planetary mixer, the metakaolin was added in small proportions with the activator solution and mixed for 180 seconds at level 2 (i.e., 82 rpm) to produce GP binder. After completion of the GP binder mixing, the sand was added slowly within 60 seconds and allowed to mix for an extra 120 seconds at level 2. Finally, the fibers were added slowly within a 60 second interval at stir (i.e., 60 rpm). Once the fibers were added, they are further mixed at level 2 for 120 seconds and then at level 4 (i.e., 125 rpm) until homogeneity was achieved. Upon completion of the EGC preparation, dog-bone and beam specimens were cast. Dog-bone and beam specimens were cured inside sealed plastic bags and demolded after 48 and 72 hours, respectively. Subsequently, specimens were placed back in sealed plastic bags until testing.

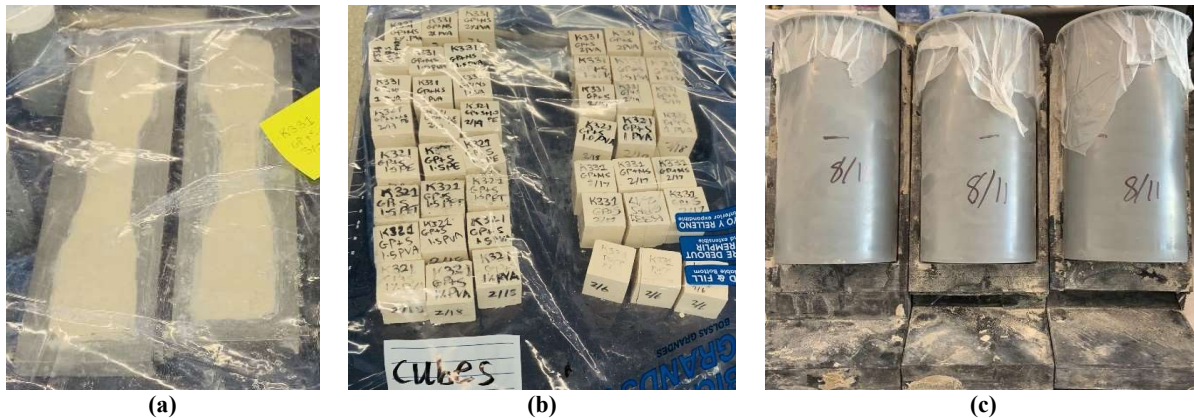| (a) | (b) | (c) |

Figure 7. Casting and curing of GP materials: (a) dog-bone specimens after casting, (b) cube specimens during curing, and (c) slant shear test setup.

4.2.2.2 Manufacturing of MKFA Based GP Materials

The manufacturing of MKFA specimens for compressive strength test, uniaxial tensile test, and third-point bending test was conducted using the tabletop planetary mixer. The manufacturing procedure started by mixing the precursor in small proportions with the activator solution adding fly ash prior to the metakaolin. Once the precursors were added, they were mixed for 180 seconds at 82 rpm (i.e., level 2) to produce MKFA GP binder. To produce MKFA mortars, sand was slowly added within 60 seconds and allowed to mix for an extra 120 seconds at level 2. Finally, to produce MKFA EGCs, the fibers were slowly added within a 60 second interval at stir (i.e., 60 rpm). Once all fibers were added, they were further mixed at level 2 for 120 seconds and then at level 4 (i.e., 125 rpm) until homogeneity was achieved.

Upon completion of the preparation of the different MKFA GP materials, the mixtures were casted into cube, dog-bone, and beam molds to prepare specimens for compressive strength test, uniaxial tensile test, and third-point bending test, respectively. After casting, specimens were placed inside sealed plastic bags to prevent moisture loss. All MKFA specimens were demolded after 72 hours. This was the case since the specimens were relatively weak in comparison to the MK GP materials; and therefore, additional time was given to allow for strength gain prior to demolding. Right after demolding, specimens were placed back in sealed plastic bags for an additional 4 days. The specimens were then allowed to air cure until their respective testing date under ambient laboratory conditions (i.e., 22±1°C).

4.2.3 GP Feasibility Study in Ecuador

Geopolymer is a mixture of varied components being adjusted to meet technical requirements. This adjustment must be done statistically to assure robustness in design. In this study simplex experimental design of three-component mixture was used to explore the possibility of usage three different solid precursors, i.e., mordenite-rich tuff, metakaolin and volcanic ashes as a ternary mixture. All remaining synthesis parameters were kept constant during the experiment.

Table 7 GP mixture proportions by mass

Mix ID	Zeolite (x1)	Volcanic Ash (x2)	Metakaolin (x3)
C1	0.6	0.2	0.2
C2	0.7	0.2	0.1
C3	0.7	0.1	0.2
C4	0.7	0.15	0.15
C5	0.75	0	0.25
C6	0.5	0.25	0.25
C7	0.75	0.25	0

4.3 Experimental Testing

4.3.1 Task I: GP Binder and Mortar Development for EGC Application

4.3.1.1 Water Loss, Shrinkage, and Density Measurement

Weight measurements are taken weekly to calculate the water loss during the curing process. After curing, the samples' dimension is taken with a caliper and the shrinkage is calculated using the average of 3 measurements on the same sample. The density and of the samples were measured using Archimedes' method according to ASTM C830-00. Density and was calculated using following equation:

$$\rho = \frac{m_{dry} * \rho_{ethanol}}{m_{wet} - m_{suspended} + m_{wire}} \qquad [7]$$

where ρ is measured density (g/cm^3), m_{dry} is dry mass (g), $\rho_{ethanol}$ is density of ethanol (g/cm^3), m_{wet} is mass of sample with ethanol occupying the open pores (g), $m_{suspended}$ is mass of sample while suspended in ethanol (g), and m_{wire} is mass of the part of Archimedes' set up that's used to suspend sample in ethanol (g).

4.3.1.2 Compressive Strength Test

The compressive strength of the pure GP binder and GP mortar were evaluated with an 810 Materials Testing System (MTS System Corporation, MN) with a constant displacement rate of 0.60 mm/minute.

4.3.1.3 Scanning Electron Microscopy (SEM)

To get a better understanding of the difference between the compositions, SEM was conduct on selected samples to gain some insight from a morphological perspective. The samples are sputter coated with 5 nm of platinum-palladium alloy to avoid charge build up. SEM analyses of the samples were conducted with the JEOL JSM-7500F (JEOL USA Inc, MA) FE-SEM to study the microstructure of the samples under back-scattered imaging.

4.3.2 Task II: EGC Performance Evaluation and Composite Optimization

4.3.2.1 Compressive Strength Test and Density

The compressive strength of all the GP mixtures prepared in this phase of the project were evaluated according to ASTM C109 on 2-inch cube specimens after 28±1 days of curing (*61*). Three specimens were prepared and tested for each material listed in Table 5 and a minimum of two specimens were prepared for mixtures presented in

Binder Type	Mix #	Type of Mix	SiO$_2$/Al$_2$O$_3$	H$_2$O/(SiO$_2$+Al$_2$O$_3$)	Cation/Al$_2$O$_3$	Sand/Binder (wt.%)	Fiber (vol.%)
K321	1	GP	3	2	1	0.36	0
	2	GP-RS					0
	3	GP-MS					0
	4	GP-RS-0.8%PVA					0.8
	5	GP-RS-1.2%PVA					1.2
	6	GP-RS-1.6%PVA					1.6
	7	GP-MS-0.8%PVA					0.8
	8	GP-MS-1.2%PVA					1.2
	9	GP-MS-1.6%PVA					1.6
K331	10	GP		3			0
	11	GP-RS					0
	12	GP-MS					0
	13	GP-RS-0.9%PVA					0.9
	14	GP-RS-1.3%PVA					1.3
	15	GP-RS-1.7%PVA					1.7
	16	GP-MS-0.9%PVA					0.9
	17	GP-MS-1.3%PVA					1.3
	18	GP-MS-1.7%PVA					1.7
Na431	19	GP	4				0
	20	GP-RS					0

	21	GP-MS					0
	22	GP-RS-0.8%PVA					0.8
	23	GP-RS-1.2%PVA					1.2
	24	GP-RS-1.5%PVA					1.5
	25	GP-MS-0.8%PVA					0.8
	26	GP-MS-1.2%PVA					1.2
	27	GP-MS-1.5%PVA					1.5

Table 6. The experimental tests were performed by applying pressure with a constant loading rate of 1800 N/sec. The experimental setup is shown in Figure 8 during the evaluation of an EGC cube specimen.

Figure 8. Compressive strength test experimental setup.

4.3.2.2 Uniaxial Tensile Test

The tensile properties of the different GP mixtures were evaluated by conducting a uniaxial tensile test according to recommendations of the Japan Society of Civil Engineers (JSCE) (*62*). Three dog-bone shaped specimens (Figure 9a) were tested after 28±1 days of curing for each selected material. The uniaxial tensile test was conducted using a deformation-controlled loading rate of 0.5 mm/min. Two linear variable displacement transducers (LVDTs) attached to each side of the specimen as shown in Figure 9b recorded the deformation of the specimens in the testing area.
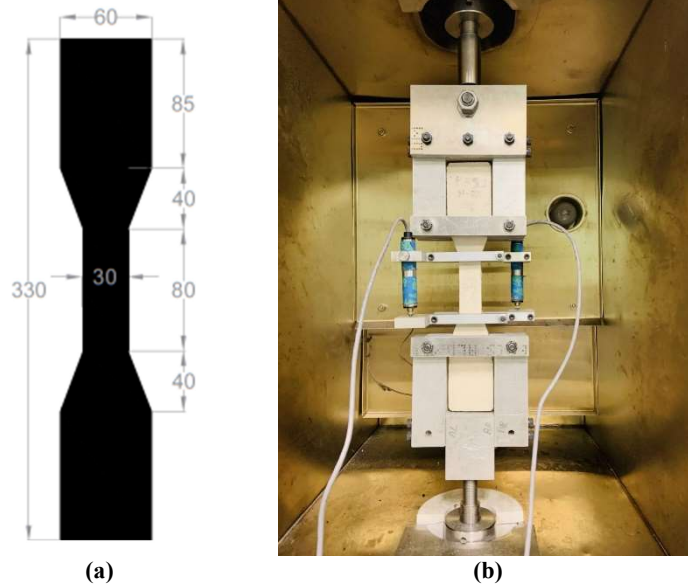
Figure 9. Uniaxial tensile test setup: (a) dog-bone specimen dimensions (in mm) and (b) uniaxial tensile test.

4.3.2.3 Third-Point Bending Test

A third-point bending testing procedure similar to ASTM C 1609 (Flexural Performance of Fiber-Reinforced Concrete) was conducted by utilizing a closed-loop, servo-controlled hydraulic universal testing system to assess flexural strength and deformation capacity of EGC mixtures (*63*). Three beam specimens with the following dimensions: 38 x 76 x 330 mm (1.5 x 3 x 13 in.) were cast for the materials selected for testing. The load was applied at a rate of 0.5 mm/min. The span length of the beam was 300 mm with a center span length of 100 mm, where loading was applied. The beam net deflection and load were recorded on an automated information recording system during the third point bending test. Figure 10 shows the dimensions of the EGC beam specimens (Figure 10a) and third point bending test setup (Figure 10b). Two linear variable displacement transducers (LVDTs) were attached to the testing setup to measure the flexural deflection of the EGC specimens.
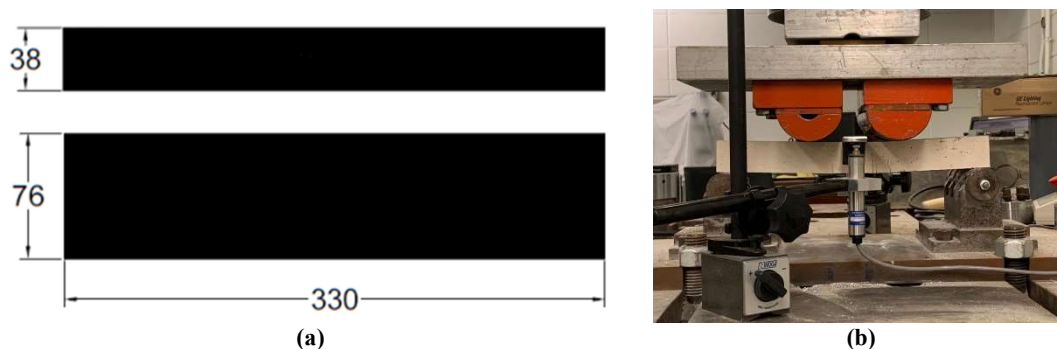
Figure 10. Flexural performance test setup: (a) beam specimen dimensions (in mm) and (b) flexural test setup.

4.3.2.4 Slant Shear Test

For the repair of concrete structures, the bond strength of the repair material with the concrete substrate is one of the most important characteristics. To this end, slant shear test similar to ASTM C882 was conducted on a 101.6 by 203.2 mm (4 by 8 inch) cylinders with LADOTD Type D Portland Cement concrete (PCC) pavement mixture as the bottom half layer at a 30 degree angle

from the horizontal and the EGC material as the top layer. To manufacture the PCC, all the dry components (i.e., coarse aggregate, cement, and concrete sand) were hand mixed in a pan until homogeneity was achieved. Afterwards, water and high range water reducer (HRWR) were added, and the concrete was further mixed. Table 8 presents the mixture proportions in kg/m^3 of the PCC material used. Upon completion of the mixing procedure, the PCC was placed in two 4" by 8" cylinders to determine the 28-day compressive strength. Furthermore three 4" by 8" cylinders were filled halfway and slanted at a 30-degree angle to form the substrate. Subsequently, the cylinder molds were covered with a plastic wrap and the concrete substrate was allowed to cure for 28 days prior to the application of the EGC top layer (as shown in Figure 7c). The top EGC layer was manufactured using the mixing procedure described in section 4.2.2 for the tabletop planetary mixer and used to fill the remaining half of the cylinder mold. The concrete/EGC specimen was then sealed with a plastic wrap and allowed to cure for 28 additional days. Upon completion of the curing regime, a compression test was conducted on the three concrete/EGC cylinders where the age of the PCC and GP layers were 56 and 28 days, respectively.

Table 8. Portland cement concrete mixture proportions in (kg/m^3).

Material	Type I Cement	Coarse Aggregate	Concrete Sand	Water
PCC	282	1594	830	114

4.3.2.5 Setting Time
The initial and final setting times of MK-based and MFA-based GP binders and mortars were evaluated per ASTM C191(*64*). The initial setting time is the time passed between the initial contact of the precursor and activator solution and a measured or calculated Vicat needle penetration of 25 mm (*64*). On the other hand, the final setting time is the time passed from the initial contact of the precursor and the activator solution until the Vicat needle no longer leave a complete circular impression on the GP surface (*64*).

4.3.2.6 Crack Width
Upon completion of the uniaxial tensile test, dogbone specimens were analyzed under the light microscope to analyze the residual cracks. A light microscope was utilized to take images of the specimens. The images were digitally analyzed to obtain the number of cracks, maximum crack width, as well as mean and standard deviation of the residual crack width.

4.3.2.7 pH
A safety assessment was conducted to determine the pH of the alkaline activators and GP binder by using a pH meter device. The pH was be measured for three replicate tests for each alkaline activator.

4.3.3 GP Feasibility Study in Ecuador
4.3.3.4 Quantitative X-ray diffraction
The mineralogy of tuff, kaolin, and metakaolin was studied by quantitative X-ray powder diffraction (QXRD). PANanalytical X'pert XRD with KαCu anode tube was used. As detector, X'celerator, a multi position detector was used. The operating conditions were 40 mA and 40 kV, 0.02 of step size. High Score Plus software was used for quantifying the crystalline phases and the amorphous content. For quantification, Rietveld refinement methodology was applied similar to that found in Snellings et al.(*65*).

4.3.3.7 Scanning Electron microscopy (SEM-EDS)

In order to study the morphology and elemental composition of GP precursors, an Inspect FEI SEM was used. The operating parameters at high vacuum mode were 15 kV and 2.0 as spot size. Samples were coated at 18 mA for 120 s with a thin Platinum layer.

4.3.3.8 Compressive strength

Compressive strength tests were carried out in a SHIMADZUUTM-600KN universal testing machine. In this study, 50 mm cube molds were used according to ASTM C109 standard. In addition, three specimens were tested for each composition, thus allowing the calculation of standard deviations and means

5. ANALYSIS AND FINDINGS

5.1 Task I: GP Binder and Mortar Development for EGC Application

5.1.1 Water Loss Measurement

The water loss measurements of pure GP binder are presented below in Figure 11 and Figure 12. The water content that's denoted in the graph is calculated as the weight of water over the weight of the entire sample. It is interesting to note that even though the samples are cured under a closed environment for the first 2 weeks curing, most of the compositions already have lost the majority water with the exceptions of K421 and K(2.5)31, indicating that these compositions have a slower curing kinetics than the other compositions. It can also be pointed out that regardless of the starting water content, all the Na-GP compositions end up with ~10-15wt% of water while all the K-GP compositions end up with ~5-10wt% of water. This is likely because Na ion has a smaller ionic radius than K ion, and therefore has a stronger ionic potential and is able to attract more water molecules.
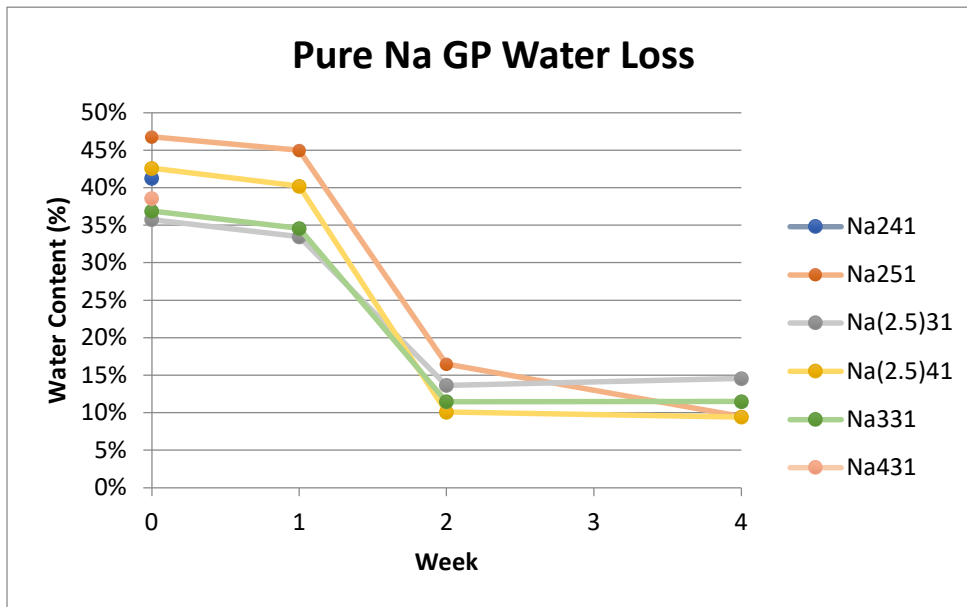
Figure 11. Water loss of pure Na GP binder.
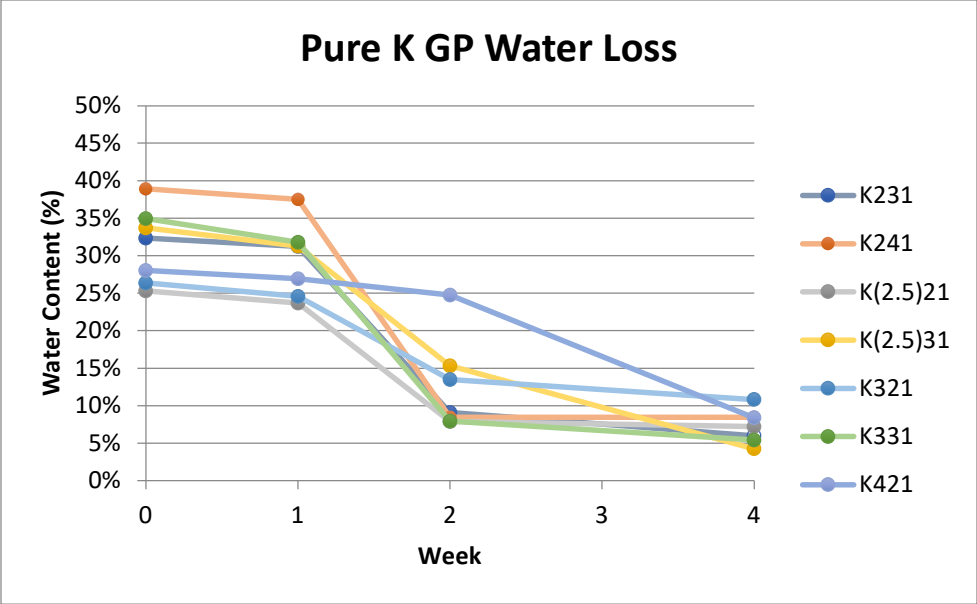
Figure 12. Water loss of pure K GP binder.

Similar to pure GP binders, GP mortars (Figure 13 and Figure 14) also show minimal water loss within the first week, and the majority of water loss between the first and the second week of curing. Na GP mortar seems to all converge to somewhere between 3-4% water content, while K GP mortar seems to converge to between 2-3% water content.
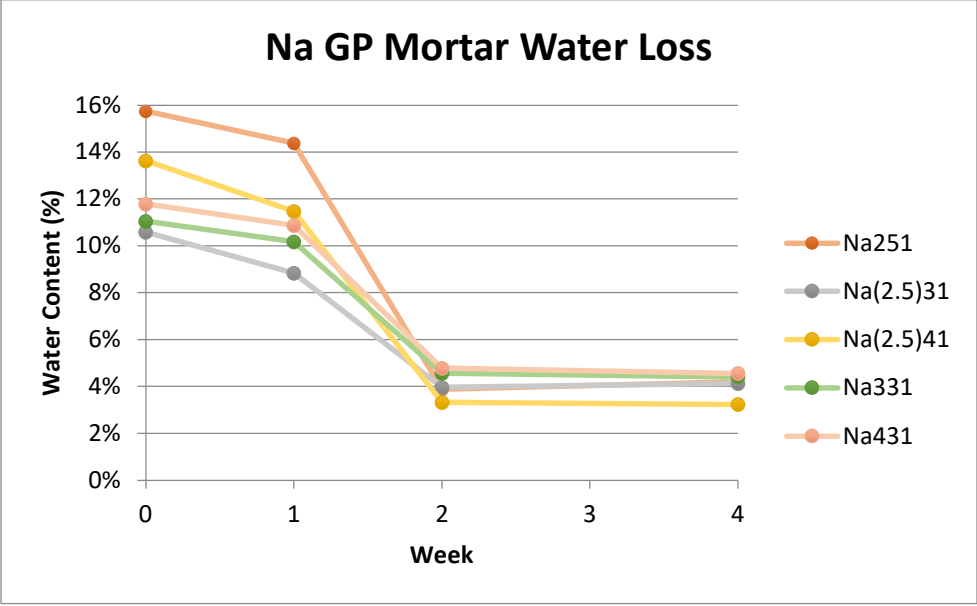
Figure 13. Water loss of Na GP mortar.
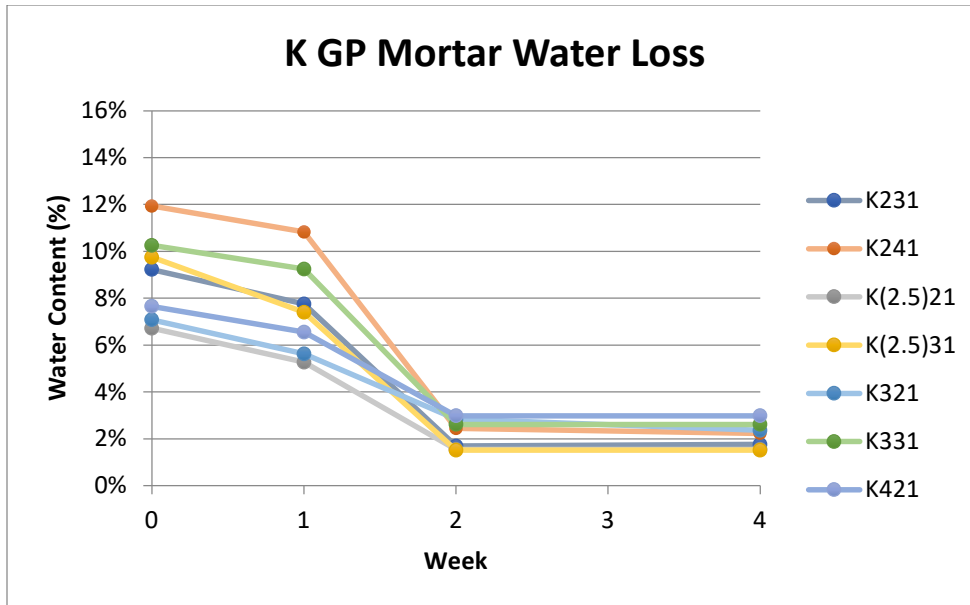
Figure 14. Water loss of K GP mortar.

5.1.2 Density

The results for density measurement of pure GP binder is presented below in Figure 15. The plot is presented as a scatter plot which each point represents a composition, where the legend gives information about the alkali cation and the x-axis gives information about the water/solids molar ratio. For example, a yellow cross with x = 3 would be K331. Overall, the plot demonstrates the trend that as water content increases, the density of the dried GP decreases. This makes sense since the water is first consumed during the geopolymerization process and then released as the process continues, which means the water would eventually leave the structure and create void in the structure.
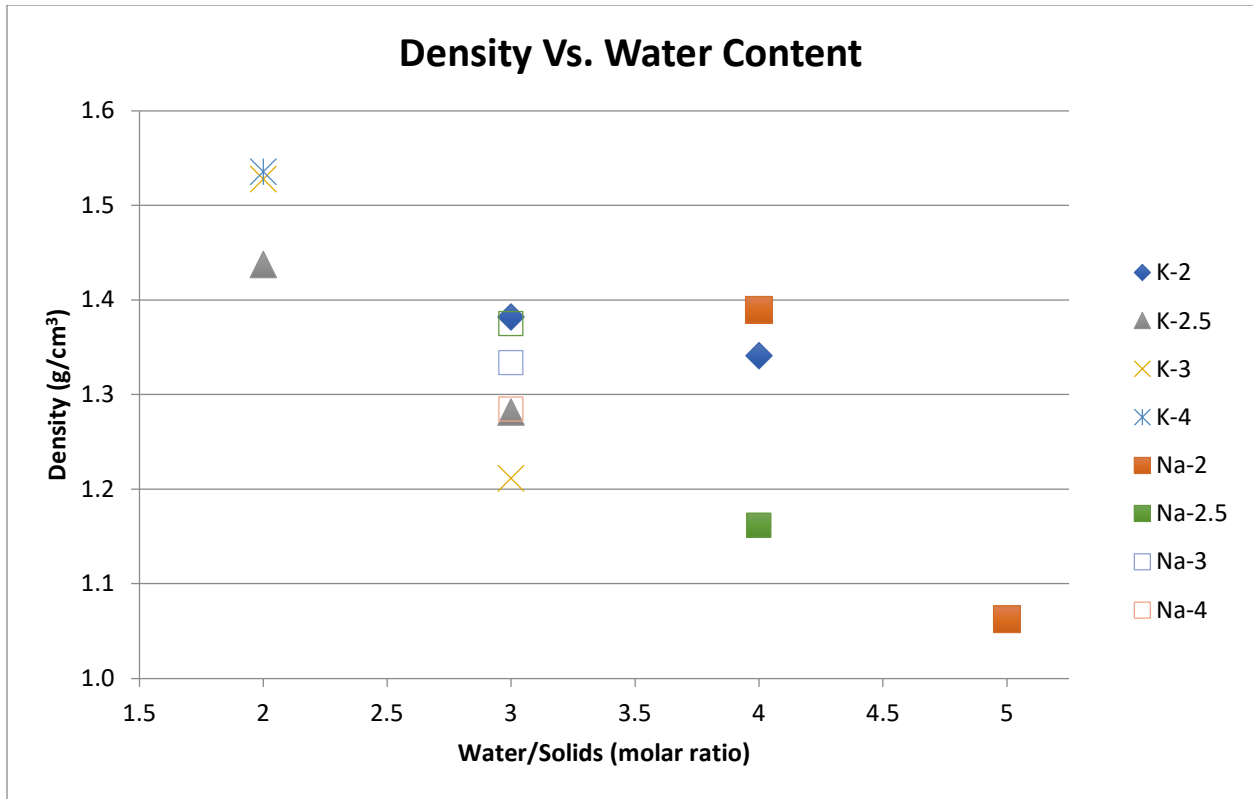
Figure 15. Plot of density vs. molar water amount.

5.1.3 Shrinkage

Shrinkage of the pure GP binder can be found in Figure 16 and Figure 17. For pure Na-GP, the shrinkage seems to become more prominent with the increase in SiO_2/Al_2O_3 ratio and decrease in water/solids ratio. K-GP do not have as clear of a trend as Na-GP have shown, instead, all that's observed is that the shrinkage seems to level off at 1% when SiO_2/Al_2O_3 is above or equal to 3. The shrinkage data for GP mortars are not presented since there's no significant shrinkage among difference compositions
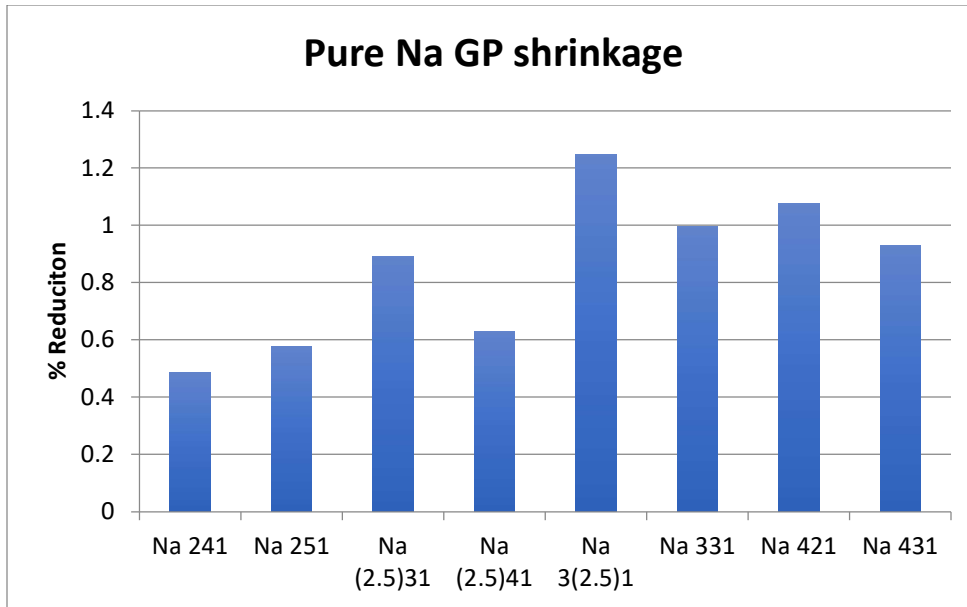
Figure 16. Shrinkage of pure Na GP binder.
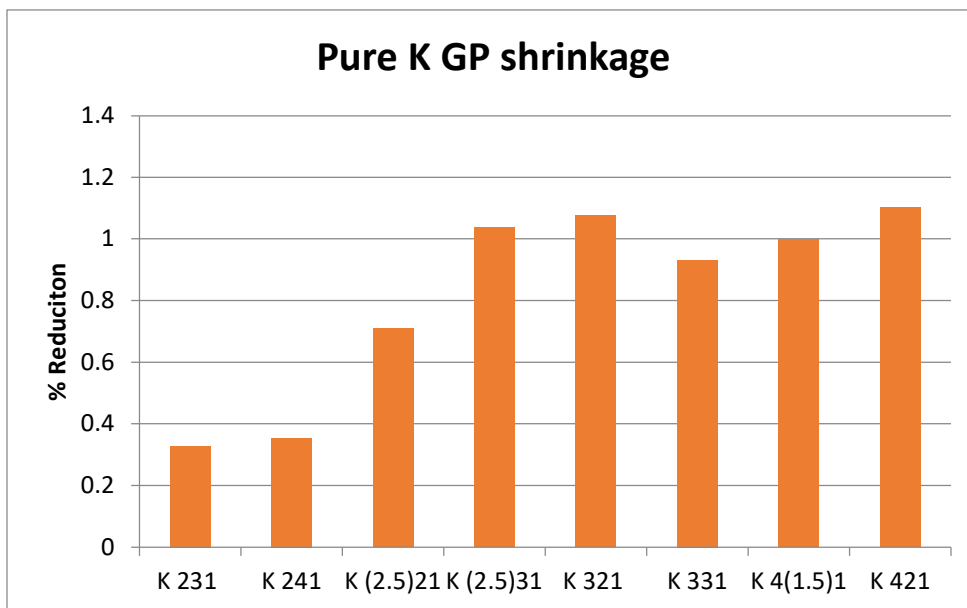
Figure 17. Shrinkage of pure K GP binder.

5.1.4 Compressive Strength

For the compressive strength of GP (see Figure 18 and Figure 19), it is expected that the strength would increase with an increase in SiO_2/Al_2O_3 ratio and/or decrease in water/solids ratio. This is essentially the case for pure Na GP except for Na421 since it has very low workability making the samples highly porous. As for pure K GP, there's not a clear trend as pure Na GP do, except that the strength significantly increases when SiO_2/Al_2O_3 is greater than or equal to 2.5.
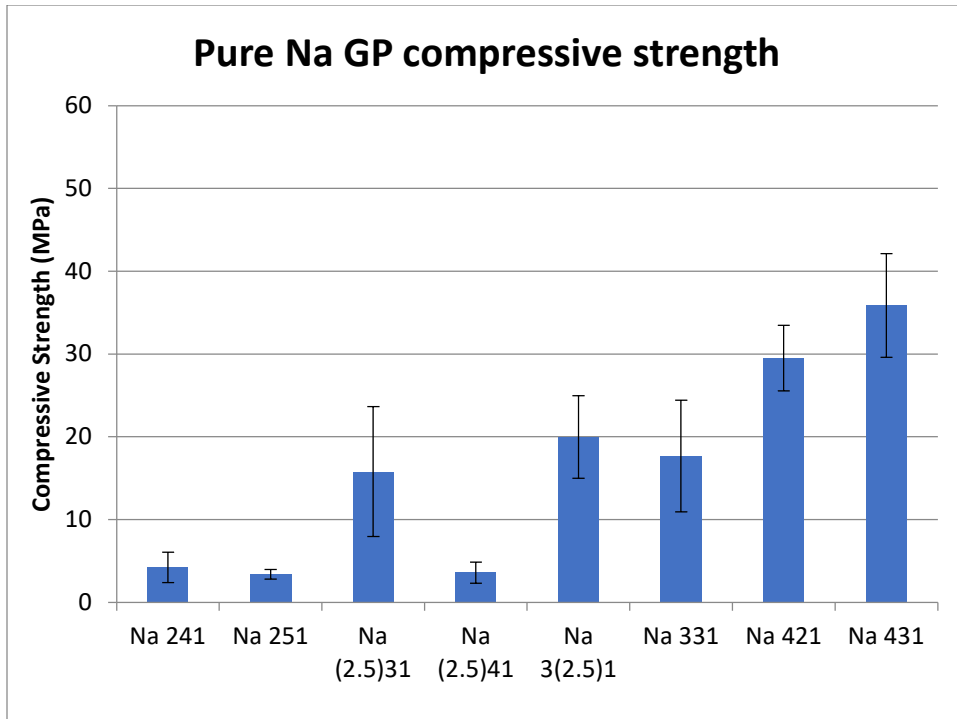
Figure 18. Compressive strength of pure Na GP.
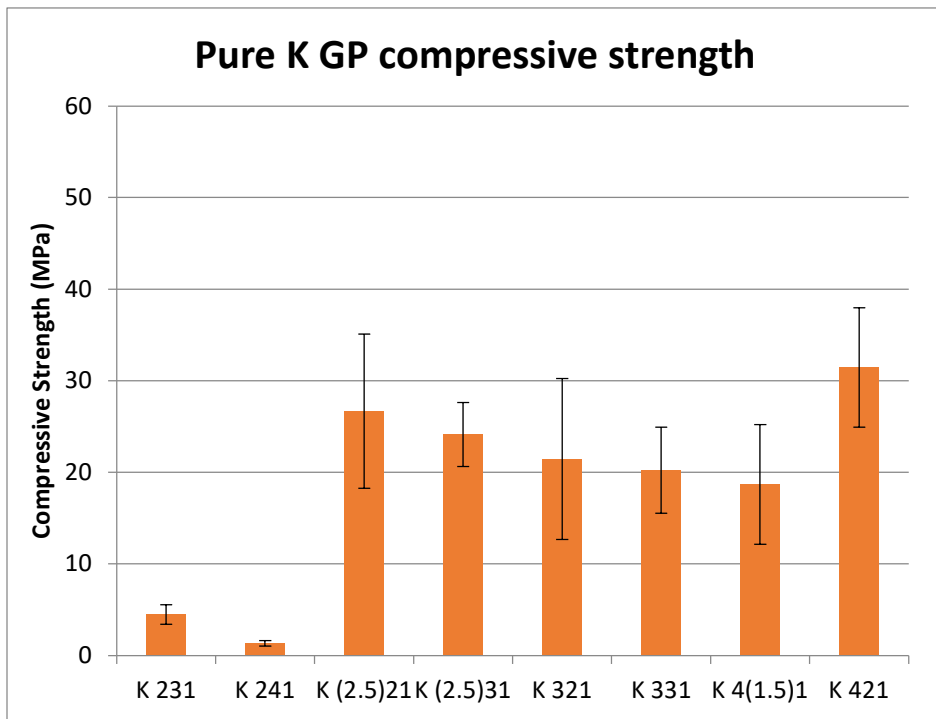
Figure 19. Compressive strength of pure K GP.

Figure 20 and Figure 21 shows the result from compressive strength test of GP mortar samples. To compare with the results from pure GP binder, similar trends are observed. It can be generalized

that GP show a significant increase in strength with the addition of sand. Notably, Na331, Na431, and K331 have the most increase.
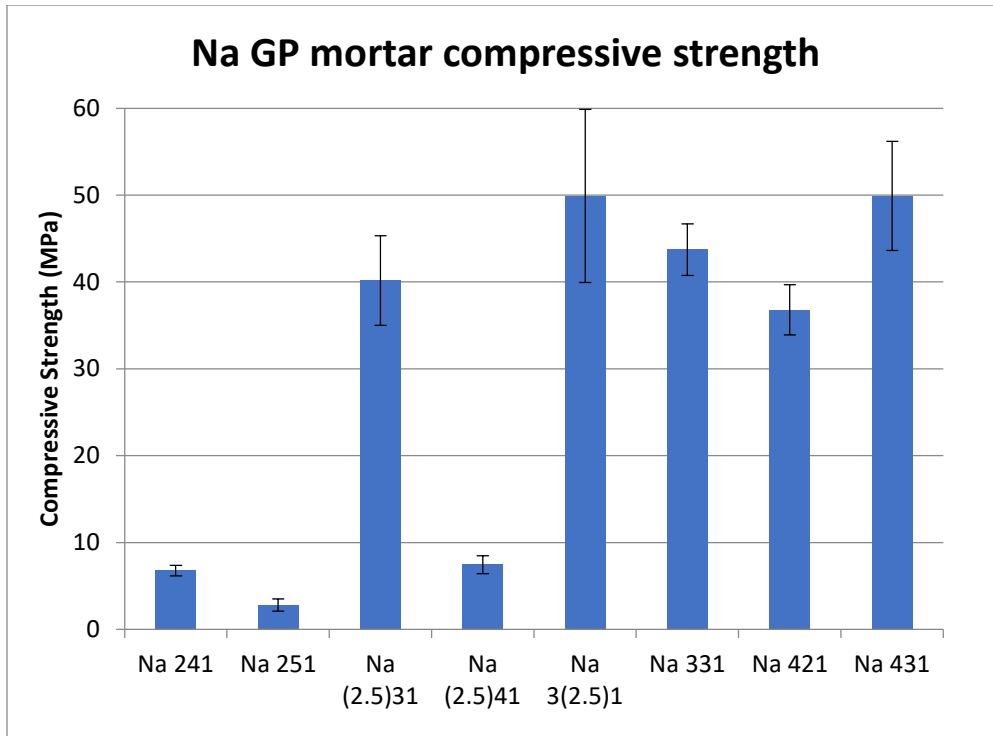
Figure 20. Compressive strength of Na GP mortar.
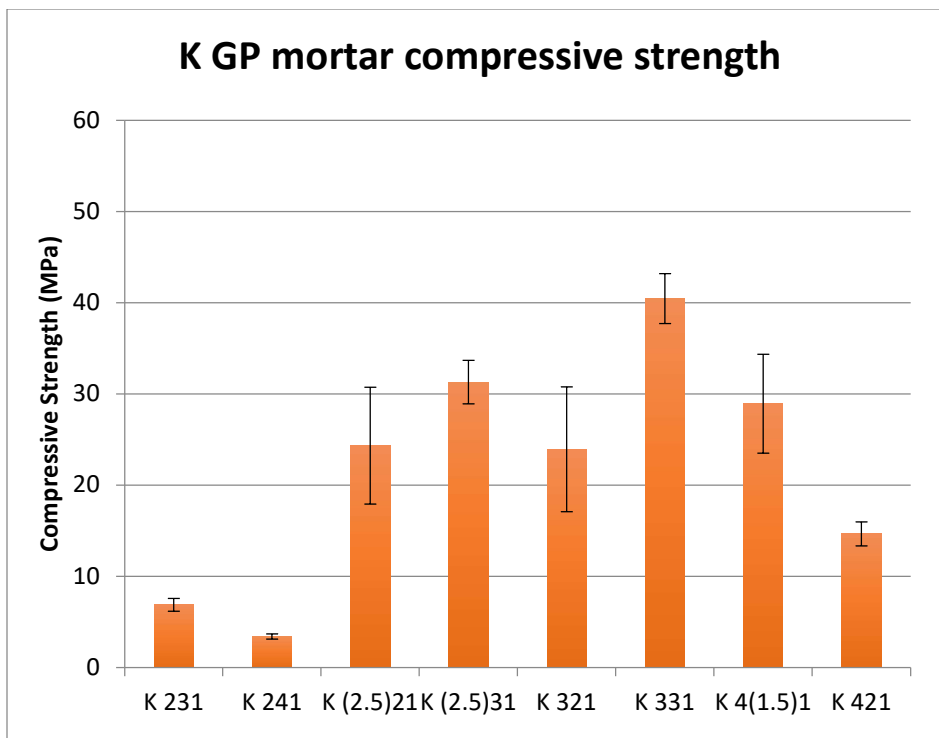
Figure 21. Compressive strength of K GP mortar.

5.1.5 SEM

Based on the results shown above, the GP mortars prepared with Na431 and K231 GP binders show one of the highest and lowest UCSs, respectively. SEM imaging of those two samples in Figure 22 clearly shows different morphology of GP binder in Na431 and K231 mortar samples. This suggests that the degree of reaction of MK in GP binder is crucial for strength of the mortar samples. This can be qualitatively determined through the larger amount of observable unreacted MK particles in the K231 GP binder (Figure 22a and b) when compared to the Na431 GP binder in Figure 22c and d. In addition, although Na431 GP binder contains some larger cracks, it seems to adhere much better to the sand particles, as compared to the K231 binder. The better adhesion to sand particles also can contribute the higher compressive strength observed in those samples.
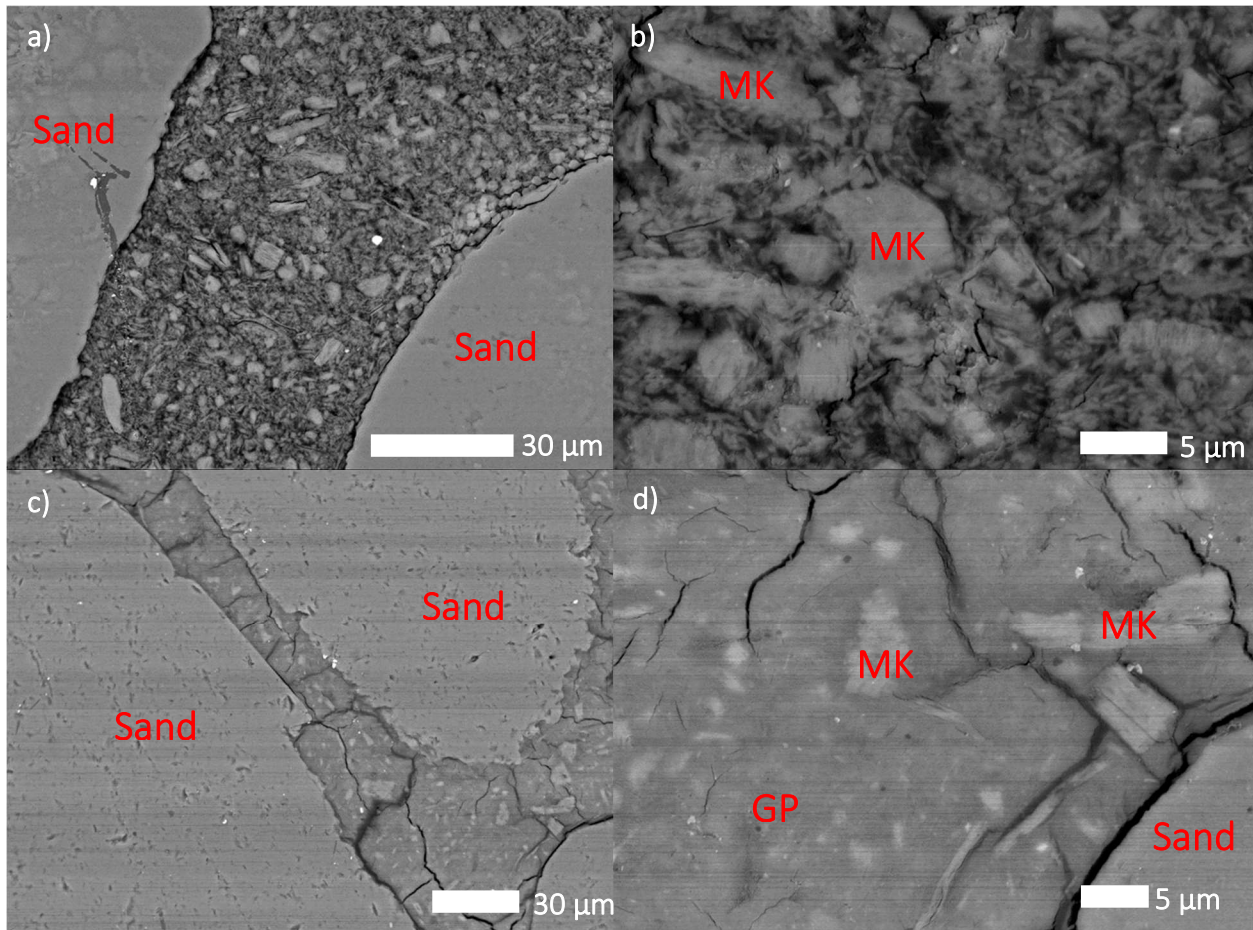
Figure 22. Back-scattered electron SEM micrograph of: (a) K231 mortar at low magnification, (b) K231 mortar at high magnification, (c) Na431 mortar at low magnification, and (d) Na431 mortar at high magnification.

5.2 Task II: EGC Performance Evaluation and Composite Optimization

5.2.1 Compressive Strength and Density
5.2.1.1 MK Based GP Materials

The compressive strength test results for the MK-based GP mixtures shown in Table 5 are presented in Figure 23. As it can be seen, the K-based GP binders presented similar strengths with K321 and K331 exhibiting compressive strengths of 18.15 and 18.71 MPa, respectively. This was unexpected since the K331 binder uses higher amounts of water during processing (compared to K321), which has been demonstrated to be detrimental to GP strength development as this results in a more porous GP microstructure (47). The effect of processing water on the GP microstructure porosity was evident in the measured GP hardened densities as shown in Figure 24, where K321 GP materials consistently exhibited greater densities compared to K331 GP materials. The hardened densities were determined by dividing the mass of the cube specimens (measured prior to the compressive strength test) by their volume. The relatively low compressive strength performance of the K321 GP binder is possibly attributed to its reduced workability compared to the K331 GP binder. Low workability can result in the occurrence of large, entrapped air bubbles during mixing and casting, which can act as defects and negatively affect compressive strength. In the case of the Na-based GP binder evaluated (i.e., Na431), it significantly outperformed the K-based binders with a compressive strength of 30.04 MPa.
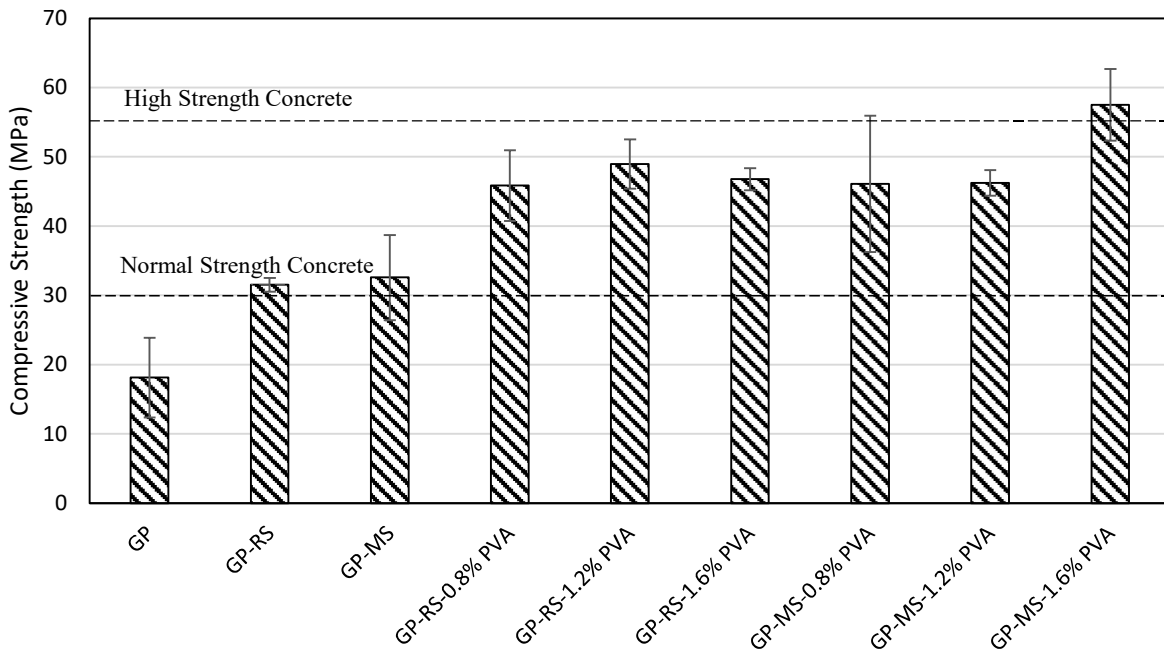

(a)
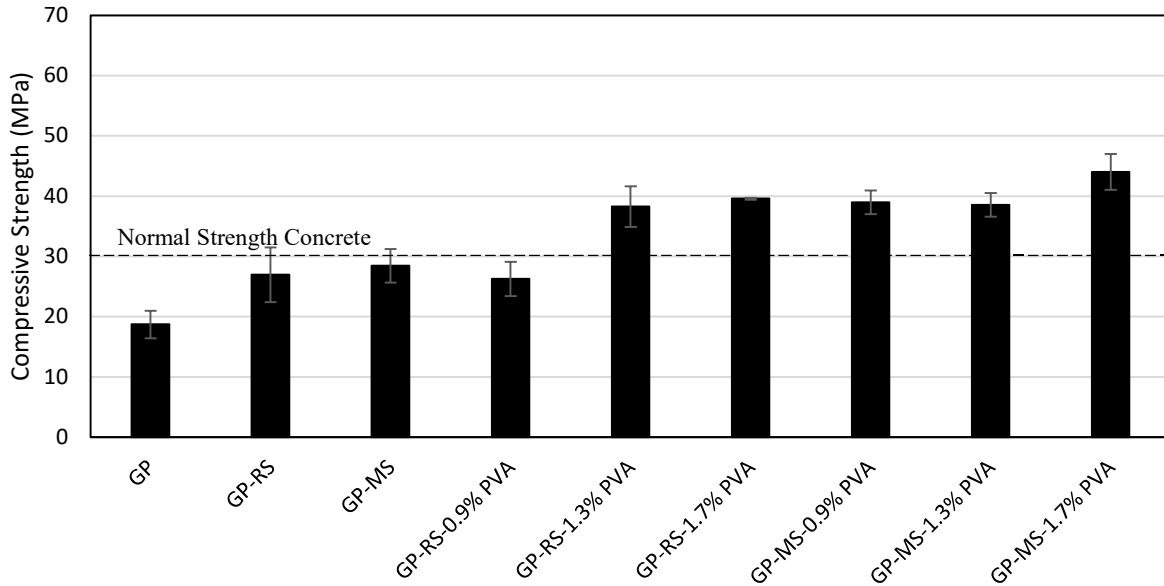
(b)
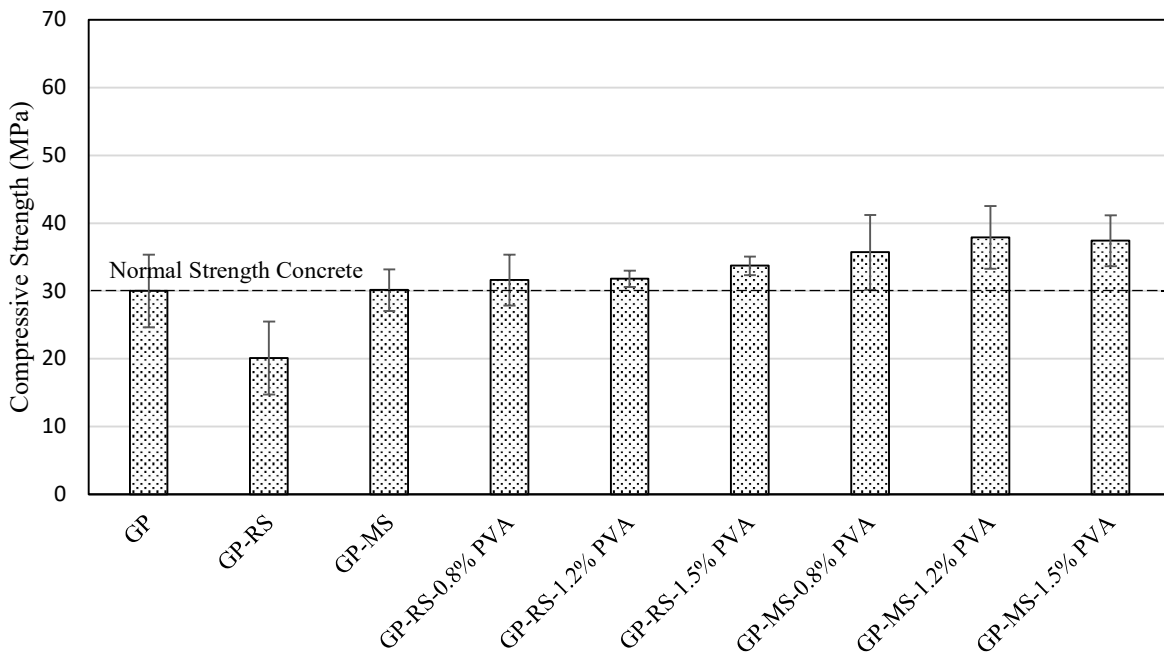
(c)

Figure 23. Average 28-Day compressive strength of MK-based GP materials (a) K321 (b) K331 (c) Na431.

Interestingly, the addition of RS (i.e., GP-RS) and MS (i.e., GP-MS) to produce GP mortars dramatically changed the results observed for pure GP binders. In the case of K-based mortars, the use of both types of sand had a clear effect of enhancing the compressive strength (compared to pure GP binder), where GP mortars implementing MS slightly outperformed those using RS. It is hypothesized that the positive effect of sand addition on compressive strength is associated with

the strong interfacial transition zone (ITZ) formed by GP binders with aggregate particles (*66–69*). Another relevant trend observed was the higher compressive strength of K321 GP mortars (compared to the K331 GP mortars) for both types of sand. This was attributed to the expected increase in porosity of the K331 GP binder microstructure compared to that of K321 (due to higher amount of water used during processing) as well as the stark differences in the workability of these binders. In contrast to the K321 GP binder, the K331 GP binder was highly workable. Consequently, this produced some segregation of the fine aggregate when producing the GP mortars with the K331 GP binder, which likely contributed to a reduction in strength. In the case of the Na-based GP mortars, a different trend was observed compared to K-based GP mortars. When implementing RS, the compressive strength of the Na431 GP mortar dramatically decreased compared to the Na431 GP binder, whereas the use of MS did not produce any increase in strength. These results were attributed to the workability of the Na-based GP binder, which exhibited the greatest workability. This in turn, caused significant problems with fine aggregate segregation, which negatively affected the strength of the material. It is important to mention that the segregation problem was much more pronounced in GP mortars using RS, due to the large particle size of this sand compared to MS. Accordingly, lower strengths were observed for RS specimens.
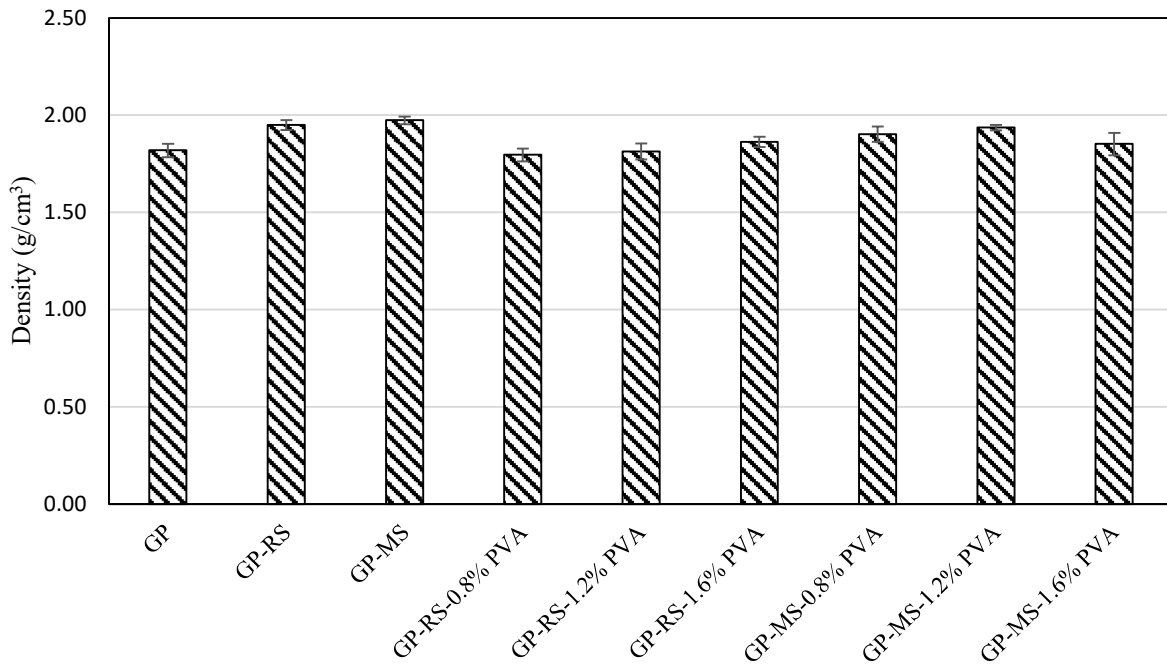
(a)
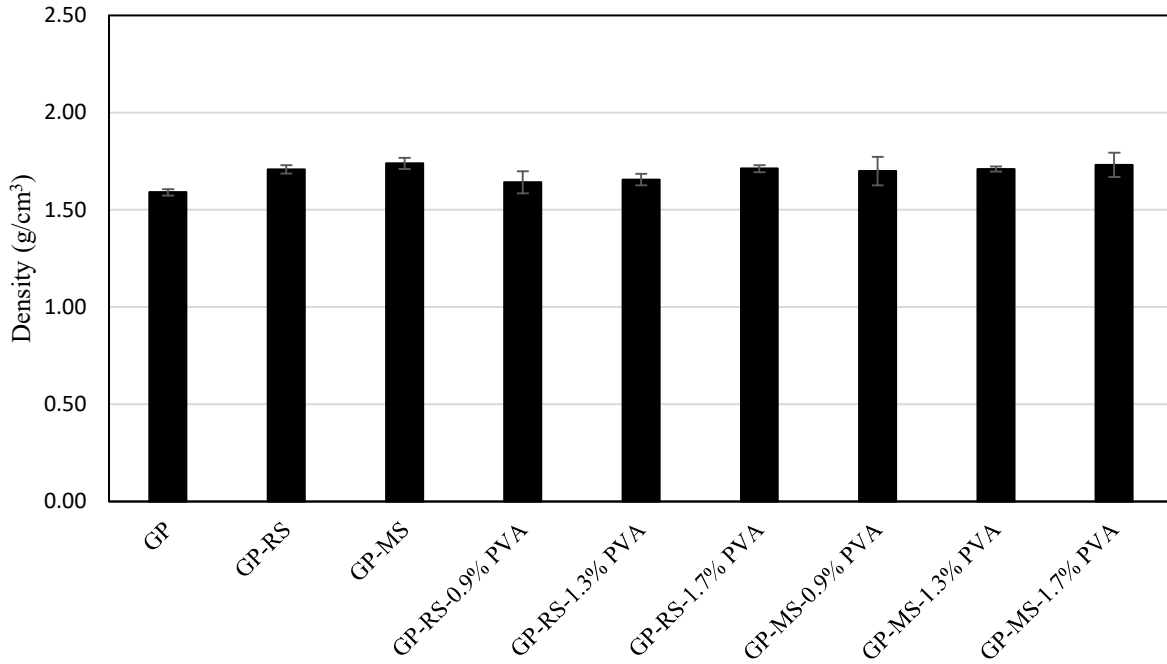
(b)
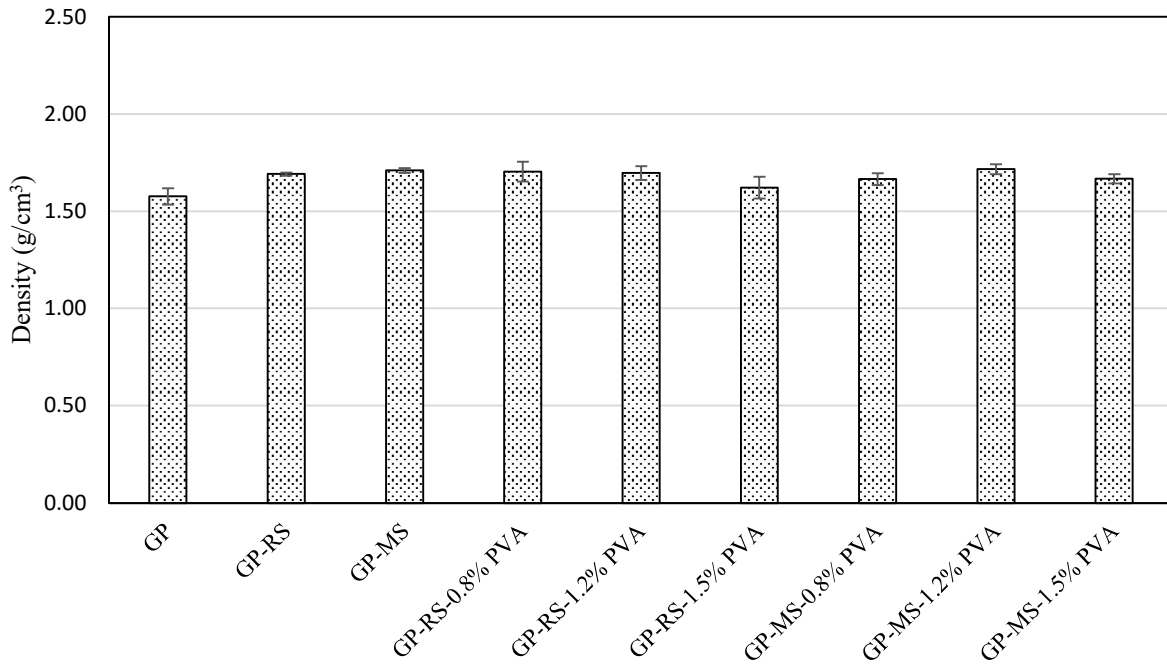
(c)

Figure 24. Average density of MK GP materials (a) K321 (b) K331 (c) Na431.

To produce EGCs, GP mortars were reinforced with PVA fibers at contents of 0.8, 1.2 and 1.6% volume fraction for K321; 0.9, 1.3, and 1.7% for K331; and 0.8, 1.2, and 1.5% for Na431. As seen in Figure 23, generally, the inclusion of PVA fibers resulted in a clear increment in compressive

strength for all MK-based GP materials evaluated. The only exception to this trend was the K331 EGC using RS and 1.3% fiber content (i.e., K331 GP-RS-1.3%PVA), which exhibited a compressive strength comparable to that of the plain K331 GP mortar (i.e., K331 GP-RS). Furthermore, the increase in fiber content generally produced enhancements in the compressive strength of the composites. K331 and Na431 EGCs incorporating RS, exhibited the highest compressive strength at 1.7% and 1.5% fiber content, while the K321 EGCs with RS achieved the maximum compressive strength at 1.2% content, respectively. On the other hand, K321 and K331 EGCs incorporating MS, presented the highest compressive strength at 1.6% and 1.7% fiber content, while the Na431 EGCs achieved this at 1.2% fiber content, respectively. Overall, the positive effect of fiber reinforcement on compressive strength is attributed to the crack bridging mechanism of fibers, which limits crack growth and propagation. This same mechanism is also responsible for altering the failure mode of GPs from brittle to ductile. As shown in Figure 25, EGCs experienced significant amounts of deformation and splitting columnar vertical cracks similar at failure. Conversely, plain GP binders crumbled into pieces. In the case of plain GP mortars, conical type failures were observed; however, upon removal of the specimens from the testing equipment the specimens crumbled. Consequently, no images are presented for plain GP binders and mortars.
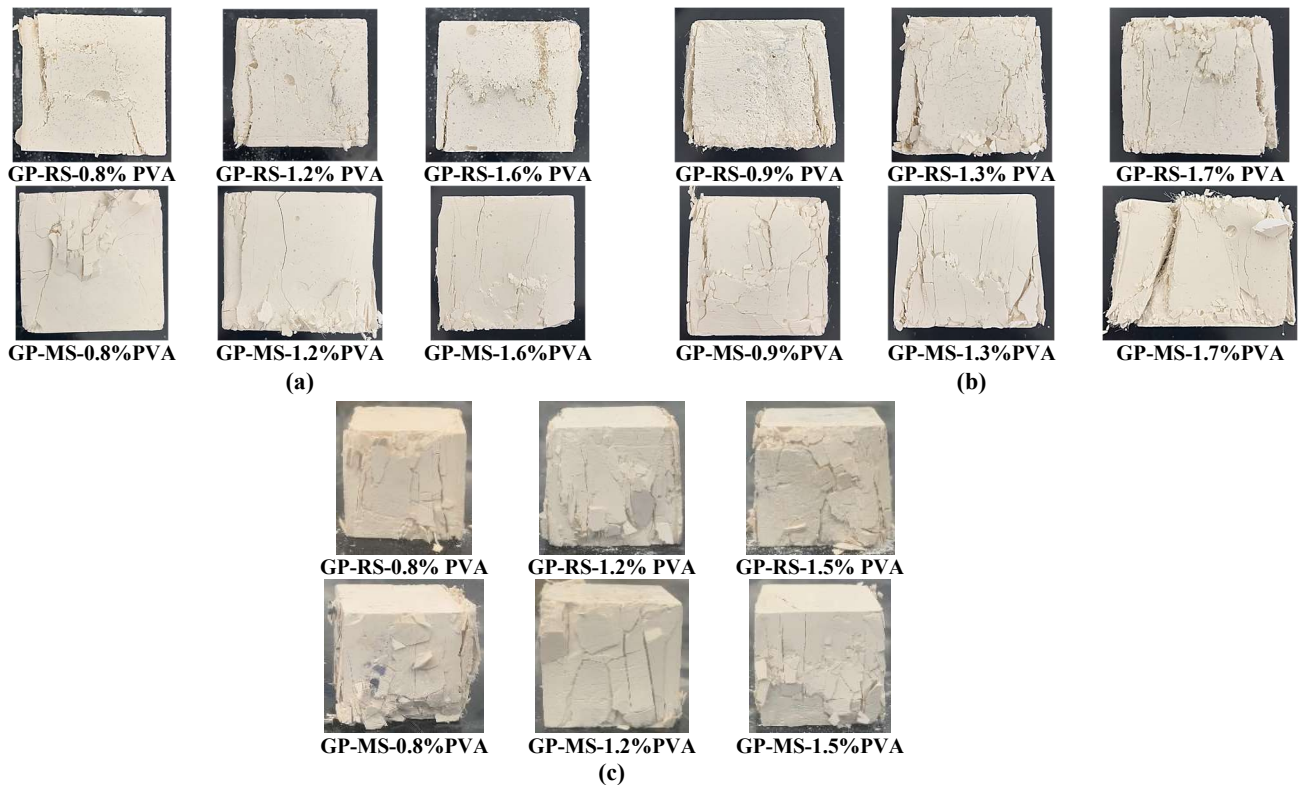

Figure 25. Compressive strength failure mode: (a) K321 EGCs (b) K331 EGCs (c) Na431 EGCs.

As shown in Figure 24, the densities of the MK-based GP materials ranged from 1.58 to 1.97 g/cm^3. As such, the GP materials evaluated exhibited densities significantly lower than the density of conventional concrete (i.e., 2.40 g/cm^3). Nevertheless, in the case of fiber-reinforced GP materials (i.e., EGCs), except for K331 GP-RS-1.3%PVA, the compressive strength of conventional concrete (i.e., 30 MPa) was surpassed. This highlights the excellent strength of these materials relative to their weight. It is relevant to note that the EGC presenting the highest

compressive strength (i.e., K321 GP-MS-1.6%PVA) of 57.52 MPa could be classified as a high-strength concrete material according to the ACI Committee 363 definition (i.e., f'c>55 MPa) while exhibiting a density 22.9% lower to that of conventional concrete.

5.2.1.2 MKFA Based GP Materials

The 28-day compressive strength of MKFA GP binder EGC mixtures shown in

Binder Type	Mix #	Type of Mix	SiO$_2$/Al$_2$O$_3$	H$_2$O/(SiO$_2$+Al$_2$O$_3$)	Cation/Al$_2$O$_3$	Sand/Binder (wt.%)	Fiber (vol.%)
K321	1	GP					0
	2	GP-RS					0
	3	GP-MS					0
	4	GP-RS-0.8%PVA					0.8
	5	GP-RS-1.2%PVA		2			1.2
	6	GP-RS-1.6%PVA					1.6
	7	GP-MS-0.8%PVA					0.8
	8	GP-MS-1.2%PVA					1.2
	9	GP-MS-1.6%PVA	3				1.6
K331	10	GP					0
	11	GP-RS					0
	12	GP-MS					0
	13	GP-RS-0.9%PVA					0.9
	14	GP-RS-1.3%PVA			1	0.36	1.3
	15	GP-RS-1.7%PVA					1.7
	16	GP-MS-0.9%PVA					0.9
	17	GP-MS-1.3%PVA					1.3
	18	GP-MS-1.7%PVA		3			1.7
Na431	19	GP					0
	20	GP-RS					0
	21	GP-MS					0
	22	GP-RS-0.8%PVA					0.8
	23	GP-RS-1.2%PVA	4				1.2
	24	GP-RS-1.5%PVA					1.5
	25	GP-MS-0.8%PVA					0.8
	26	GP-MS-1.2%PVA					1.2
	27	GP-MS-1.5%PVA					1.5

Table 6 are presented in Figure 26. As it can be observed, the compressive strength of the MKFA GP materials ranged from 4.94 to 10.10 MPa, which is in all cases lower than the compressive strength of normal concrete (i.e., 30 MPa). Low strengths observed were attributed to the replacement of highly reactive silica fume with fly ash, which likely remained partially unreacted limiting the strength gain of the materials. Figure **27** support this hypothesis as unreacted fly ash particles were encountered within the GP microstructure after 28 days of curing. Furthermore, three interesting trends were observed: (1) the implementation of sand produced an increment in strength, with MS producing the largest strength gain; (2) the addition of PVA fibers produced an enhancement in the compressive strength; and (3) the increment in fiber content produced further

strength gain. It is important to mention that the trends observed for MKFA GP materials were similar to those observed in MK GP materials.
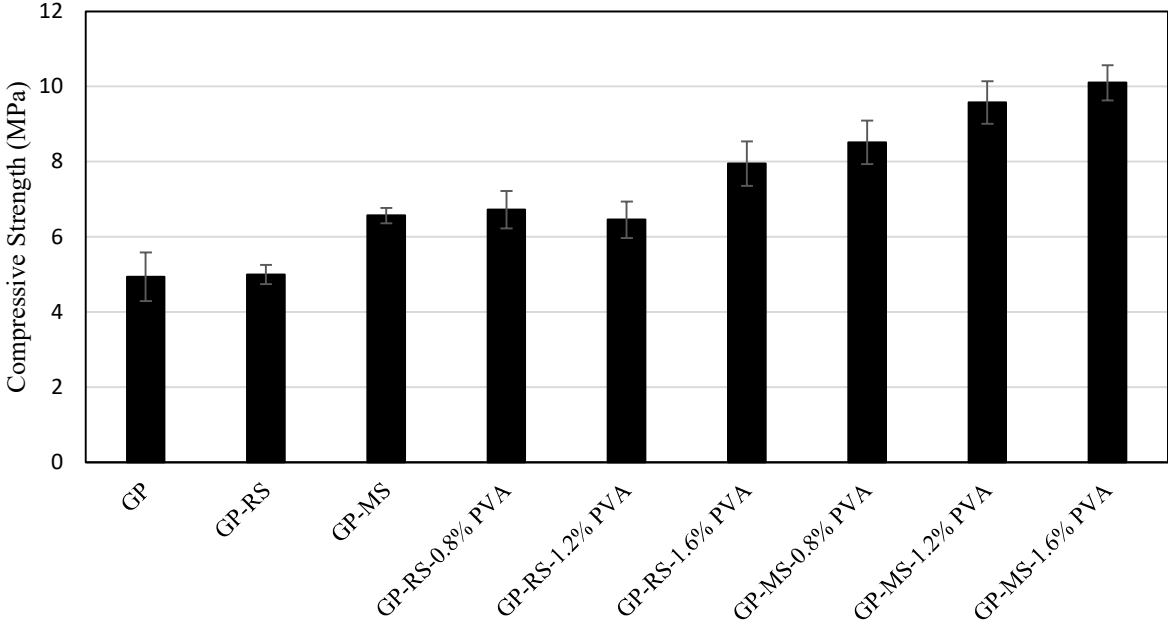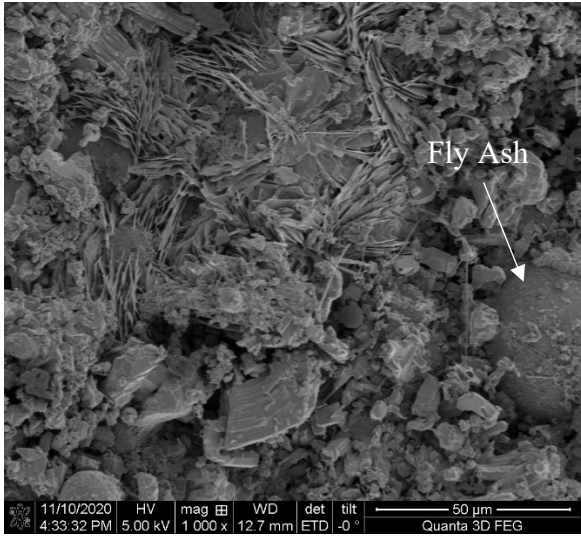

Figure 26. M*K*FA-based GP materials average 28-Day compressive strength.

(a)

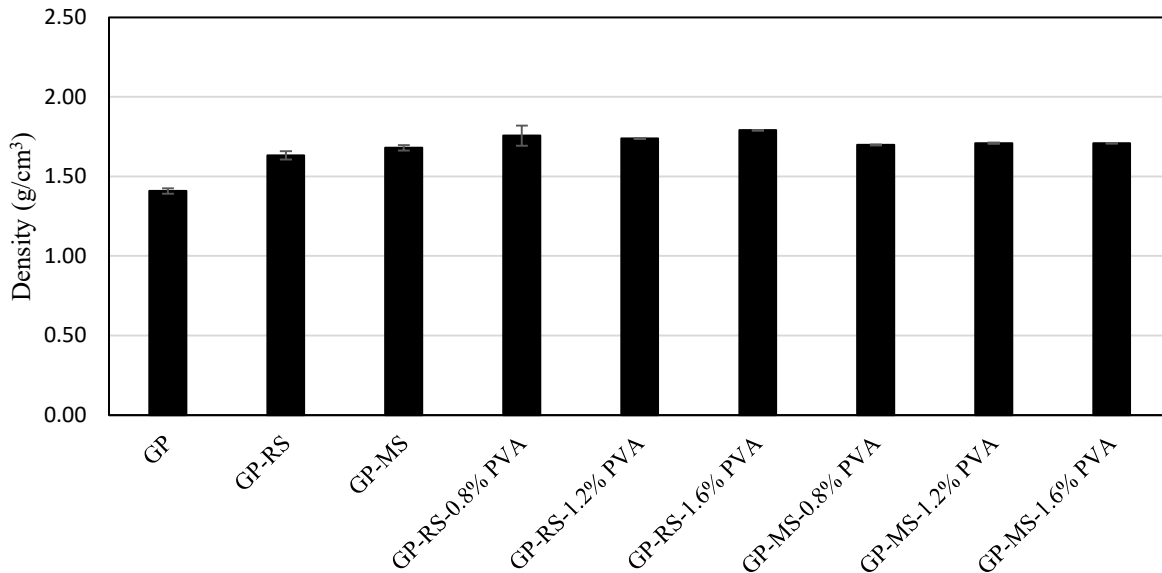**Figure 27. Pure MKFA SEM image.**

Figure 28 M*K*FA-based GP materials fresh and hardened density.

As shown in Figure 28, the hardened densities of the MKFA-based GP materials ranged from 1.41 to 1.79 g/cm³. Therefore, similar to MK based GP materials, the MKFA-based GP materials did also exhibit densities significantly lower than conventional concrete. However, as previously mentioned the strengths of the MKFA based materials were low. Future research should focus on evaluating MKFA GP materials implementing partial replacement of fly ash with silica fume to achieve composites exhibiting higher mechanical strength. Furthermore, different curing methods including heat curing should be evaluated to further explant the potential of MKFA based GPs.

5.2.2 Uniaxial Tensile Test

5.2.2.1 MK Based GP Materials

As discussed in the compressive strength section, from the GP binders evaluated, K321 exhibited the greatest promise as it produced EGCs with excellent mechanical strength while presenting proper workability to prevent aggregate segregation. As such, uniaxial tensile tests were conducted on the EGCs produced with K321 GP mortars using RS and MS. Both EGCs were evaluated using 1.6% PVA fiber content.

The tensile stress vs. strain curves for the MK EGCs evaluated are presented in Figure 29. It can be observed that while multiple cracking behavior occurred in some specimens, a robust PSH behavior was not achieved for any of the composites. Figure 30 reports the average tensile properties of the composites obtained from the tensile stress vs. strain curves. From these results it is evident that from the two different composites evaluated, the one using MS (i.e., K321 GP-MS-1.6%PVA) presented the best tensile performance by exhibiting a greater tensile strength and tensile strain capacity. In contrast to the composite implementing RS (i.e., K321 GP-RS-1.6%PVA), the one using MS (i.e., K321 GP-MS-1.6%PVA) produced an increase in the tensile strength and tensile strain capacity of 66.5% (2.12 to 3.53 MPa) and 109.1% (0.22 to 0.46%), respectively. The important improvement in tensile strength observed, was attributed to the stronger GP matrix produced by the composite implementing MS, which likely improved the

40

fiber/matrix interfacial frictional bond. Evidence of GP matrix strengthening with MS was identified as the matrix cracking strength of the MS composite exceeded that of the RS composite by 50.0% (2.10 to 3.15 MPa). Furthermore, an improvement in fiber distribution is expected in EGCs using MS due to the small particle size of this sand (*70*). This in turn, can lead to the enhancement of the fiber bridging capacity; and thus, to the improvement of the tensile strength of the composite. In the case of the improvement in tensile ductility when implementing MS, it is believed that the improvement in the fiber bridging capacity is also associated with this phenomenon as this can produce an enhancement in the complementary energy of the fiber bridging relation. Furthermore, it is well known that the implementation of aggregate with small particle size reduces the fracture toughness of the cementitious matrices due to a decrease in the tortuosity of the fracture path (*70*). As such, it is believed that use of MS can reduce the fracture toughness of the GP matrix, and therefore, enhance the PSH behavior of the EGC leading to a greater tensile ductility.

(a)

(b)
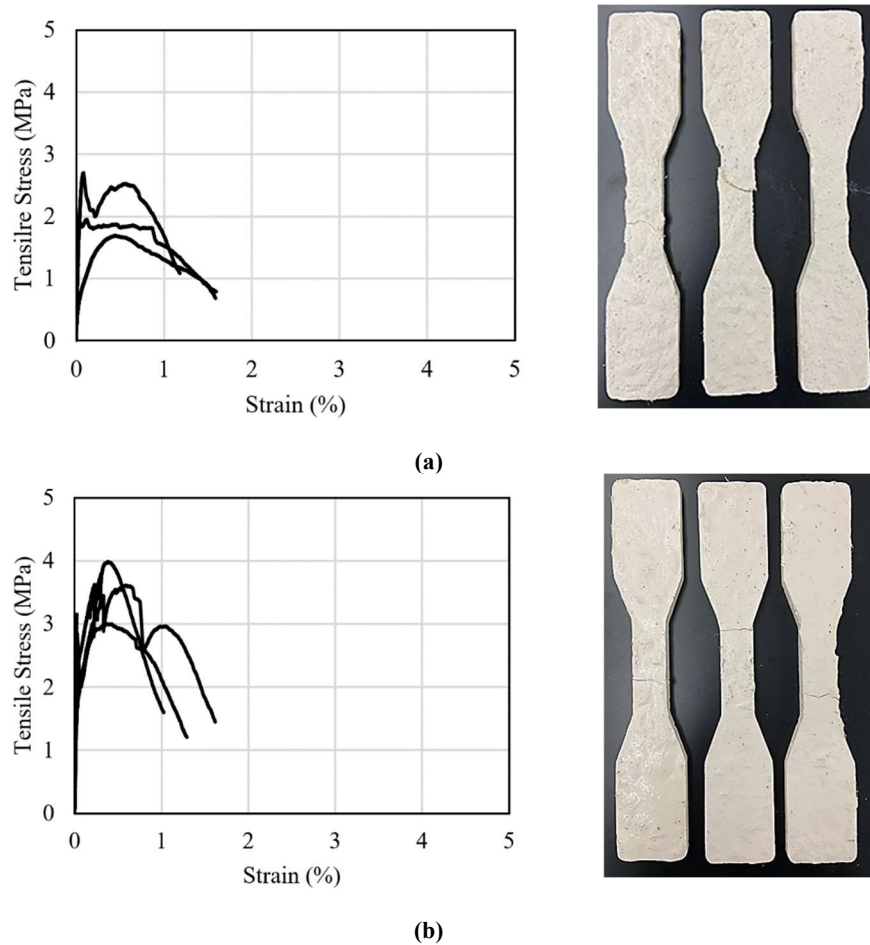
Figure 29. Tensile stress vs. strain curves of MK EGCs using VPM2 mixer: (a) K321 GP-RS-1.6%PVA and (b) K321 GP-MS-1.6%PVA.
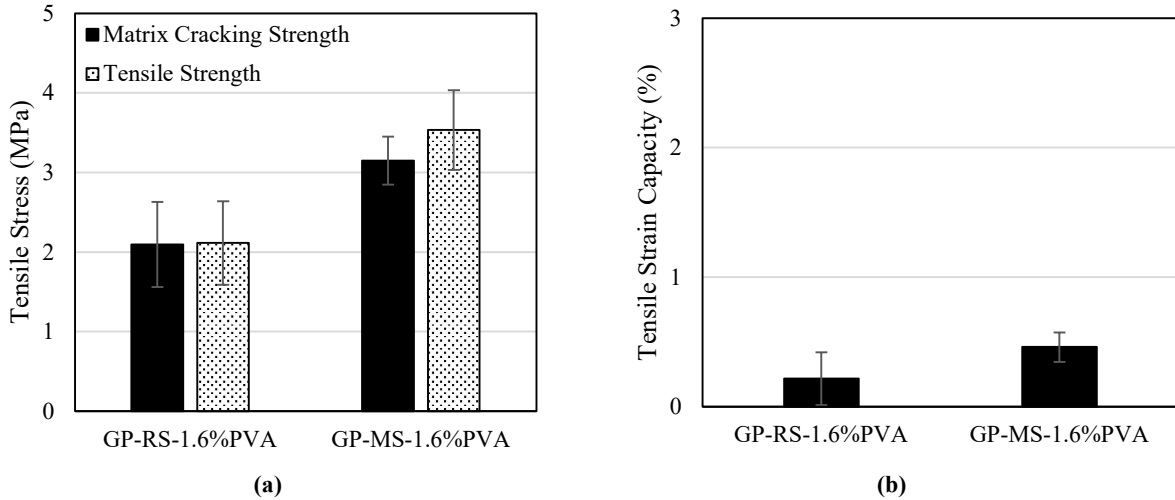
Figure 30. Tensile properties of MK EGCs using VPM2 mixer: (a) matrix cracking strength and tensile strength and (b) tensile strain capacity.

While the K321 GP binder exhibited the best workability for preventing segregation, optimal fiber was not achieved. This was clearly observed as the tensile strain capacity of both composites evaluated did not surpass 1%, which is typically associated as a lower bound for ECC materials (*71*). Consequently, a different mixing procedure was attempted in an effort to enhance fiber distribution by using a tabletop planetary mixer a described in section 4.2.2. Figure 31 presents the tensile stress vs. strain curves of the K321 GP-RS-1.6%PVA and K321 GP-MS-1.6%PVA composites using the modified mixing procedure. As it can be seen, a significant enhancement in the PSH behavior of both composites was observed. It is important to mention that one K321 GP-RS-1.6%PVA specimen and two K321 GP-MS-1.6%PVA specimens exhibited failure outside of the testing zone (i.e., neck failure). Therefore, these materials were not considered in the computation of tensile properties presented in Figure 32.

(a)

42
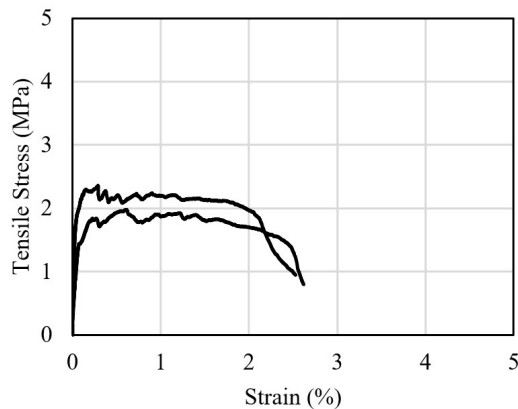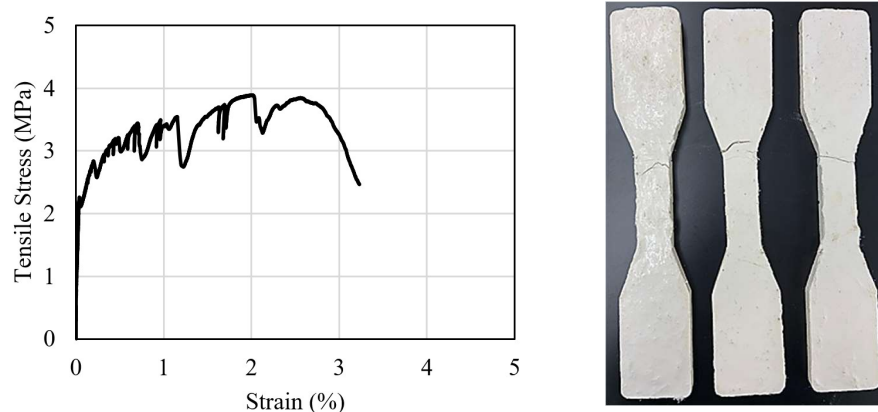
(b)

Figure 31. Tensile stress vs. strain curves of EGCs using tabletop planetary mixer: (a) K321 GP-RS-1.6%PVA (b) K321 GP-MS-1.6%PVA.

From Figure 32, it can be observed that the tensile strain capacity of both composites improved by 105% (0.22 to 0.45) and 339% (0.46 to 2.02) for RS and MS composites, respectively, by using the modified mixing procedure. This dramatic improvement in ductility highlights, the importance of fiber distribution on composite performance. Upon completion of the uniaxial tensile test, all the specimens were evaluated under the light microscope to assess the number and size of the cracks. Crack analysis of specimens exhibiting more than one crack are presented in Table 9. As shown, the crack analysis revealed 10 cracks within the testing section of the K321 GP-MS-1.6%PVA specimen shown in Figure 31b averaging 148.5 μm in width (excluding the failure crack). While MK based GP binders show potential for utilization in the development of EGCs, future research should be directed towards the optimization of MK GP binder's rheology to provide with homogenous fiber distribution. In turn, this will allow to fully exploit the potential of MK binders in the manufacture of EGCs.
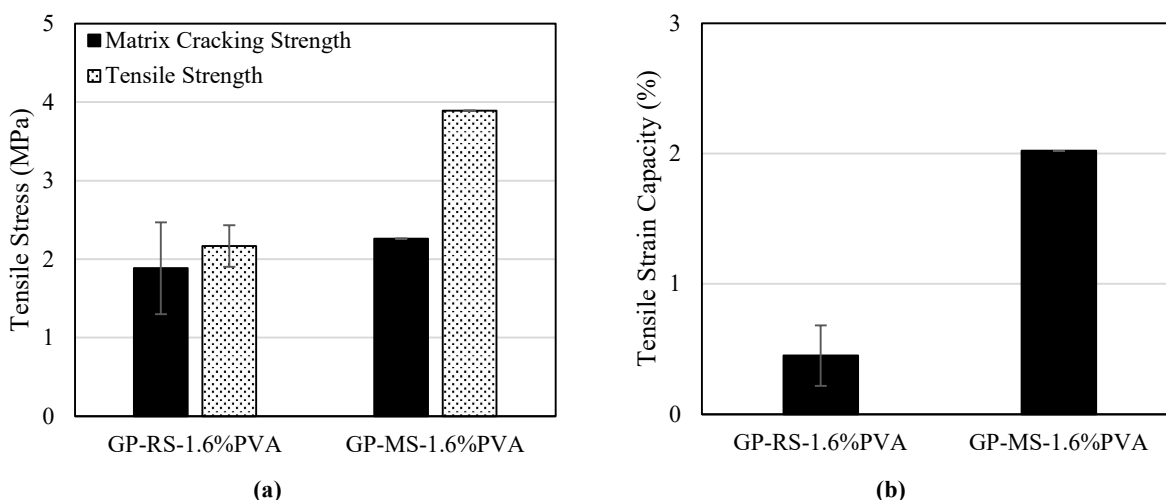
(a)

(b)

Figure 32. Tensile properties of MK EGCs using planetary mixer: (a) matrix cracking strength and tensile strength and (b) tensile strain capacity.

Table 9 Crack Analysis.

Binder Type	Mixing Type	Material	Number of Specimens	Avg. Number of Cracks	Avg. Crack Width (μm)

K321	VPM2	GP-RS-1.6%PVA	1	3	170.0
		GP-MS-1.6%PVA	2	2.5	148.3
	Planetary Mixer	GP-RS-1.6%PVA	1	3	90.3
		GP-MS-1.6%PVA	1	10	148.5

5.2.2.2 MKFA Based GP Materials

Uniaxial tensile tests were conducted on the EGCs produced with K321 MKFA mortars using RS and MS at 1.6% PVA fiber content. Three replicates were tested after 28±1 days of curing per each EGC mixture (i.e., K321 MKFA-RS-1.6%PVA and K321 MKFA-MS-1.6%PVA). The tensile stress vs. strain curves for the MKFA EGCs evaluated are presented in Figure 33. It is important to notice that some specimens failed outside of the testing zone (i.e., exhibited neck failure as shown in Figure 33); and therefore, were excluded from the analysis.

From the tensile stress vs. strain curves, it is evident that the MKFA compositions did not exhibit a PSH behavior as a single crack localized failure occurred in all specimens evaluated. However, after the GP matrix cracked, an increase in load carrying capacity did occur associated with the fiber-reinforcement. Figure 34 reports the average tensile properties of the composites obtained from the tensile stress vs. strain curves. As observed, the tensile strength achieved for both mixtures evaluated were low with 0.52 and 0.33 MPa for RS and MS mixtures, respectively. Yet, improvements from the matrix cracking strength to the tensile strength were of 33.3% (0.39 to 0.52 MPa) and 266.7% (0.09 to 0.33 MPa) for RS and MS mixtures, respectively. Furthermore, the tensile strain capacity of the composites was also low with 0.51 and 0.59% for RS and MS mixtures, respectively. It is important to mention that MKFA specimens were mixed using the enhanced mixing procedure using the tabletop planetary mixer. As such, compared to the MK EGCs manufacture under the same conditions, the MKFA composites significantly underperformed in terms of tensile strength and ductility. The poor performance of the MKFA composites is attributed to the low strength of the GP matrix. As observed from the compressive strength results, MKFA GPs were very weak. Consequently, this produced a poor fiber/matrix interface leading to the deficient tensile performance.

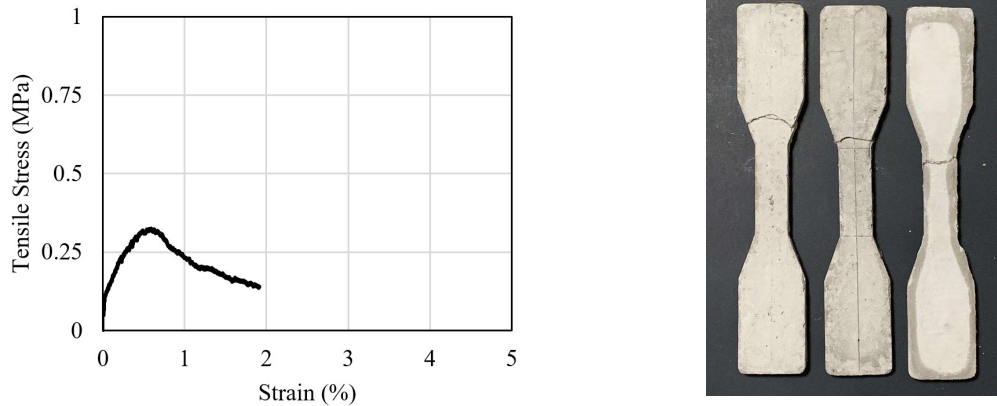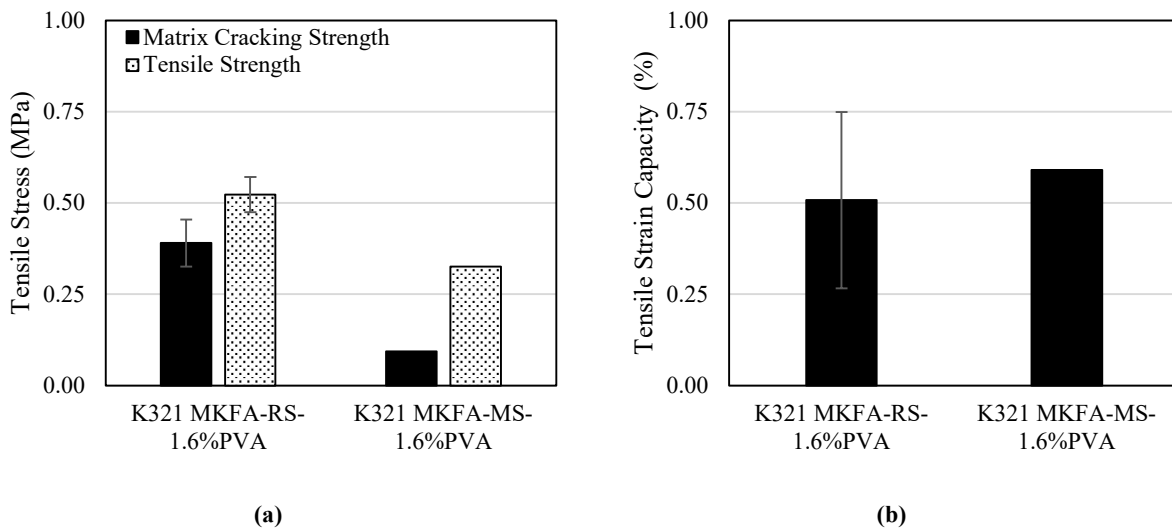**(a)**

(b)
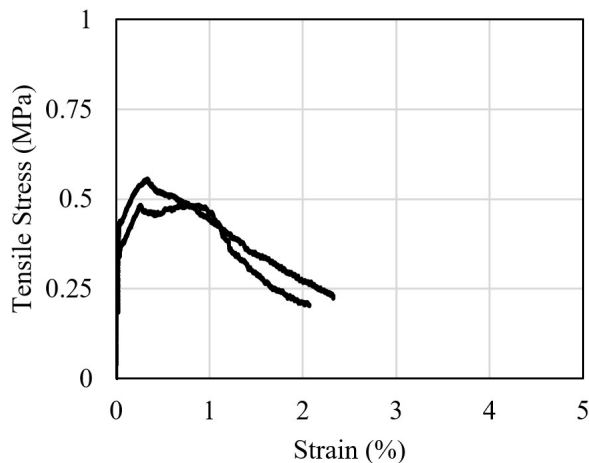
Figure 33. Tensile stress vs. strain curves of EGCs using planetary mixer: (a) K321 MKFA-RS-1.6%PVA (b) K321 MKFA-MS-1.6%PVA.

(a)   **(b)**

Figure 34. Tensile properties of MKFA EGCs using planetary mixer: (a) matrix cracking strength and tensile strength and (b) tensile strain capacity.

5.2.3 Flexural Performance Test

5.2.3.1 MK Based GP Materials

A third point bending test similar to ASTM C1609 was conducted on two MK EGC compositions (i.e., K321 GP-RS-1.6%PVA and K321 GP-MS-1.6%PVA) after 28±1 day of curing to determine the flexural performance of the EGC beams. Figure 35 presents the flexural stress vs deflection curves of the two EGC mixtures. As shown in, the several specimens exhibited PSH behavior where an increase in load carrying capacity after the first cracking strength (summarized in Figure 36) accompanied with significant deformation occurred (through a process of multiple microcracking). Similar to what was observed in the uniaxial tensile test, the type of sand (RS or MS) affected the strength and deformation capacity of the composites. As illustrated in Figure 36, the MS specimens exhibited an enhanced flexural strength and deflection capacity in contrast to RS specimens. It is important to mention that two of the MS specimens evaluated reached the LVDTs deformation limit before reaching the flexural strength. As a result, the flexural strength

and deformation capacity reported for K321 GP-MS-1.6%PVA is an underestimate. The flexural strength of K321 GP-RS-1.6%PVA and K321 GP-MS-1.6%PVA were 3.9 and 5.0 MPa, respectively. As such, the flexural strength of these composites was comparable to that of conventional concrete, which typically ranges between 4 to 6 MPa.
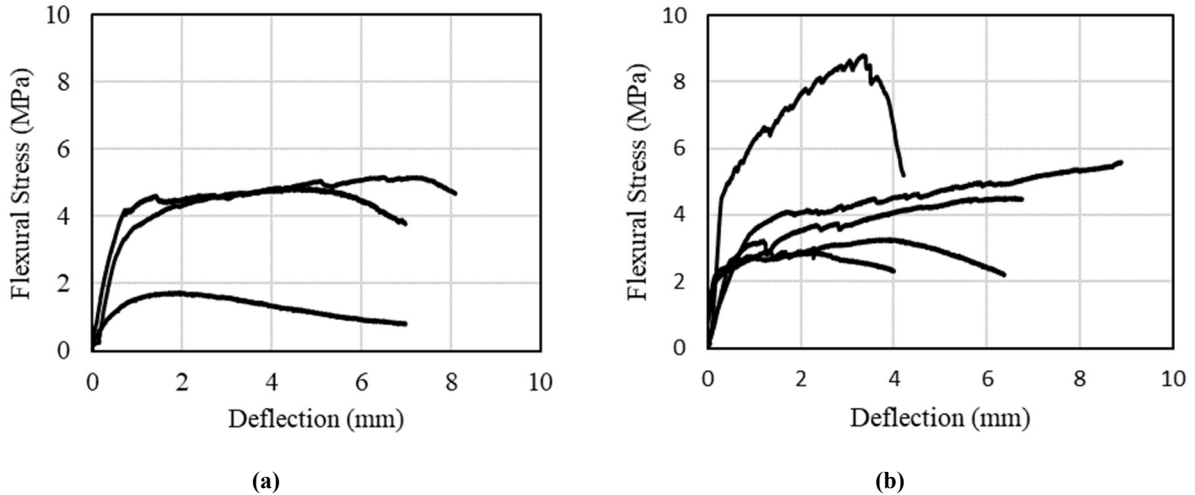

(a)   (b)

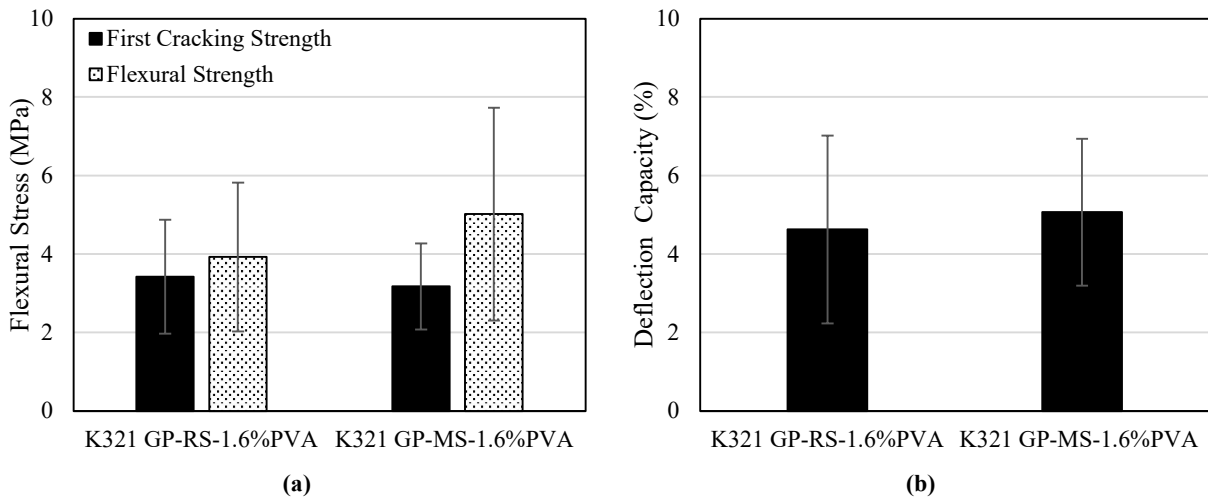**Figure 35. Flexural stress vs. deflection curves of: (a) K321 GP-RS-1.6%PVA and (b) K321 GP-MS-1.6%PVA.**

(a)   (b)

Figure 36. MK average flexural performance test results: (a) first cracking strength and flexural Strength and (b) deflection capacity.

5.2.3.2 MKFA Based GP Materials

Similar to MK EGC beams, the third point bending test was conducted on two MKFA EGC compositions (i.e., K321 MKFA-RS-1.6%PVA and K321 MKFA-MS-1.6%PVA) after 28±1 day of curing to determine their flexural performance. The flexural stress vs deflection curves of the two EGC mixtures is presented in Figure 37. As shown, all specimens exhibited a single crack failure similar to conventional FRC. The average first cracking strength, flexural strength, and flexural deflection capacity are presented in Figure 38. It was observed that compared to MKFA composites using RS, composites using MS exhibited a slight increase in the first cracking strength and flexural strength of 9.0% and 3.2%, respectively. On the other hand, the flexural deflection capacity of the RS specimens was 84.0% higher than that observed for MS specimens. As expected

from the tensile results, the flexural strength and deflection capacity of the MKFA composites was much lower than that of the MK EGC specimens. Furthermore, the flexural strength of the MKFA composites was significantly lower than the flexural strength of conventional concrete.
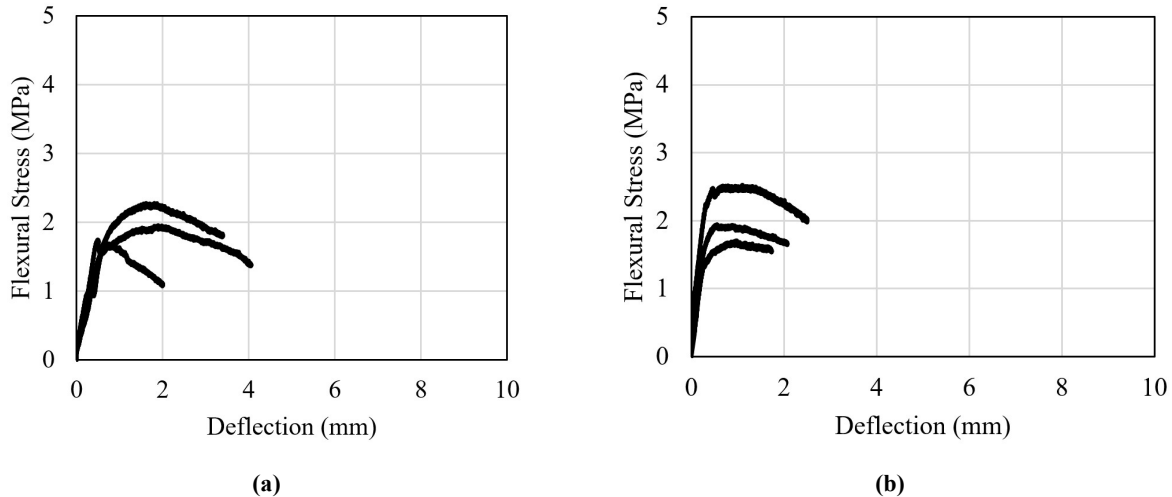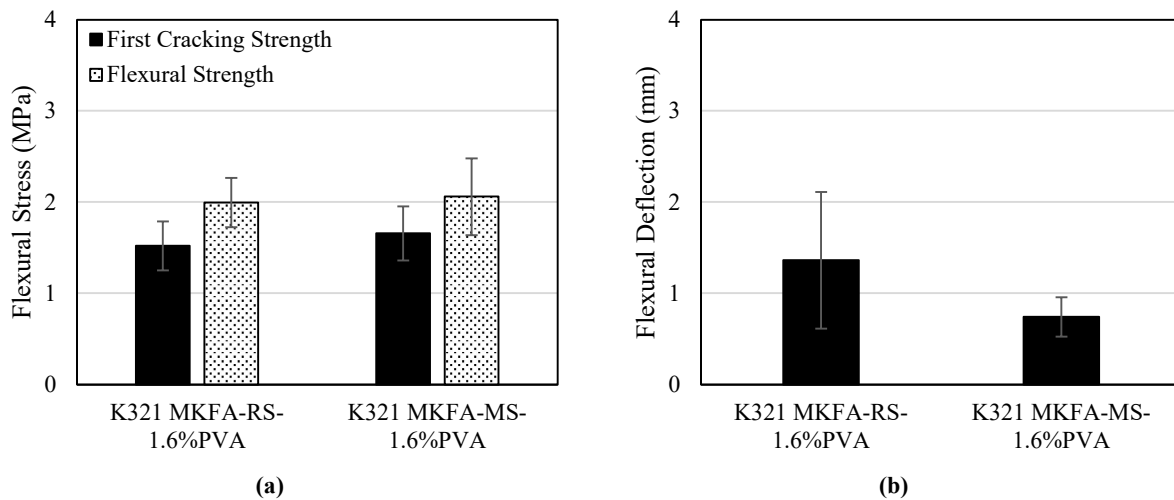

(a) **(b)**

Figure 37. Flexural stress vs. deflection curves of: (a) K321 MKFA-RS-1.6%PVA and (b) K321 MKFA-MS-1.6%PVA

(a) **(b)**

Figure 38. MKFA flexural performance test results: (a) first cracking strength and flexural strength and (b) deflection capacity.

5.2.4 Slant Shear Test

Based on the experimental results, it was determined that K321 GP-MS-1.6%PVA exhibited the highest strength and ductility among all EGCs. As such, to evaluate the potential of this material for repair applications, the bond strength of K321 GP-MS-1.6%PVA with conventional concrete was evaluated by slant shear test. Figure 39a shows a K321 GP-MS-1.6%PVA slant shear specimen during testing. There are three types of failures when conducting slant shear test: substrate failure, interfacial failure, and surface (*72*). As shown in and Figure 39b, substrate failure was observed. This was the case since the PCC substrate had a lower compressive strength than

the surface layer and the bond between the GP material and the concrete substrate was sound. However, since substrate failure occurred, the calculated shear stress at failure of 15.64 MPa (presented in Table 10) is an underestimate of the slant shear bond strength of the of the EGC with concrete. It is important to mention that the compressive strength of the slant shear specimen was higher than the 28-day compressive strength of the PCC substrate due to the continued hydration and strength gain concrete exhibits over time (since the PCC age at testing was 56 days).

Table 10. PCC compressive strength and slant shear (SS) test results.

Property	Average	STD	CV (%)
PCC (28-Day Compressive Strength, MPa)	29.49	0.84	0.03
SS (Compressive Strength, MPa)	36.74	1.06	0.03
SS (Shear Stress, MPa)	15.64	0.34	0.02

| (a) | (b) |
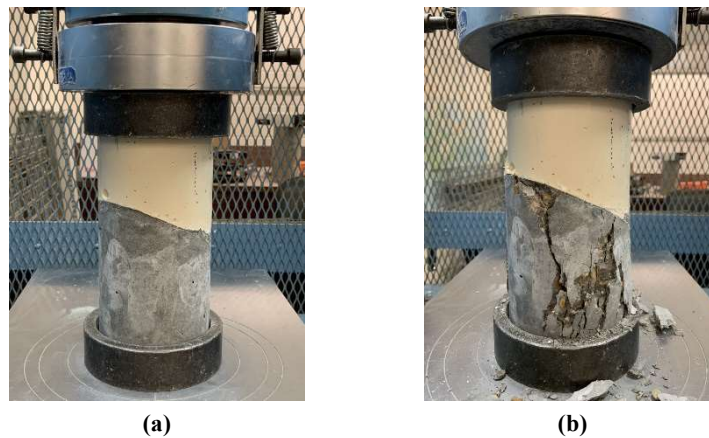
Figure 39. Slant shear test: (a) specimen during testing and (b) specimen at failure.

5.2.5 Setting Time

5.2.5.1 MK Based GP Materials

Per ASTM C191, Vicat needle penetration vs time curves for MK GP binders and mortars are presented in Figure 40 and Figure 41. From these curves, the initial and final setting times were obtained and are shown in **Error! Reference source not found.**. From the experimental results, K321 GP materials are observed to have the fastest setting time followed by K331 and Na431 GP materials. Interestingly, the increase in water content used during processing significantly increased the initial and final setting times for K-based GP binders. Compared to the K321 GP binder, the increases in the initial and final setting time for the K331 GP binder were of 96.8% (from 127 to 250 minutes) and 90.9% (from 165 to 315 minutes), respectively. This phenomenon is attributed to the effect of excess water in delaying the geopolymerization process; thus, preventing rapid hardening of the GP. Regarding the Na-based GP binder, this material exhibited by far the highest initial and final setting times of 2044 and 2205 minutes, respectively, among all the MK GPs evaluated. Surprisingly, while the Na431 GP binder used the same amount of water of K331 during processing (i.e., W/GP solids of 3), its initial and final setting times exceeded those of the K331 binder by 7.2 and 6 times, respectively.

A consistent trend observed for all MK GP materials was that the addition of sand increased the initial and final setting times, with RS producing a higher increase than MS. This behavior may

be attributed to the effect of aggregate in retaining water inside the GP mortars. For instance, in Portland cement concrete (PCC), internal bleeding is a well-known phenomenon in which water is retained on the lower surface of the aggregate and prevented to easily rise to the concrete surface (*73*). Internal bleeding is usually exacerbated by the increase in aggregate size, which in turn, may explain the effect of RS in producing higher setting times compared to MS in GP mortars (*73*). It is important to mention that significant segregation was observed in K331 and Na431 mortars incorporating RS, which can introduce error in the setting time measurements. Furthermore, due to Na431 being more workable than K331, the effect of segregation was more pronounced in Na431 than in K331.
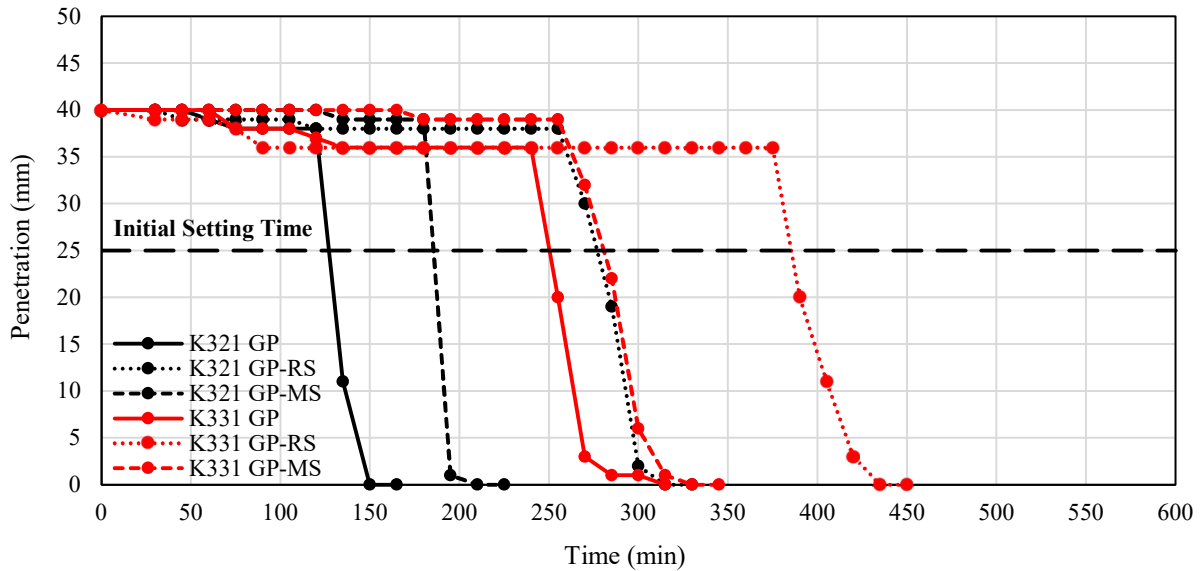
Figure 40. K321 and K331 setting time experimental results.
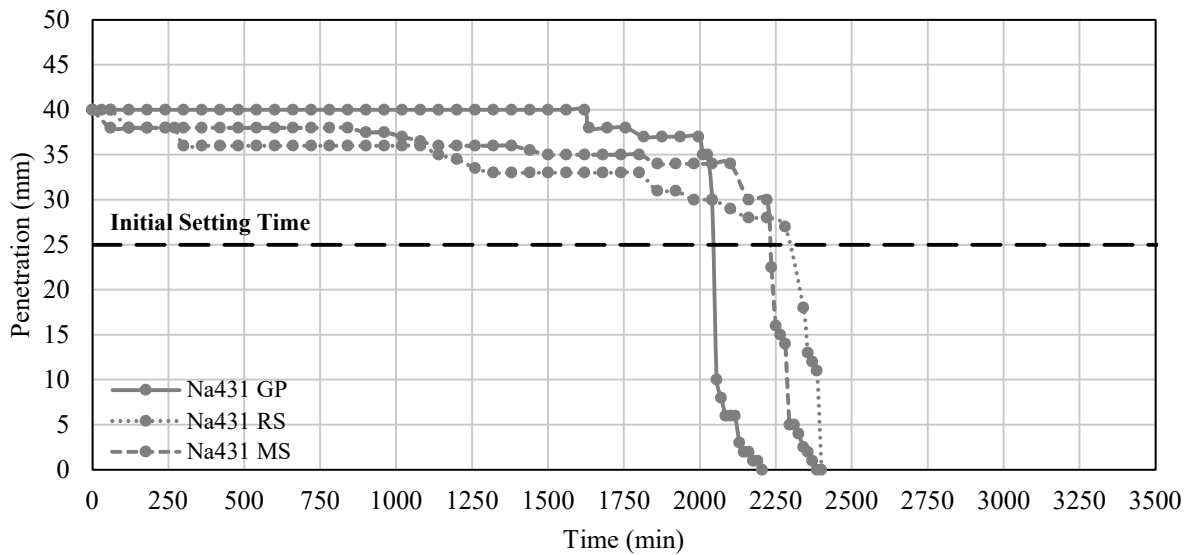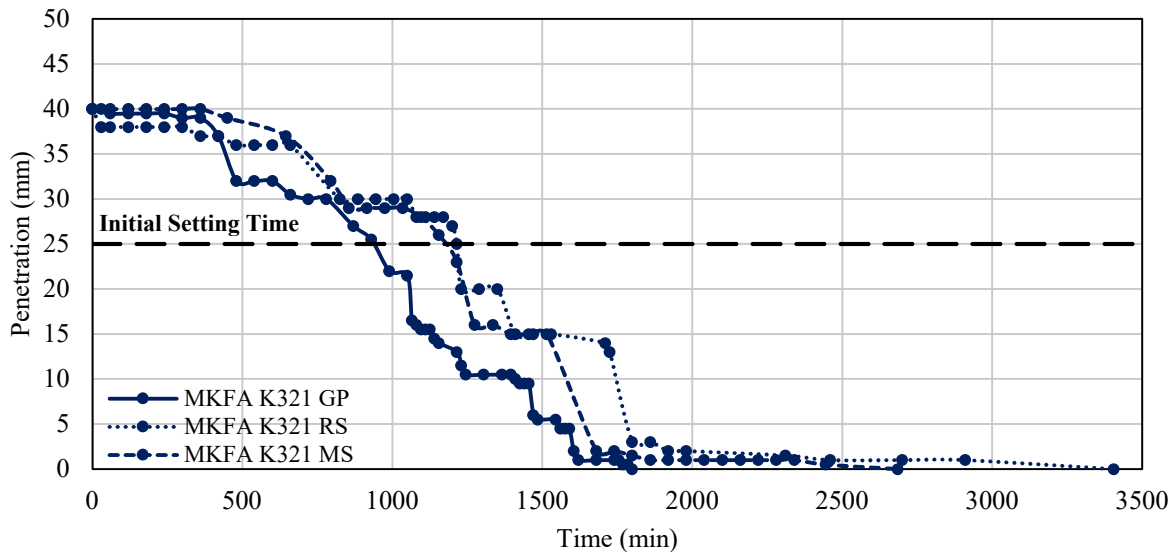

Figure 41. Na431 setting time experimental results.

Table 11. Setting Time Results.

Mixture	Initial Setting Time (min)	Final Setting Time (min)
K321 GP	127	165
K321 RS	277	330
K321 MS	186	225
K331 GP	250	315
K331 RS	385	450
K331 MS	281	345
Na431 GP	2044	2205
Na431 RS	2300	2565
Na431 MS	2230	2610

5.2.5.1 MKFA Based GP Materials

Similar to MK GP materials, the setting time for MKFA binder and mortars were evaluated per ASTM C191. The Vicat needle penetration vs time curves are shown in Figure 42. From these curves the initial and final setting times were obtained and are shown in Table 12. It can be observed that a similar trend was obtained in which the addition of sand led to an increase in initial and final setting time, with RS producing a higher increase than MS. This was attributed to the same internal bleeding phenomenon mentioned in section 5.10.1. Compared to MK K321 GP materials, a significant increase in initial and final setting time was observed when silica fume was completely replaced with fly ash. For example, the MKFA K321 binder exhibited an increase in the initial and final setting time of 679.5% (from 127 to 990 minutes) and 2009.1% (from 165 to 3480 minutes), respectively, compared to the MK K321 GP. The dramatic increase in setting time of the MKFA binder is likely attributed to the lower reactivity of fly ash compared to silica fume.

Figure 42. MKFA K321 setting time experimental results.

Table 12. Setting time results.

Mixture	Initial Setting Time (min)	Final Setting Time (min)
MFA K321 GP	990	3480
MFA K321 RS	1215	4920
MFA K321 MS	1160	4800

5.2.7 pH

The pH of the MK-based activator solution and GP binders are shown in Figure 43. For all the MK GP binders the pH ranges between 13.09 and 14.65, whereas typical Portland cement concrete has a pH level between 12 and 13. Consequently, safety precautions should be taken when working with these materials including the use of personal protective equipment and appropriate training of workforce.
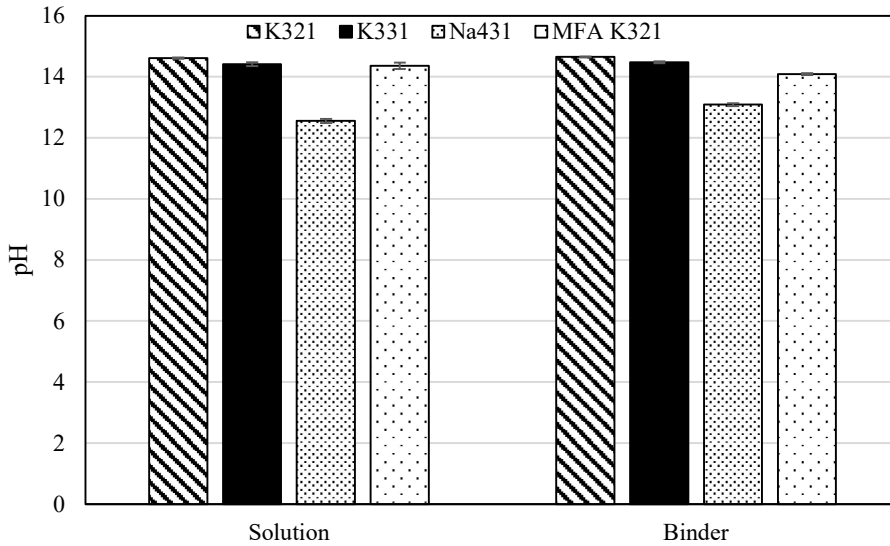

Figure 43. pH of activator solution and GP binder.

5.3 GP Feasibility Study in Ecuador

5.3.1 Characterization

The samples of kaolin, composed mainly of kaolinite, were successfully transformed to metakaolin after 3h at 600°C as can be seen in Figure 44 and Figure 45. On the other hand, Figure 46 shows that mordenite is the major mineralogical phase in the tuff. In all these samples, quartz was present and ranged from 10 to 25% by weight.
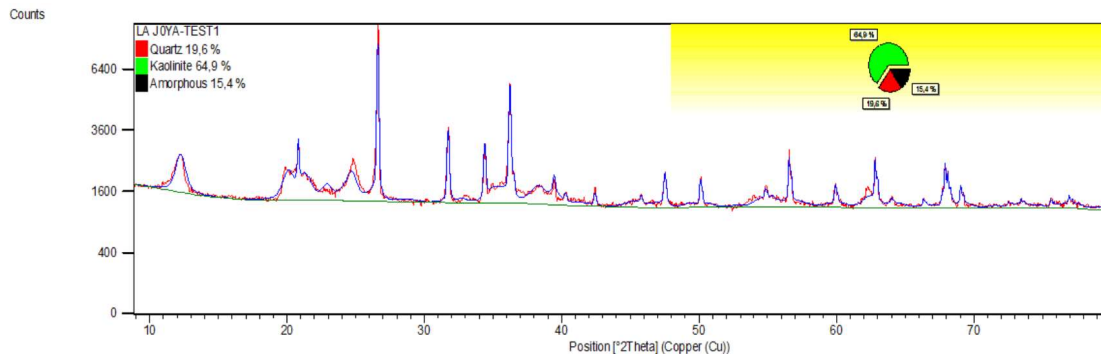
Figure 44 Quantitative X-ray diffractogram of as-receive kaolin.
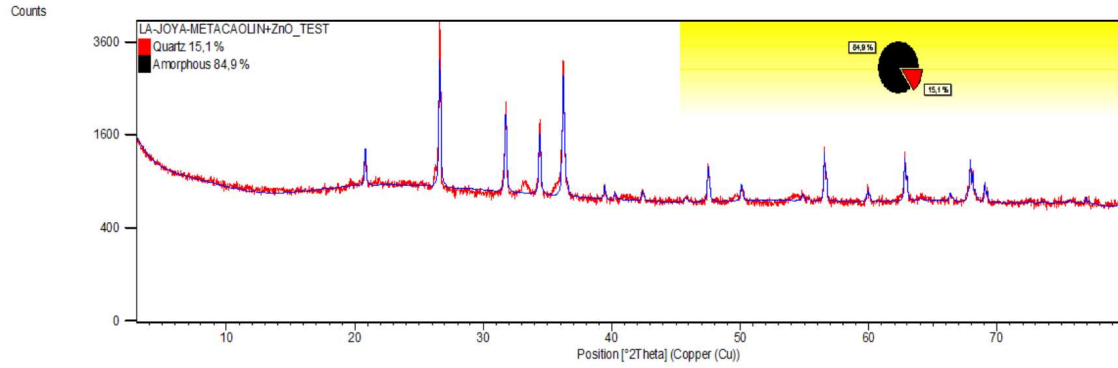
Figure 45 Quantitative X-ray diffraction of metakaolin (MK) after 3 h at 600°C.
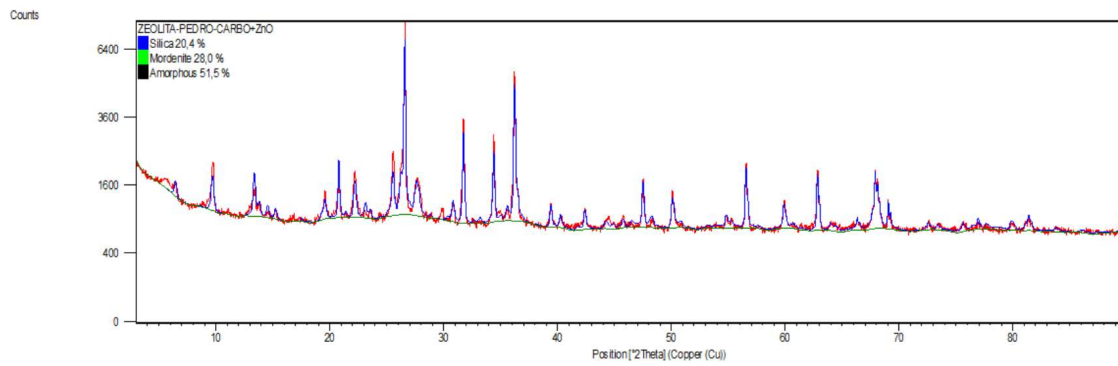
Figure 46 Quantitative X-ray diffractogram of as-receive zeolite-rich tuff.

Figure 47 displays an image of amorphous volcanic ash conjointly with elemental analysis whose Si/Al ratio is about 3. In addition, Figure 48 shows an image of zeolite tuff with quantitative analysis confirming that mordenite is the major mineralogical phase. Based on its Si/Al, this area showed a Si/Al of 5 similar to mordenites.
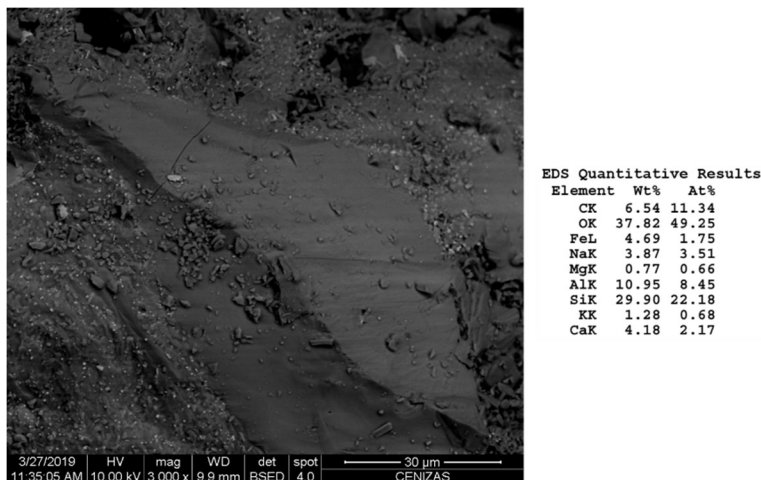

Figure 47 SEM image with EDS quantitative result of volcanic ash.

```
EDS Quantitative Results
Element  Wt%    At%
   CK    5.04   8.69
   OK   40.46  52.42
  NaK    1.43   1.29
  MgK    0.75   0.64
  AlK    7.86   6.04
  SiK   37.79  27.89
   KK    1.86   0.98
  CaK    1.81   0.94
  FeK    3.01   1.12
```
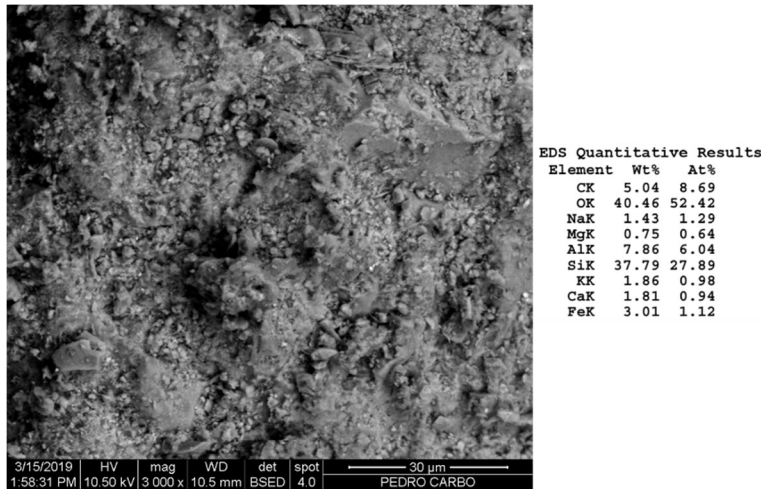
Figure 48 SEM image with EDS quantitative result of zeolite-rich tuff.

5.3.2 Compressive Strength

In order to determine the optimal composition of geopolymer mortars, three components as solid precursor were used to synthesize this geopolymer, i.e., mordenite tuff (x1), volcanic ash (x2), and metakaolin (x3). The combination of components according to the simplex experimental design were evaluated at 7, 28 and 91 days. **Error! Reference source not found.** present mixture contour plots, which show the lowest level of compressive strength in red, and the highest in yellow. Mixtures shown in the contour plots displayed the mixtures that showed higher strength at testing days. We can observe that the content of MK produced meaningfully higher strengths at early ages, but as time proceeded, the component of zeolite tuff in geopolymer produces similar effects to MK. The effect plot confirmed that result as can be seen in Figure 50. MK showed the highest effect over compressive strength during testing followed by the zeolite tuff (composed mainly of mordenite). Hence, a mixture between zeolite and MK presents an excellent potential as solid precursors in synthesis of geopolymers. On the other hand, volcanic ash content in the geopolymer composition showed the least effect over compressive strength. It is hypothesized that under the evaluated synthesis conditions, i.e., molar concentration of NaOH solution (SH) of 8 M, $Na_4Si_5O_{12}$/NaOH ratio of 3, a liquid to solid ratio of 0.5, and curing temperature of 60°C for 24h, volcanic ash was not fully activated. In addition, the nature of zeolites and MK is similar as both are aluminosilicates and can similarly respond to the same alkaline solution. Unlike zeolite and MK, volcanic ash is different in nature because of its genesis. In summary, volcanic ash could not be properly activated by the alkaline solution and curing conditions that can active zeolites and MK.
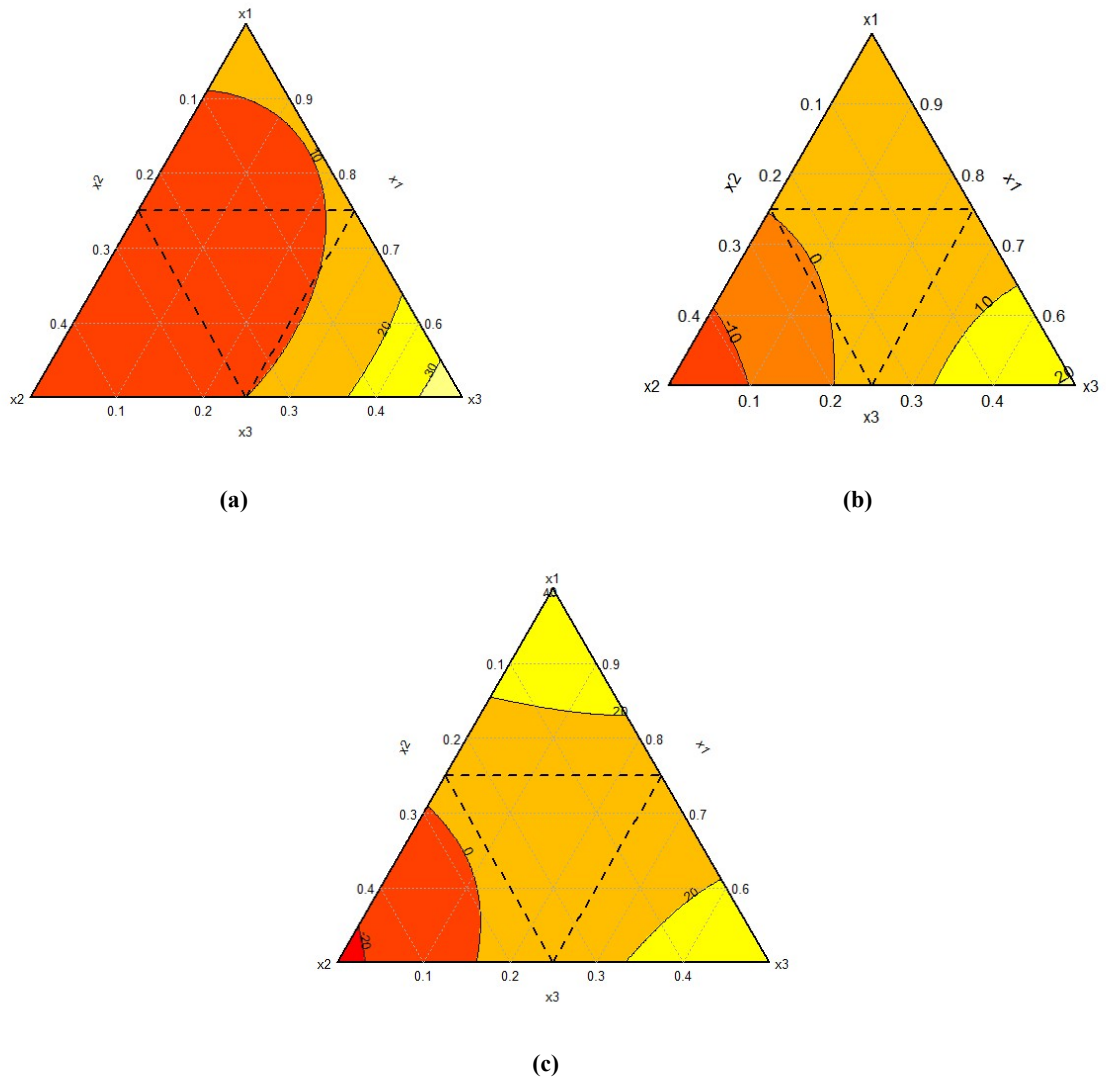
(a)

(b)

(c)

Figure 49 Mixture contour plots between components zeolite tuff (x1), volcanic ash (x2), metakaolin (x3) for compressive strength at: (a) 7 days, (b) 28 days, and (c) 91 days.
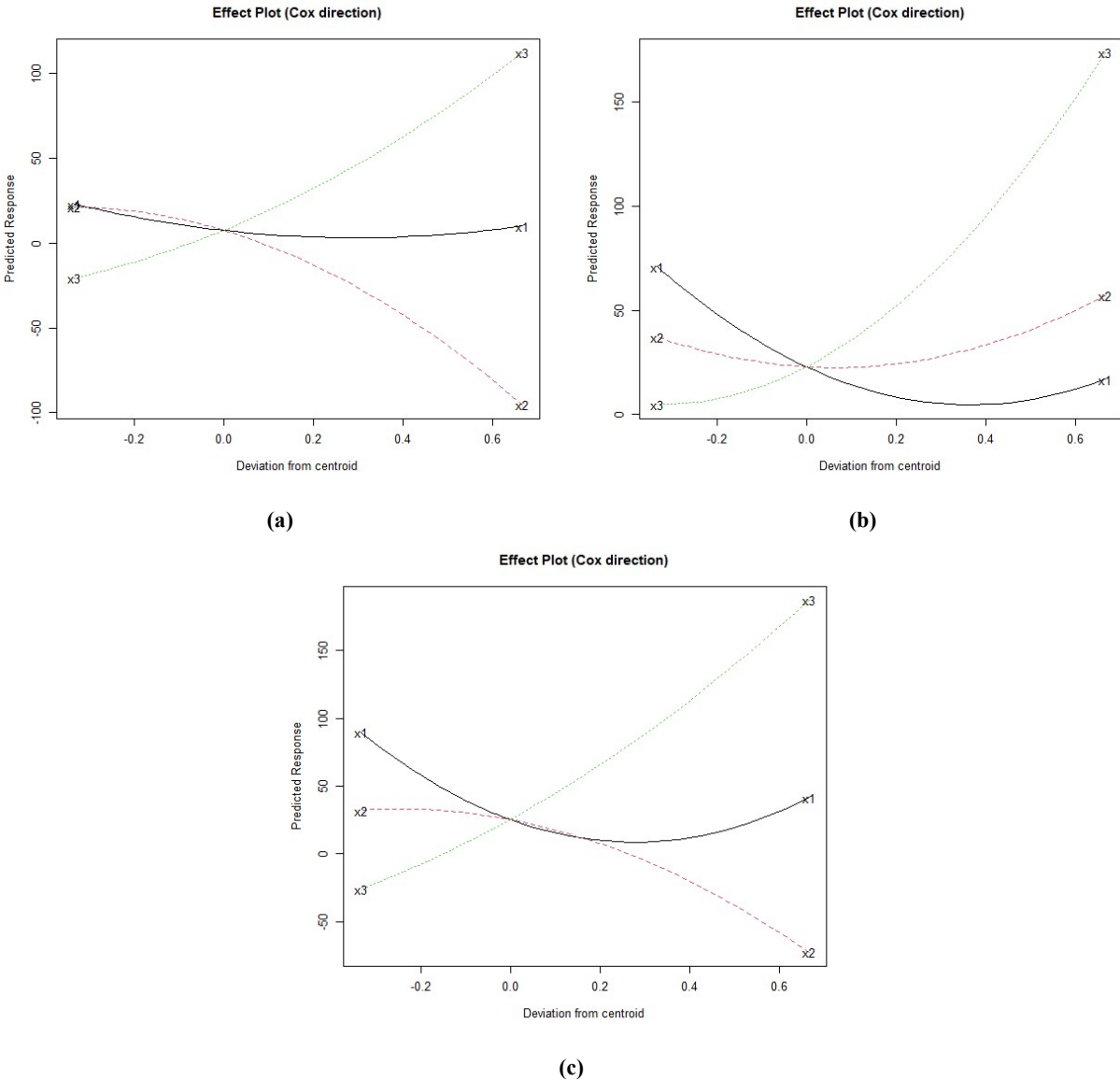
(a)

(b)

(c)

Figure 50 Effect plots of components x1, x2, x3, evaluating Cox direction, for compressive strength at: (a) 7 days, (b) 28 days, and (c) 91 days.

The compressive strength of geopolymer mixtures is presented in Table 13. Although generally samples showed hardening evolution over 91 days, the increment was very slow and in some cases mixtures kept compressive strength constant between 28 and 91 days. Because of the initial elevated temperature curing conditions, the strength is achieved at early ages by geopolymerization; after that, under ambient conditions, the hardening can be controlled by other reactions like carbonation.

55

Table 13 Values of compressive strength for mixtures with replications at 7, 28 and 91 days.

Mix ID	7 days (MPa)	28 days (MPa)	91 days (MPa)
	5.55	5.89	9.16
C1	3.20	5.92	8.46
	2.80	3.66	7.87
	1.64	3.39	7.07
C2	2.76	4.43	7.90
	1.57	1.37	9.00
	5.05	9.89	22.22
C3	2.49	7.70	13.69
	5.91	7.23	11.66
	3.44	4.06	10.41
C4	4.21	6.67	6.80
	2.58	3.83	9.42
	8.55	12.46	4.10
C5	5.67	12.26	16.20
	4.48	12.92	20.25
	4.03	10.16	11.43
C6	7.27	9.04	13.87
	3.49	10.77	5.65
C7	0.29	2.81	5.28

Mixtures C3 and C5 were the most promising showing the highest compressive strength over 91 days. These mixtures were mainly composed of zeolite and MK. As explained before, the major component in the mixture was zeolite, then MK acted as a mineral addition. In these cases, MK ranged from 10 to 20% by weight and could react with zeolite to form geopolymer with compressive strength of approximately 20 MPa after 91 days. On the other hand, C7, a mixture between zeolite and volcanic ash, was not able to show compressive strength at early ages, but as time proceeded, it was only capable of achieving 5 MPa. Figure 51 show images of the geopolymer mortars before and after compressive strength tests. Reddish color of samples C3 and C5 was attributed to the MK content. Compressive strength can be related to the porosity of the matrix. The samples whose compressive strength were low showed bigger pores as can be seen in C1, C6 and C7.

	Before	After 7 Days	After 28 Days	After 91 Days
C1				
C2				
C3				
C4				
C5				
C6				
C7				

Figure 51 Images of cubic samples of geopolymer before and after testing at 7, 28 and 91 days.

6. CONCLUSIONS

The objective of this study was to develop novel Engineered Geopolymer Composite (EGC) materials implementing locally available ingredients to produce practical and cost-effective EGCs for repair and new construction of transportation infrastructure in the region. To this end, MK and MKFA based GP binders, mortars, and fiber-reinforced composites were developed and thoroughly evaluated. In addition, a feasibility study was conducted in Ecuador to evaluate use of natural zeolite, volcanic ash, and metakaolin for the development of GP matrices. Based on the experimental findings the following conclusions can be drawn:

- Regardless of the starting water composition, the water content of all K- and Na-based GP binders stabilized at ~5-10wt% and ~10-15wt%, respectively. A similar tendency was observed for K- and Na-based GP mortars were the water content converged to ~2-3% and ~3-4%, respectively. Interestingly, the final water content of GP mortars reduced compared to pure GPs. Furthermore Na-based compositions exhibited a greater tendency to retain water in contrast to K-based compositions. This phenomenon was attributed to the fact that the Na ion has a smaller ionic radius than the K ion, and consequently has a stronger ionic potential and is able to attract more water molecules. Furthermore, the density of the dried GP decreased as the initial water content increased. This was attributed to the fact that water is eventually released as the geopolymerization process progresses, which create voids within the GP structure. Generally, the strength of Na-based GP binders increased as the SiO_2/Al_2O_3 ratio increased and/or the water/solids ratio decreased. In the case of K-based GP binders, the strength increased significantly when the SiO_2/Al_2O_3 ratio was equal or greater than 2.5. In addition, the strength of the GPs significantly increased with the addition of sand, which was attributed to the formation of a strong ITZ between the GP binder and aggregate particles. SEM microstructure analysis of GPs revealed that larger quantities of unreacted metakaolin correlated with low strengths. Based on satisfactory strength and workability characteristics K321, K331, and Na431 GP compositions were selected for further evaluation as fiber reinforced composites (i.e., EGCs).

- The addition of PVA fibers in GP mortars produced important improvements in compressive strength. Furthermore, the increment in PVA fiber dosage generally enhanced the compressive strength of the GP composites. In addition, specimens using MS sand tended to exhibit greater compressive strengths compared to those using RS. Interestingly, from the binder compositions studied for developing EGCs (i.e., K321, K331, and Na431), K321 produced the composites exhibiting the highest compressive strengths. This was a surprising finding since both K331 and Na431 pure GP binders exhibited higher strength compared to K321 pure GP. However, K331 and Na431 GP binders presented excessive workability, which caused aggregate and fiber segregation problems as well as poor fiber distribution. It was also found that the K321 GP mortars exhibited the fastest initial setting time, which ranged between 186 and 277 minutes. The greatest compressive strength achieved in this study of 57.52 MPa occurred for the K321 GP-MS-1.6%PVA composite. This material classified as a high-strength concrete material while exhibiting a density 22.9% lower to that of conventional PCC. Consequently, the K321 GP-MS-1.6%PVA

composite along with K321 GP-RS-1.6%PVA (for comparative purposes) were selected for further evaluation in uniaxial tension and bending. Experimental findings revealed a mild PSH behavior of both composites in uniaxial tension, with K321 GP-MS-1.6%PVA outperforming in terms of both tensile strength and ductility. The lack of robust PSH characteristics of the composites was mainly attributed to the unsatisfactory fiber distribution. Consequently, a modified mixing procedure was attempted to improve fiber dispersion using a tabletop planetary mixer. This in turn, produced significant enhancements in the tensile properties of the composites and allow the K321 GP-MS-1.6%PVA composite to exhibit a tensile strength and strain capacity of up to 3.89 MPa and 2.02%, respectively. Findings observed in the uniaxial tensile test were reflected in the flexural performance of the composites were the K321 GP-MS-1.6%PVA composite presented the highest flexural strength and deflection capacity of 5.0 MPa and 5.1 mm, respectively. The K321 GP-MS-1.6%PVA composite was also selected to evaluate the bond strength of MK EGCs with conventional concrete through slant shear test. Experimental findings suggested excellent bond characteristics of the MK-based EGC as failure of the slant shear specimens occurred in the concrete substrate. Overall, it was concluded that MK based GP matrices are promising for the development of EGCs, however securing proper fiber dispersion is challenging. As such, future research should be directed towards the optimization of rheological characteristics of the GP matrices and mixing procedures to consistently yield proper fiber distribution.

- To produce more cost-effective composites, the development of K321 MKFA GP compositions were evaluated by replacing silica fume with fly ash. However, compared to K321 MK GP compositions, the resulting materials exhibited low compressive strengths ranging from 4.94 to 10.10 MPa and exceedingly high initial settings times ranging from 990 to 1215 minutes. It is important to mention that like K321 MK GP materials, the compressive strength of K321 MKFA GP compositions was enhanced when MS was implemented and when fiber dosage increased. MKFA fiber-reinforced composites evaluated in tension and bending (i.e., K321 MKFA-RS-1.6%PVA and K321 MKFA-MS-%PVA) did not produce PSH behavior and exhibited low tensile and flexural strengths. This was attributed to the low strength of the MKFA GP matrices, which produced a poor fiber/matrix interface. Based on current findings, future research should be directed towards evaluating partial replacements of silica fume with fly ash to yield composites exhibiting satisfactory mechanical strength and cost-effectiveness.

- The pH of the different GP binders evaluated for EGC application (i.e., K321, K331, Na431, and MKFA K321) was assessed. The pH of these binders ranged between 13.1 and 14.7, whereas that of PCC typically ranges between 12 and 13. As such, all the GP binders evaluated were more alkaline than conventional concrete. Consequently, safety precautions should be taken when working with these materials including the use of personal protective equipment and appropriate training of the workforce.

- A feasibility study was conducted in Ecuador to evaluate the use of natural zeolite, volcanic ash, and metakaolin for the development of geopolymer matrices for EGC application. The experimental results showed that MK had the highest effect on strength of the GPs, followed by the zeolite. Volcanic ash had the least effect over the GP strength. It is hypothesized that under the evaluated synthesis conditions volcanic ash was not fully activated. The highest of compressive strength obtained was approximately 20 MPa. Experimental findings suggested that an optimal Si/Al ratio may be achieved by mixing 70% of zeolite and 30 of MK.

REFERENCES

1. Mindess, S., F. J. Young, and D. Darwin. *Concrete*. Prentice Hall, 2003.

2. Ohno, M., and V. C. Li. An Integrated Design Method of Engineered Geopolymer Composite. *Cement and Concrete Composites*, Vol. 88, 2018, pp. 73–85. https://doi.org/10.1016/j.cemconcomp.2018.02.001.

3. Nematollahi, B., J. Sanjayan, and F. U. Ahmed Shaikh. Tensile Strain Hardening Behavior of PVA Fiber-Reinforced Engineered Geopolymer Composite. *Journal of Materials in Civil Engineering*, Vol. 27, No. 10, 2015, pp. 1–12. https://doi.org/10.1061/(ASCE)MT.1943-5533.0001242.

4. Alrefaei, Y., and J. G. Dai. Tensile Behavior and Microstructure of Hybrid Fiber Ambient Cured One-Part Engineered Geopolymer Composites. *Construction and Building Materials*, Vol. 184, 2018, pp. 419–431. https://doi.org/10.1016/j.conbuildmat.2018.07.012.

5. Li, V. C. Engineered Cementitious Composite (Ecc): Material, Structural, and Durability Performance. *Concrete Construction Engineering Handbook, Second Edition*, 2008, pp. 1001–1048.

6. Li, V. C., T. Horikoshi, A. Ogawa, S. Torigoe, and T. Saito. Micromechanics-Based Durability Study of Polyvinyl Alcohol-Engineered Cementitious Composite. *ACI Materials Journal*, Vol. 101, No. 3, 2004, pp. 242–248. https://doi.org/10.14359/13120.

7. Li, V. C. On Engineered Cementitious Composites (ECC). A Review of the Material and Its Applications. *Journal of Advanced Concrete Technology*, Vol. 1, No. 3, 2003, pp. 215–230. https://doi.org/10.3151/jact.1.215.

8. Li, V. C. *Engineered Cementitious Composites (ECC) Bendable Concrete for Sustainable and Resilient Infrastructure*.

9. Arce, G., H. Noorvand, M. Hassan, T. Rupnow, and R. Hungria. Cost-Effective ECC with Low Fiber Content for Pavement Application. *MATEC Web of Conferences*, Vol. 271, 2019, p. 07001. https://doi.org/10.1051/matecconf/201927107001.

10. Noorvand, H., G. Arce, M. Hassan, and T. Rupnow. Investigation of the Mechanical Properties of Engineered Cementitious Composites with Low Fiber Content and with Crumb Rubber and High Fly Ash Content. Vol. 2673, No. 5, 2019, pp. 418–428. https://doi.org/10.1177/0361198119837510.

11. Reda Taha, M. M., X. Xiao, J. Yi, and N. G. Shrive. Evaluation of Flexural Fracture Toughness for Quasi-Brittle Structural Materials Using a Simple Test Method. *Canadian Journal of Civil Engineering*, Vol. 29, No. 4, 2002, pp. 567–575. https://doi.org/10.1139/l02-044.

12. Li, V. C., C. Wu, S. Wang, A. Ogawa, and T. Saito. Interface Tailoring for Strain-Hardening Polyvinyl Alcohol-Engineered Cementitious Composite (PVA-ECC). *ACI Materials Journal*, Vol. 99, No. 5, 2002, pp. 463–472. https://doi.org/10.14359/12325.

13. Pakravan, H. R., M. Jamshidi, and M. Latifi. The Effect of Hydrophilic (Polyvinyl Alcohol)

Fiber Content on the Flexural Behavior of Engineered Cementitious Composites (ECC). *Journal of the Textile Institute*, Vol. 109, No. 1, 2018, pp. 79–84. https://doi.org/10.1080/00405000.2017.1329132.

14. Ling, Y., K. Wang, W. Li, G. Shi, and P. Lu. Effect of Slag on the Mechanical Properties and Bond Strength of Fly Ash-Based Engineered Geopolymer Composites. *Composites Part B: Engineering*, Vol. 164, No. February, 2019, pp. 747–757. https://doi.org/10.1016/j.compositesb.2019.01.092.

15. Ma, H., S. Qian, Z. Zhang, Z. Lin, and V. C. Li. Tailoring Engineered Cementitious Composites with Local Ingredients. *Construction and Building Materials*, Vol. 101, No. Part 1, 2015, pp. 584–595. https://doi.org/10.1016/j.conbuildmat.2015.10.146.

16. Nematollahi, B., J. Sanjayan, and F. U. A. Shaikh. Strain Hardening Behavior of Engineered Geopolymer Composites: Effects of the Activator Combination. *Journal of the Australian Ceramic Society*, Vol. 51, No. 1, 2015, pp. 54–60.

17. Redon, C., V. C. Li, C. Wu, H. Hoshiro, T. Saito, and A. Ogawa. Measuring and Modifiying Interface Properties Od PVA Fibers in ECC Matrix. *Manager*, Vol. 13, No. December, 2001, pp. 399–406.

18. Kan, L. li, W. song Wang, W. dong Liu, and M. Wu. Development and Characterization of Fly Ash Based PVA Fiber Reinforced Engineered Geopolymer Composites Incorporating Metakaolin. *Cement and Concrete Composites*, Vol. 108, No. May 2019, 2020, p. 103521. https://doi.org/10.1016/j.cemconcomp.2020.103521.

19. Kan, L. li, J. wei Lv, B. bei Duan, and M. Wu. Self-Healing of Engineered Geopolymer Composites Prepared by Fly Ash and Metakaolin. *Cement and Concrete Research*, Vol. 125, No. September, 2019, p. 105895. https://doi.org/10.1016/j.cemconres.2019.105895.

20. Osman, B. H., X. Sun, Z. Tian, H. Lu, and G. Jiang. Dynamic Compressive and Tensile Characteristics of a New Type of Ultra-High-Molecular Weight Polyethylene (UHMWPE) and Polyvinyl Alcohol (PVA) Fibers Reinforced Concrete. *Shock and Vibration*, Vol. 2019, 2019. https://doi.org/10.1155/2019/6382934.

21. Choi, J. Il, B. Y. Lee, R. Ranade, V. C. Li, and Y. Lee. Ultra-High-Ductile Behavior of a Polyethylene Fiber-Reinforced Alkali-Activated Slag-Based Composite. *Cement and Concrete Composites*, Vol. 70, 2016, pp. 153–158. https://doi.org/10.1016/j.cemconcomp.2016.04.002.

22. Yu, K. Q., J. T. Yu, J. G. Dai, Z. D. Lu, and S. P. Shah. Development of Ultra-High Performance Engineered Cementitious Composites Using Polyethylene (PE) Fibers. *Construction and Building Materials*, Vol. 158, 2018, pp. 217–227. https://doi.org/10.1016/j.conbuildmat.2017.10.040.

23. Ding, Y., K. Q. Yu, J. tao Yu, and S. lang Xu. Structural Behaviors of Ultra-High Performance Engineered Cementitious Composites (UHP-ECC) Beams Subjected to Bending-Experimental Study. *Construction and Building Materials*, Vol. 177, 2018, pp. 102–115. https://doi.org/10.1016/j.conbuildmat.2018.05.122.

24. Singh, N. B. Fly Ash-Based Geopolymer Binder: A Future Construction Material. *Minerals*,

Vol. 8, No. 7, 2018. https://doi.org/10.3390/min8070299.

25.	Ohno, M., and V. C. Li. A Feasibility Study of Strain Hardening Fiber Reinforced Fly Ash-Based Geopolymer Composites. *Construction and Building Materials*, Vol. 57, 2014, pp. 163–168. https://doi.org/10.1016/j.conbuildmat.2014.02.005.

26.	Nematollahi, B., J. Sanjayan, and F. U. A. Shaikh. Matrix Design of Strain Hardening Fiber Reinforced Engineered Geopolymer Composite. *Composites Part B: Engineering*, Vol. 89, 2016, pp. 253–265. https://doi.org/10.1016/j.compositesb.2015.11.039.

27.	Ma, C., G. Long, Y. Shi, and Y. Xie. Preparation of Cleaner One-Part Geopolymer by Investigating Different Types of Commercial Sodium Metasilicate in China. *Journal of Cleaner Production*, Vol. 201, 2018, pp. 636–647. https://doi.org/10.1016/j.jclepro.2018.08.060.

28.	Nematollahi, B., J. Sanjayan, and F. U. A. Shaikh. Comparative Deflection Hardening Behavior of Short Fiber Reinforced Geopolymer Composites. *Construction and Building Materials*, Vol. 70, 2014, pp. 54–64. https://doi.org/10.1016/j.conbuildmat.2014.07.085.

29.	Yang, E. H., S. Wang, Y. Yang, and V. C. Li. Fiber-Bridging Constitutive Law of Engineered Cementitious Composites. *Journal of Advanced Concrete Technology*, Vol. 6, No. 1, 2008, pp. 181–193. https://doi.org/10.3151/jact.6.181.

30.	Marshall, D., and B. N. Cox. A J-Integral Method for Calculating Steady-State Matrix Cracking Stresses in Composites. Vol. 7, 1988, pp. 127–133.

31.	Li, V. C. *Engineered Cementitious Composites (ECC)*. 2019.

32.	Li, V. C. From Micromechanics Engineering Design for Compo- of Cementitious Engineering. *JSCE Journal of Structural Mechanics Earthquake Eng.*, Vol. 471, No. I–24, 1993, pp. 37s-48s.

33.	Kanda, T., and V. C. Li. Practical Design Criteria for Saturated Pseudo Strain Hardening Behavior in ECC. Vol. 4, No. 1, 2006, pp. 59–72.

34.	Weissberger, A. *Technique of Organic Chemistry*. 2020.

35.	MARK, J. E.; ALLCOCK, H. R.; WEST, R. *Inorganic Polymers*. xford University Press, 2005.

36.	Davidovitis, J. *Geopolymer Chemistry & Applications*. Institut Geopolymer, 2015.

37.	Provis, J. L., and J. S. J. van Deventer. *Geopolymers Structure, Processing, Properties and Industrial Applications*. Woodhead Publishing Limited and CRC Press LLC, 2009.

38.	Ryu, G. S., Y. B. Lee, K. T. Koh, and Y. S. Chung. The Mechanical Properties of Fly Ash-Based Geopolymer Concrete with Alkaline Activators. *Construction and Building Materials*, Vol. 47, No. 2013, 2013, pp. 409–418. https://doi.org/10.1016/j.conbuildmat.2013.05.069.

39.	Sata, V., A. Sathonsaowaphak, and P. Chindaprasirt. Resistance of Lignite Bottom Ash Geopolymer Mortar to Sulfate and Sulfuric Acid Attack. *Cement and Concrete Composites*, Vol. 34, No. 5, 2012, pp. 700–708. https://doi.org/10.1016/j.cemconcomp.2012.01.010.

40. Bakharev, T. Resistance of Geopolymer Materials to Acid Attack. *Cement and Concrete Research*, Vol. 35, No. 4, 2005, pp. 658–670. https://doi.org/10.1016/j.cemconres.2004.06.005.

41. Vickers, L., A. van Riessen, and W. Rickard. *Fire-Resistant Geopolymers: Role of Fibres and Fillers to Enhance Thermal Properties*. 2015.

42. Komnitsas, K. A. Potential of Geopolymer Technology towards Green Buildings and Sustainable Cities. *Procedia Engineering*, Vol. 21, 2011, pp. 1023–1032. https://doi.org/10.1016/j.proeng.2011.11.2108.

43. Turner, L. K., and F. G. Collins. Carbon Dioxide Equivalent (CO2-e) Emissions: A Comparison between Geopolymer and OPC Cement Concrete. *Construction and Building Materials*, Vol. 43, 2013, pp. 125–130. https://doi.org/10.1016/j.conbuildmat.2013.01.023.

44. McLellan, B. C., R. P. Williams, J. Lay, A. Van Riessen, and G. D. Corder. Costs and Carbon Emissions for Geopolymer Pastes in Comparison to Ordinary Portland Cement. *Journal of Cleaner Production*, Vol. 19, No. 9–10, 2011, pp. 1080–1090. https://doi.org/10.1016/j.jclepro.2011.02.010.

45. P. Duxson, A. Fernández-Jiménez, J. L. Provis, G. C. Lukey, A. Palomo, and J. S. J. V. D. *Geopolymer Technology: The Current State of the Art*. J. Mater. Sci., 2007.

46. He, P., M. Wang, S. Fu, D. Jia, S. Yan, J. Yuan, J. Xu, P. Wang, and Y. Zhou. Effects of Si/Al Ratio on the Structure and Properties of Metakaolin Based Geopolymer. *Ceramics International*, Vol. 42, No. 13, 2016, pp. 14416–14422. https://doi.org/10.1016/j.ceramint.2016.06.033.

47. Lizcano, M., A. Gonzalez, S. Basu, K. Lozano, and M. Radovic. Effects of Water Content and Chemical Composition on Structural Properties of Alkaline Activated Metakaolin-Based Geopolymers. *Journal of the American Ceramic Society*, Vol. 95, No. 7, 2012, pp. 2169–2177. https://doi.org/10.1111/j.1551-2916.2012.05184.x.

48. Lizcano, M., H. S. Kim, S. Basu, and M. Radovic. Mechanical Properties of Sodium and Potassium Activated Metakaolin-Based Geopolymers. *Journal of Materials Science*, Vol. 47, No. 6, 2012, pp. 2607–2616. https://doi.org/10.1007/s10853-011-6085-4.

49. Tarbuck, E. J., and F. K. Lutgens. *Earth An Introduction to Physical Geology*. 2017.

50. Morsy FA, El-Sherbiny S, Hassan MS, M. H. Modification and Evaluation of Egyptian Kaolinite as Pigment for Paper Coating. 2014, pp. 264,430-438. https://doi.org/10.1016.

51. Ilić, B. R., A. A. Mitrović, and L. R. Miličić. Thermal Treatment of Kaolin Clay to Obtain Metakaolin. *Hemijska Industrija*, Vol. 64, No. 4, 2010, pp. 351–356. https://doi.org/10.2298/HEMIND100322014I.

52. BASF. MetaMax ®. 2007, p. 2007.

53. Panesar, D. K. *Developments in the Formulation and Reinforcement of Concrete*. 2019.

54. Zahid, M., and N. Shafiq. Effects of Sand / Fly Ash and the Water / Solid Ratio on the Mechanical Properties of Engineered Geopolymer. 2020.

55. Trindade, A. C. C., A. A. Heravi, I. Curosu, M. Liebscher, F. de Andrade Silva, and V. Mechtcherine. Tensile Behavior of Strain-Hardening Geopolymer Composites (SHGC) under Impact Loading. *Cement and Concrete Composites*, Vol. 113, No. June, 2020. https://doi.org/10.1016/j.cemconcomp.2020.103703.

56. Constâncio Trindade, A. C., I. Curosu, M. Liebscher, V. Mechtcherine, and F. de Andrade Silva. On the Mechanical Performance of K- and Na-Based Strain-Hardening Geopolymer Composites (SHGC) Reinforced with PVA Fibers. *Construction and Building Materials*, Vol. 248, 2020. https://doi.org/10.1016/j.conbuildmat.2020.118558.

57. Salami, B. A., M. A. Megat Johari, Z. A. Ahmad, and M. Maslehuddin. Impact of Added Water and Superplasticizer on Early Compressive Strength of Selected Mixtures of Palm Oil Fuel Ash-Based Engineered Geopolymer Composites. *Construction and Building Materials*, Vol. 109, 2016, pp. 198–206. https://doi.org/10.1016/j.conbuildmat.2016.01.033.

58. Abdullah, M. M. A. B., R. A. Razak, and Z. Yahya. *Geopolymer Composite for High Temperature Exposure*. 2012.

59. Analyses, C., C. Ash, B. X. Fluorescence, I. Coupled, P. Mass, F. Atomic, and A. Spectrometry. ASTM: D 7348 – 08: Standard Test Methods for Loss on Ignition (LOI) of Solid Combustion Residues 1. Vol. i, 2009, pp. 1–7. https://doi.org/10.1520/D7348-13.2.

60. ASTM. ASTM C128-12, Standard Test Method for Density, Relative Density (Specific Gravity), and Absorption of Fine Aggregate. *ASTM International, West Conshohocken, PA*, Vol. i, 2012, pp. 2–7. https://doi.org/10.1520/C0128-15.2.

61. Materials, A. S. for T. &. Standard Test Method for Compressive Strength of Hydraulic Cement Mortars (Using 2-in. or [50-Mm] Cube Specimens). *Engineered Concrete*, 2009, pp. 29–31. https://doi.org/10.1201/9781420091175-c5.

62. Zhang, Z., Q. Zhang, S. Qian, and V. C. Li. Low E Modulus Early Strength Engineered Cementitious Composites Material Development for Ultrathin Whitetopping Overlay. *Transportation Research Record*, Vol. 2481, 2015, pp. 41–47. https://doi.org/10.3141/2481-06.

63. Test, C. C., T. Drilled, C. Concrete, and S. T. Panels. C 1609/C 1609M-05 Standard Test Method for Flexural Performance of Fiber-Reinforced Concrete (Using Beam With Third-Point Loading) 1. *Astm*, Vol. i, No. C 1609/C 1609M-05, 2005, pp. 1–8. https://doi.org/10.1520/C1609.

64. American Society for Testing & Materials. Standard Test Methods for Time of Setting of Hydraulic Cement by Vicat Needle. 1987, pp. 1–8. https://doi.org/10.1520/C0191-19.2.

65. Snellings, R., L. Machiels, G. Mertens, and J. Elsen. Rietveld Refinement Strategy for Quantitative Phase Analysis of Partially Amorphous Zeolitized Tuffaceous Rocks. *Geologica Belgica*, Vol. 13, No. 3, 2010, pp. 183–196.

66. Qian, L. P., Y. S. Wang, Y. Alrefaei, and J. G. Dai. Experimental Study on Full-Volume Fly Ash Geopolymer Mortars: Sintered Fly Ash versus Sand as Fine Aggregates. *Journal of Cleaner Production*, Vol. 263, 2020. https://doi.org/10.1016/j.jclepro.2020.121445.

67. Peng, H., C. Cui, C. S. Cai, Y. Liu, and Z. Liu. Microstructure and Microhardness Property of the Interface between a Metakaolin/GGBFS-Based Geopolymer Paste and Granite Aggregate. *Construction and Building Materials*, Vol. 221, 2019, pp. 263–273. https://doi.org/10.1016/j.conbuildmat.2019.06.090.

68. Ren, X., and L. Zhang. Experimental Study of Interfacial Transition Zones between Geopolymer Binder and Recycled Aggregate. *Construction and Building Materials*, Vol. 167, 2018, pp. 749–756. https://doi.org/10.1016/j.conbuildmat.2018.02.111.

69. Singh, B., M. R. Rahman, R. Paswan, and S. K. Bhattacharyya. Effect of Activator Concentration on the Strength, ITZ and Drying Shrinkage of Fly Ash/Slag Geopolymer Concrete. *Construction and Building Materials*, Vol. 118, 2016, pp. 171–179. https://doi.org/10.1016/j.conbuildmat.2016.05.008.

70. Sahmaran, M., M. Lachemi, K. M. A. Hossain, R. Ranade, and V. C. Li. Influence of Aggregate Type and Size on Ductility and Mechanical Properties of Engineered Cementitious Composites. *ACI Materials Journal*, Vol. 106, No. 3, 2009, pp. 308–316. https://doi.org/10.14359/56556.

71. Li, V. C. *Engineered Cementitious Composites (ECC)*. 2019.

72. Tayeh, B. A., B. H. Abu Bakar, M. A. Megat Johari, and Y. L. Voo. Evaluation of Bond Strength between Normal Concrete Substrate and Ultra High Performance Fiber Concrete as a Repair Material. *Procedia Engineering*, Vol. 54, No. Farhat 2010, 2013, pp. 554–563. https://doi.org/10.1016/j.proeng.2013.03.050.

73. Monteiro, P. *Concrete: Microstructure, Properties, and Materials*. 2006.